Title
Brain-Mimetic, Three-Dimensional Hyaluronic Acid-Based Hydrogels to Investigate Effects of the Tumor Microenvironment on Glioblastoma Progression

Author
Sohrabi, Alireza

Publication Date
2021

Peer reviewed|Thesis/dissertation

UNIVERSITY OF CALIFORNIA

Los Angeles

Brain-Mimetic, Three-Dimensional Hyaluronic Acid-Based Hydrogels to Investigate Effects of the Tumor Microenvironment on Glioblastoma Progression

A dissertation submitted in partial satisfaction of the

requirements for the degree of Doctor of Philosophy

in Bioengineering

by

Alireza Sohrabi

2021

ABSTRACT OF THE DISSERTATION

Brain-Mimetic, Three-Dimensional Hyaluronic Acid-Based Hydrogels to Investigate Effects of the Tumor Microenvironment on Glioblastoma Progression

by

Alireza Sohrabi
Doctor of Philosophy in Bioengineering
University of California, Los Angeles, 2021
Professor Stephanie Kristin Seidlits, Chair

Glioblastoma (GBM) is the most common and lethal type of brain cancers with median survival of 12-15 months. The poor patient prognosis is partially due to the highly infiltrative nature of GBM. GBM cells invasion through brain parenchyma is the main reason for secondary tumor formation. We posit that the unique brain extracellular matrix (ECM) facilitates GBM invasion. Specifically, we focused on the perivasculature niche surrounding the GBM tumor and the biophysical properties of the tumor. To study these, we fabricated a brain-mimetic, three-dimensional hydrogel platform based on hyaluronic acid (HA) with orthogonal control on biochemical and biophysical properties. First, we used this platform to study the crosstalk between GBM cells and the perivasculature. We found that cells derived from perivascular niche of GBM patient tumors induced a migratory phenotype in patient-derived GBM cells. Second, mimicking biophysical properties of a GBM tumor within the HA hydrogel platform enabled us to demonstrate that the ECM stiffness directly caused a switch in GBM metabolism pathway. By using this novel *in vitro* platform, we were able to uncover effects of the ECM on GBM progression which have not been observable with traditional methods.

Acknowledgment

In the first place, I would like to express my deepest appreciation to my thesis chair, supervisor, and mentor, Dr. Stephanie Seidlits. Under your supervision, I learned how to be a better researcher, a better mentor and a better human. Your dedication, hard-work and keen interest to help all of your students has set a great example for me to look up to. Your support and mentorship made this bumpy journey more pleasant.

I would like to thank my PhD committee members, Dr. Kornblum, Dr. Di Carlo, Dr. Deming and Dr. Nathanson. I consider myself lucky that I could benefit from your knowledge and experience in different aspects of my thesis. I appreciate all of your academic and scientific advice along this road.

I am grateful for all of my colleagues in Seidlits research lab. Specially Dr. Xiao, Dr. Ehsanipour and Jesse Liang. The four of us have been through many challenges together from the day 1 of Seidlits lab. It has been a blessing to have each one of you as a colleague and more importantly as a friend. To all other Seidlits lab members, who have helped me with my thesis, thank you. I consider all of you a friend before a colleague.

I would love to thank my parents Saied and Ladan, my siblings Amirreza and Niusha, my In-laws Parmiss and Amin, and my nieces Amitis and Bahar. Although far apart physically, your support along the way warmed my heart and pushed me toward my goals.

As an international student here, friends became my family, and I was lucky to have a great one. Shadi, my best friend since college, I appreciate your mental support in every day of this journey. We have been going through our daily PhD lives together. There have been numerous occasions that your support helped me moving forward. For these I am eternally grateful. To my friends, Alireza, Ebrahim and Mostafa who are like brothers to

me, befriending you has been a blessing for me. Just knowing that each of you are here for me made the challenges of living abroad easier to handle. Thank you for your support. Finally, Mai, my amazing friend, you gave me a better perspective about life in graduate school. Thank you!

Table of Contents

Chapter 1: Introduction and background *1*

Chapter 2: Role of microvasculature in glioblastoma invasion *28*

Chapter 3: Role of tumor mechanical properties on glioblastoma progression *47*

Chapter 4: Future development *79*

Chapter 5: Broader impact *90*

Chapter 6: Bibliography *93*

List of figures

1.1: Schematic representation of GBM tumor microenvironment ……12
1.2: An evolutionary diagram of models developed to study GBM ……...19
1.3: Controlling hydrogel mechanical and chemical properties in 3D ……..……30
1.4: Cell-ECM and Cell-Cell interactions at the level of a single cell ……35
2.1: ^{1}HNMR spectrum of a thiolated HA ……44
2.2: Photochemical thiol-ene method to fabricate HA hydrogels ……...45
2.3: Role of the interactome target proteins in GBM migration ……47
2.4: Comparison of GBM migration in HA-IBSP hydrogels against HA-RGD gels ……48
2.5: Interfacing hydrogels used to study GBM/ECs interaction ……..50
2.6: Western blot verification of IBSP knockdown in TECs ……51
2.7: IBSP knock down in TECs immensely decreased GBM cell migration ……52
3.1: AFM micro-compression investigation of xenografted GBM tumors ……..67
3.2: Photogels characterization ……...69
3.3: Uniform size of GBM spheroids was achieved using Aggrewell™ ……71
3.4: Live/Dead staining of GBM spheroids ……72
3.5: Bulk RNA-sequencing results ……...74
3.6: FLIM investigation of GBM spheroids in different stiffness ……..76
3.7: CD44 and integrin interaction with ECM influence GBM cells metabolism ……...79
3.8: GBM cells migration is stiff VS soft and the environment pH ……..81
3.9: FLIM comparison of a GBM spheroid and GBM migratory population is soft hydrogels……82
4.1: Schematic representation of a new Interfacing hydrogel system ……...89
4.2: AFM mechanical studies of an interfacing hydrogel ……91
4.3: GBM cells migration in an interfacing hydrogel ……92
4.4: Rheology data of soft and stiff hydrogels ……..……94
4.5: EDC/NHS modification of HA and 4-arm PEG-COOH to add hydrazide functional groups ……..96
4.6: Michael-addition click chemistry modification of HA-SH and 4 arm PEG-SH to introduce hydrazide functional group ……..97

BIOGRAPHICAL SKETCH

NAME Sohrabi, Alireza	POSITION TITLE Graduate Student Researcher
eRA COMMONS USER NAME (credential, e.g., agency login) ASOHRABI	

INSTITUTION AND LOCATION	DEGREE *(if applicable)*	MM/YY	FIELD OF STUDY
University of AmirKabir, Tehran, Iran	B.S.	06/2006-02/2011	Polymer Science and Engineering
University of Twente, Enschede, Netherlands	M.Sc.	08/2012-08/2014	Chemical Engineering
University of California, Los Angeles (UCLA), USA	Ph.D. candidate	09/2014-present	Bioengineering

A. Positions and Honors

Positions and Employment

2012-2014 Master student researcher, Prof. Vancso lab, University of Twente, Netherlands

2013 Intern in Prof. Kasko lab, University of California, Los Angeles

2014 - Present Graduate Student Researcher, Department of Bioengineering, University of California Los Angeles, Advisor: Stephanie Seidlits

2014-Present Member, American Chemical Society (ACS)

2016-Present Member, Biomedical Engineering Society (BMES)

2017-Present Member, American Association for Cancer Research (AACR)

Awards and Honors:

2006 Silver medal in International Young Invention symposium, Germany

2014 Cum laude award, University of Twente, Netherlands

2014, 2017, 2019 Bioengineering department graduate fellowship, UCLA

B. Synergistic activities

2016 Teaching assistant (UCLA)

2017 Teaching associate (UCLA)

2018 Teaching fellow (UCLA)

2017-2019 Co-founder, internal vice president of Bioengineering graduate association (BGA)

C. Publication

1. Zoetebier, B.*, **Sohrabi, A**., et al.* PEG stabilized DNA–poly (ferrocenylsilane) polyplexes for gene delivery. *Chem. Commun.* **52**, 7707–7710 (2016).

2. Margul, D. J. *et al.* Reducing neuroinflammation by delivery of IL-10 encoding lentivirus from multiple-channel bridges. *Bioeng. Transl. Med.* **1**, 136–148 (2016).

3. Xiao, W., **Sohrabi, A**. & Seidlits, S. K. Integrating the glioblastoma microenvironment into engineered experimental models. *Future Sci. OA* **3**, FSO189 (2017).

4. Xiao, W., Ehsanipour, A., **Sohrabi, A.** & Seidlits, S. K. Hyaluronic-acid based hydrogels for 3-dimensional culture of patient-derived glioblastoma cells. *J. Vis. Exp.* **2018**, 1–9 (2018).

5. Tay, A., **Sohrabi, A**., Poole, K., Seidlits, S. & Di Carlo, D. A 3D Magnetic Hyaluronic Acid Hydrogel for Magnetomechanical Neuromodulation of Primary Dorsal Root Ganglion Neurons. *Adv. Mater.* **30**, 1–8 (2018).

6. Xiao, W.*, Zhang R., **Sohrabi A**., et al.* Brain-mimetic 3D culture platforms allow investigation of cooperative effects of extracellular matrix features on therapeutic resistance in glioblastoma. *Cancer Res.* (2018). doi:10.1158/0008-5472.CAN-17-2429

7. Seidlits, S. K.*, Liang J., Bierman, R. D., **Sohrabi, A**.,* Peptide-modified, hyaluronic acid-based hydrogels as a 3D culture platform for neural stem/progenitor cell engineering. *J. Biomed. Mater. Res. - Part A* **107**, 704–718 (2019).

8. Sheikhi, A. *et al.* Microfluidic-enabled bottom-up hydrogels from annealable naturally-derived protein microbeads. *Biomaterials* **192**, 560–568 (2019).

9. Sheikhi, A. *et al.* Modular microporous hydrogels formed from microgel beads with orthogonal thermo-chemical responsivity: Microfluidic fabrication and characterization. *MethodsX* **6**, 1747–1752 (2019).

10. Xiao, W. *et al.* Bioengineered scaffolds for 3D culture demonstrate extracellular matrix-mediated mechanisms of chemotherapy resistance in glioblastoma. *Matrix Biol.* **85**, 128–146 (2020).

11. Bastola, S. *et al.* Tumor edge architecture in glioblastoma is constructed by inter-cellular signals from vascular endothelial cells. *bioRxiv* (2020).

12. Yu, Q. *et al.* Extracellular matrix proteins confer cell adhesion-mediated drug resistance through integrin αv in glioblastoma cells. *Front. cell Dev. Biol.* **9**, (2021).

Chapter 1: Introduction and background

Glioblastoma (GBM), grade IV glioma, is the most common and lethal type of cancer originating in the brain. Median survival time after diagnosis is 12-15 months[1]. Patients' poor prognosis is mainly due to two distinctive aspects of GBM: 1) GBM cells aggressively infiltrate healthy brain tissue and form secondary tumors, a phenomenon which renders local surgical methods ineffective, and 2) GBM tumors overwhelmingly develop resistance to standard treatments such as chemotherapies and radiotherapy. These two phenotypes combined translate into a 5-year overall survival rate of 5% for pateints[2].

GBM genetic subtype

Based on data deposited in The Cancer Genome Atlas (TCGA), GBM frequently has amplified genes like the epidermal growth factor receptor (EGFR), mutated genes like the tumor suppressor p53 (TP53), and the homozygous deletion of genes like CDKN2A/B[3]. Researchers have identified that major altered pathways in GBM are the receptor tyrosine kinases (RTK)-RAS-phosphoinositide 3-kinase (PI3K), retinoblastoma suppressor (RB), and TP53 pathways. These pathways and their alteration significantly facilitate tumor progression, proliferation and survival[3]. Interestingly, researchers have been able to induce GBM in mice by activation of RAS and Akt pathways in neural progenitor cells[4]. Based on common molecular alterations, GBM has been classified into four subtypes: proneural, classical, neural and mesenchymal. This classification is heavily based on abnormalities in the platelet-derived growth factor-α (PDGFA), EGFR and neurofibromatosis 1 (NF1). Out of these subtypes, patients diagnosed with mesenchymal subtype typically have worse prognoses. However, more recent studies have suggested this GBM classification system is inaccurate, as both tumor-associated, non-malignant

cells were included[5]. To remedy this, researchers have used three methods, 1) comparison of patient samples with their matched cell culture, 2) performing single cell RNA sequencing on GBM cells, and 3) comparison of biopsies from the tumor core versus the tumor periphery. Recent studies performed comprehensive longitudinal analysis of GBM transcriptome, excluding non-malignant cells revealed the presence of three subtypes rather than four: proneural, classical and mesenchymal.[6]

One important shortcoming of this classification is dismissing the isocitrate dehydrogenase (IDH)-mutant class of GBM tumors. IDH is an important rate-limiting enzyme in the Krebs cycle and metabolism. Recently, IDH mutation has been closely linked to GBM occurrence[7]. IDH mutants produce high levels of 2-hydroxyglutaric (2-HG), which inhibits GBM stem cell differentiation. In addition, high 2-HG can result in increased expression of vascular endothelial growth factor (VEGF), which promotes neovascularization around the tumor[7]. Finally, it has been shown that IDH mutation can induce high expression of hypoxia-inducible factor-1α (HIF-1α), which promotes GBM invasion. All of these changes eventually result in GBM tumor progression, invasion and formation of secondary tumors[7].

GBM Microenvironment

GBM tumors, originating in the brain, are isolated from the peripheral tissue behind the blood-brain barrier (BBB), which closely interacts with the unique microenvironment of the brain[8]. Even highly aggressive GBM tumors rarely metastasize outside of the brain[9]. In addition, metastatic tumors originating outside of the brain integrate minimally into the brain microenvironment[10].Together, these findings strongly imply that the unique brain microenvironment is preferred by GBM tumors. The brain extracellular matrix (ECM)

is composed of very few fibrous proteins and high amounts of specialized proteoglycans (PGs), glycosaminoglycans (GAGs) and glycoproteins[8,10]. In addition, soluble-factors, cell-cell interactions, and mechanical ques paint an exceedingly complex microenvironmental landscape. This complex ECM is altered in GBM tumors to support the growth and invasion of GBM[11]. **Figure 1.1** summarizes these interactions. In addition to brain ECM, GBM dynamically alters the microenvironment by secreting its own ECM and degrading the brain ECM around it. These dynamic changes in ECM, in turn, upregulate ECM deposition genes and degradation enzymes secreted from the GBM tumor[8,10,12].

One of the most abundant brain ECM components is hyaluronic acid (HA). HA is a negatively charged, unbranched GAG present at high molecular weights (~1 MDa) in the normal brain. HA chains act as the organizational centers of brain ECM, interacting with other molecules (proteins and PGs) through HA binding peptides (HABPs) to create a hydrogel-like microenvironment[13]. In addition, GBM upregulates HA expression which, in turn, contributes to many aspects of GBM including initial tumor development, cell proliferation, invasion and drug resistance[14,15]. In addition to HA overexpression, GBM cells overexpress HA-specific receptors, like CD44 and RHAMM. Concurrent overexpression of all of these factors can potentially lead to the hyper-aggression of the tumor[16,17]. Similar to many other cancers, it has been shown that GBM cell interactions with HA, through CD44 ,leads to tumor growth, invasion, and treatment resistance[18,19]. For instance, HA-CD44 interactions increase activation of the PI3K-AKT and MAPK-ERK1/2 signaling pathways, which results in an increase in apoptotic resistance and the migratory capacity of GBM cells[20,21]. Moreover, HA-bound CD44 interacts with many

other membrane-associated proteins such as RTKs, matrix metalloproteases (MMPs), and integrins to promote cell invasion and matrix degradation[20–23].

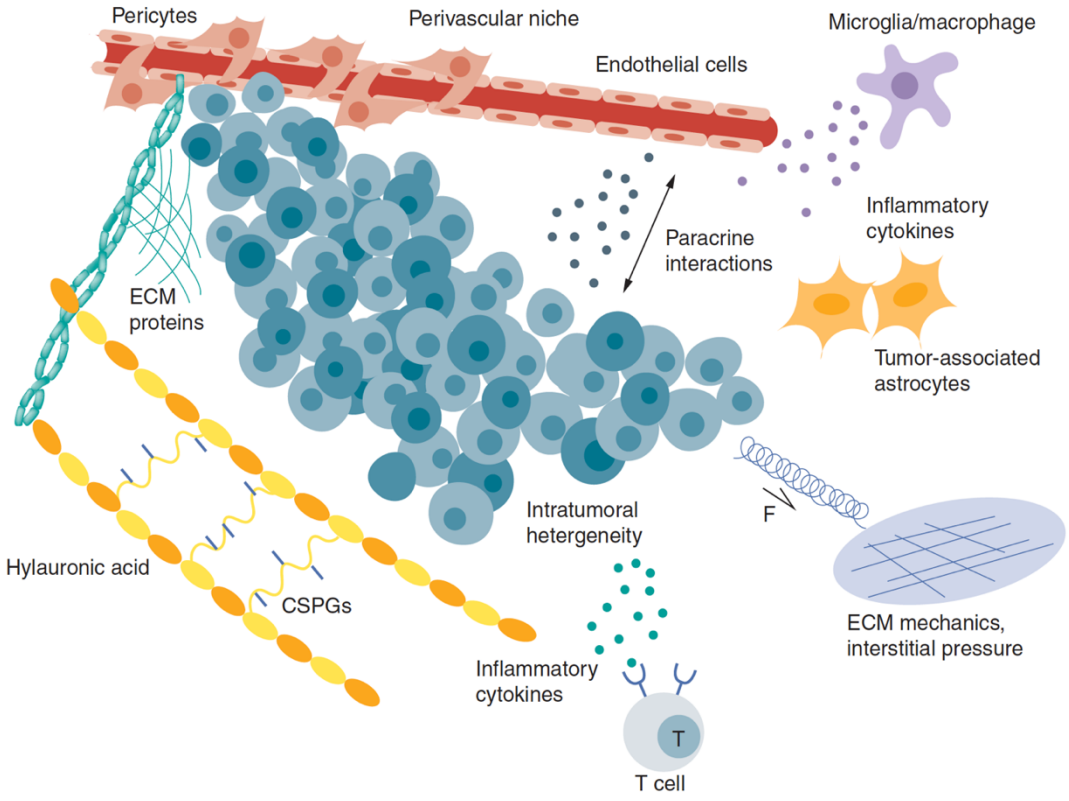

Figure 1. 1: Complex tumor microenvironment of GBM: HA, interacting with other proteins and GAGs form a hydrogel-like mesh around the tumor which relays chemical and mechanical signals to the GBM. Beside the mesh, interstitial pressure around the tumor alters mechanical signaling of tumor. In addition, GBM dynamically interacts with other cells in its microenvironments. (Figure adopted from Xiao et al., 2017)

Integrins are the main cell surface receptors for attachment to the ECM. HA-bound CD44 receptors act synergistically with many integrin subtypes (β_1, β_3, β_5 and α_v) to promote cell migration[24–26]. However, HA alone typically does not support cell adhesion and migration without additional integrin-binding proteins such as vitronectin, tenascin-C, osteopontin, etc. [8,10]. Interactions of ECM protein with integrins on GBM cells generally leads to apoptotic resistance and invasion. For instance, GBM invasion alongside vasculature is promoted through the interaction of integrins with collagen IV and laminin[24,27,28].

Beside ECM proteins, other brain ECM components, like glycoproteins and chondroitin sulfate (CS), are upregulated around GBM tumors[10,29]. Glycoproteins have a wide range of roles in cell growth and migration. For instance, heparan sulfate, by sequestering growth factors (e.g. EGF, PDGF-α and transforming growth factor-β (TGF-β)), facilitates activation of oncogenic RTKs[29–31]. Effects of PGs on GBM cells often depends on the simultaneous presence of other ECM components. For example, one study showed that migratory GBM cells cleave the PG brevican and that the product of this cleavage associates with fibronectin to enhance cell migration[32].

Soluble factors

Tumor and tumor-associated overexpression of several biological factors, such as TGF-β, TGF-α, EGF, VEGF and tumor necrosis factor-α (TNF-α), promotes GBM cell survival and proliferation[33,34]. As more than 50% of GBM tumors have either amplification or mutation of EGFR, targeted therapies against it has been extensively studied in clinical trials[33]. Moreover, GBM tumors overexpress the PDGF-α receptor (PDGFR-α). PDGF-α triggers an autocrine loop which promotes GBM proliferation[35]. Interestingly, EGFR-

dependent tumors often acquire resistance to EGFR inhibition by switching growth dependence to PDGFR-mediated pathways[36]. Several RTKs (e.g. EGF, TGF-α and PDGF-A) interact with ECM receptors to enhance tumor progression[21,23,30,37–39]. For example, CD44 localizes near EGFR on the cell membrane to activate the ERK1/2-MAPK and PI3K-AKT pathways, leading to increased GBM cell migration and apoptotic resistance[21,40].

The presence of inflammatory cytokines is also altered in a GBM tumor microenvironment compared to a healthy brain tissue. This abnormal microenvironment is thought to contribute to GBM invasion, angiogenesis around the tumor and other pathological phenotypes[34,41]. Numerous studies have shown effects of TGF-β on GBM proliferation (by increasing PDGF-β expression)[42], angiogenesis (by upregulating VEGF expression)[43] and tumor invasion (by enhancing MMP expression)[44]. In addition, TGF-β inhibits tumor clearance by cytotoxic T cells and induces an immunoprotective, M1-type phenotype in infiltrating macrophages and microglia. M1-type macrophages have been shown to support GBM tumor growth[44–46].

Another important soluble factor in the GBM microenvironment is low molecular weight HA (<50kDa). Low molecular weight HA is the product of HA degradation by hyaluronidases, which are overexpressed by GBM cells[47]. Unlike native, high molecular weight HA, low molecular weight HA can modulate toll-like receptors (TLRs) activity[48]. Although not well-studied in GBM, activation of TLRs on immune cells by low molecular weight HA has been reported to cause a proinflammatory response. For instance, it has been suggested that low molecular weight HA activates TLR4 and induces TNF-α expression in macrophages[49]. These studies indicate that, in GBM cells, low molecular

weight HA may participate in TNF-α autocrine loop described above. Interestingly, Wu et al., 2015, showed that in breast cancer patients, high serum level of HA fragments (<50KDa) and not total HA level, correlated positively with occurrence of lymph-node metastasis[50].

GBM cells migrate through brain parenchyma while degrading the matrix around them[51–53], which necessary for formation of new blood vessels around tumors to supply high metabolic demands of GBM cells[25]. GBM cells primarily overexpresses MMP-2 and MMP-9 and this overexpression directly correlates with poor survival in patients[54,55]. MMP-2 targets many brain ECM components, including fibronectin and laminin, while MMP-9 more specifically degrades laminin, osteonectin, and collagen IV[56], abundant in the a basement membrane of blood vessels[51]. In experimental models, inhibition of both MMPs reduces GBM invasion and growth[25,57].

In addition to matrix degradation, MMPs can interact with GBM cell receptors, ECM components and soluble factor to enhance GBM progression. For example, MMP-2 physically localizes close to integrin $\alpha_v\beta_3$, which mediates adhesion to vitronectin, thus enhancing cell migration in the vicinity of blood vessels[58]. In the same fashion, proteolytically active MMP-9 localizes near CD44, cleaves latent TGF-β and promote invasion and angiogensis[59].

Biophysical properties of GBM tumors

Another crucial feature of an ECM is the mechanical properties of the microenvironment in which cells reside. For instance, Engler et. al showed that while a softer matrix drove differentiation of mesenchymal stem cells (MSCs) towards a neurogenic lineage, a stiffer matrix drove them towards a myogenic lineage[60]. In the brain,

cells sense and respond to micron-scale mechanical rigidity[61]. Mechanical signals are transduced by numerous cell receptors such as integrins, CD44, stretched ion channel and G-protein-couples receptors[23,62,63]. It has been shown that in response to ECM mechanical signals, integrin-mediated pathways like FAK/PI3K/AKT and ERK/MAPK are activated. These pathways are likewise upregulated in migratory cells[23,64]. Receptors that are anchored to the actin cytoskeleton, such as CD44 and integrins, can rapidly relay mechanical cues through the release of actin-bound transcription factors and direct coupling to the nuclear membrane[65]. RTKs can also respond to mechanical cues[66]. For example, in airway epithelial cells, compressive stress increases EGFR phosphorylation followed by an increase in the ERK pathway activity[24]. Tumor stiffening with disease progression and the role of mechanical cues in drug resistance and invasion have been extensively studied[64,67]. However, previous studies investigating the mechanism of GBM cell responses to mechanical cues contain discrepancies in methods used to measure tumor stiffness as well as conclusions drawn collected data[66,68–71]. For example, while Netti, *et al., 2000,* reported that the linear compressive modulus of GBM tumors *ex vivo* was around 20 times higher than that of healthy mouse brain[72]. In contrast, Pogoda, *et al., 2014,* did not find any differences in the shear compressive moduli[73,74]. In clinical patients, indirect methods such as ultrasound-based elastography, have suggested that GBM tumors are approximately twice as stiff as tumor-free brain tissue in terms of Young's modulus. Although most studies agree that stiffness of GBM tumor increases with disease progression[75,76], it is remains unclear clear whether this can be attributed to the stiffness of ECM, the cells themselves, rising interstitial pressure or some

combination. Therefore, it is not counter-intuitive to hypothesize that GBM cells are softer than healthy brain cells around them[77–79].

As a GBM tumor grows, the local interstitial pressure increases. While cerebral spinal fluid drains through perivascular lymphatic system, in GBM, fluid accumulates which results in a sharp pressure gradient between the tumor and healthy adjacent tissue[80,81]. This elevation in pressure activates pathways similar to the ones activated by stiff ECM[74]. Recent studies have demonstrated that this buildup in interstitial pressure drives tumor growth and invasion specifically, through the CXCL12-driven chemotaxis and HA-CD44 interactions[82,83].

Cell-cell interactions

Beside the ECM, homo-interactions among GBM cells and hetero-interactions of GBM cells with other cell types play important roles in tumor progression. GBM homo-interactions, through gap junctions, can provide protection against drug-induced apoptosis. For example, Gielen et al., 2013, showed that knocking down connexin-43 (a gap junction protein) sensitized GBM cells to temozolomide (TMZ) treatment[84]. GBM cells also interact with each other through cadherins, but their role in GBM progress is not clear due to conflicting reports. While some reports suggest that lack N-cadherin-based cell junctions are necessary for cell invasion, others report that N-cadherin is upregulated in GBM and does not affect cell migration[85–87]. These contradictory results might be due to the differences in GBM subtypes.

GBM stem cells

Over a decade ago, researchers first isolated a subpopulation of GBM cells called GBM stem cells (GSCs). Although few in numbers, it is believed that tumor drug

resistance and invasion is mainly due to the presence of these cells[88]. Hence, it is believed that GSCs survive/resist treatment, invade the healthy brain tissue and form secondary tumors (recurrent tumors)[88,89]. GSC function is heavily dependent on interactions with the ECM, non-GSC tumor cells and non-cancerous cells in the tumor microenvironment[89]. As with homotypic interactions, GSCs interact with other non-GSC tumor cells through both gap and adherens junctions. Interestingly, unlike non-GSC cells which have high level of connexin-43, GSCs upregulate another gap junction protein, connexin-46, which is essential for GSC self-renewal[90,91].

Similar to other tumors, GBM tumors require excessive amounts of nutrition and oxygen. To satisfy this, GBM utilizes multiple strategies to promote neovascularization, such as high jacking normal vessels (vascular co-option)[92], sprouting of new vessels (angiogenesis)[93] and formation of vascular-like structure by tumor cells (vascular mimicry)[94]. GBM cells can attract endothelial cells (ECs) and pericytes by secreting angiogenic factors like VEGF[33,44]. Alternatively, GBM cells can physically interact with pericytes through Cdc-42 and actin-based extensions to alter pericytes contractility[95]. Finally, GSCs can trans-differentiate into ECs and pericytes to create new vessels[96,97]. In addition to providing nutrition, the GBM vasculature plays and important role in maintaining the ability of GSCs to initiate new tumors , drug resistance and invasion[98–100]. GSCs, through direct contact with vasculature, can invade large distances from the original tumor[101]. In addition, direct interactions between integrin α_5 and laminin, which is enriched near tumor vasculature, regulates GSC growth[90,102].

Experimental models of GBM

There have been numerous *in vivo* and *in vitro* models widely used to investigate GBM physiology, drug response and invasion. Each model bears some advantages and disadvantages. A summary of these models is presented **Figure 1. 2**.

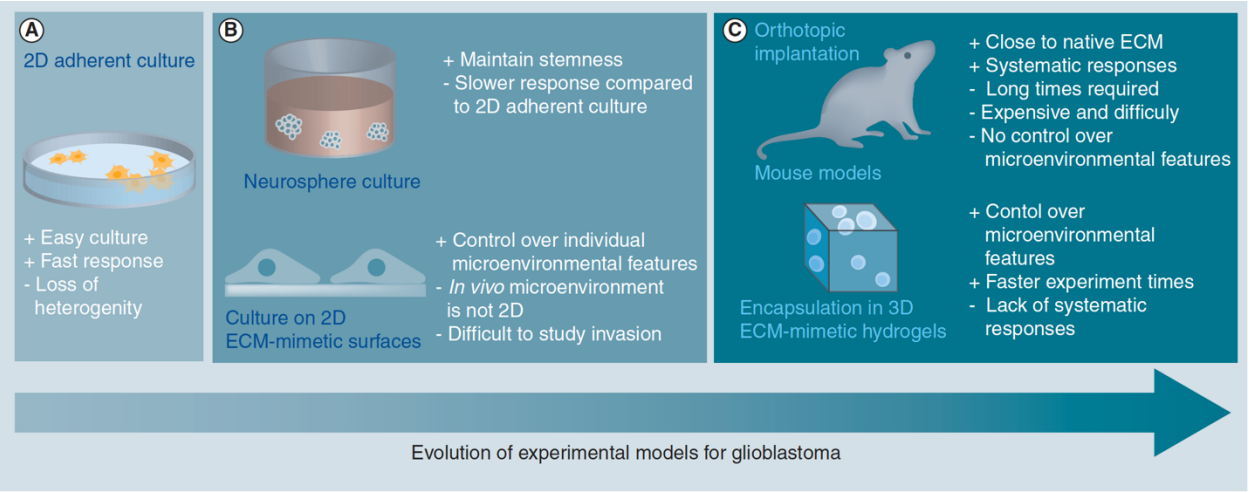

Figure 1. 2: An evolutionary diagram of models developed to study GBM. A) First model developed for GBM studies is adherent model on 2D where GBM single cells are cultured on a protein coated surface. B) To maintain stemness of GBM cells, gliomasphere culture was developed. Additionally, to control the GBM microenvironment, GBM cells were cultured on a surface with ECM-mimetic components. C) Finally, to introduce the 3D aspect of native GBM microenvironment, GBM cells (single or sphere) were encapsulated in 3D ECM-mimetic hydrogels. In addition, GBM cells were xenografted in mice brains. (Figure adopted from Xiao et. al., 2017)

Two-dimensional culture models

It has been half a century since researchers started using culturing patient-derived GBM tumor cells on two-dimensional (2D) surfaces to study GBM physiology. One of the most widely used cell lines is U-87. Although extensive data have been collected using this cell line, it is difficult to interpret results due to phenotype drift and extensive mutation since the original isolation. In addition, U-87 lacks representation of cell heterogeneity observed in GBM tumors[103].

Serum-based cell culture has been widely used to investigate effects of different agents on GBM. Serum contains various ECM components and soluble factors that facilitate cell adhesion and growth. Although simple to do, the serum method has a number of disadvantages. First, GBM cells cultured in serum lose phenotypic heterogeneity as serum induces selection of cells with specific characteristics[103]. Second, the presence of serum can cause phenotypic and genotypic changes in cells[104]. Finally, as serum is derived from animal sources, it typically suffers from poor batch-to-batch reproducibility[105].

In serum-free 2D cultures, coating surfaces with ECM proteins, which can be useful to study ECM-cell interactions, is common. The main pitfall with this method is that upon coating, proteins typically denature, compromising the relevance of results to *in vivo* cases. Moreover, it is difficult to mimic the complex mixture of ECM proteins of native brain ECM on a 2D surface. To circumvent this issue, researchers have widely used Matrigel. Matrigel, derived from the basement membrane of Engelbreth-Holm-Swarm mouse sarcoma, contains approximately 60% laminin, 30% collagen-IV and 8% entactin in addition to tethered growth factors including EGF, TGF-β and PDGF-β[106]. Beside

representing the complex ECM, Matrigel is compatible with both 2D and 3D models. Although useful for some experiments, Matrigel does not reflect GBM ECM. Another disadvantage of Matrigel is an inability to study roles of individual ECM components on GBM since one cannot control the composition. Finally, similar to serum reagents, Matrigel also suffers from batch-to-batch variability[106].

Suspension-based culture models

To improve relevance to clinical data, a suspension-based culture system was developed more recently by establishing cultures of freshly isolated patient tumor cells in serum-free media supplemented with EGF and basic FGF-2[107]. Cells are then allowed to clonally divide in suspension to yield "gliomaspheres"[108–110]. Unlike serum-based methods, gliomaspheres better preserve the genotypic, phenotypic and *in vivo* characteristics of the individual GBM tumor from which they were derived[108–110]. Another advantage of this method is that gliomaspheres deposit their own ECM, creating a semi 3D microenvironment in each sphere. Gliomasphere cultures have enabled researchers to study the GSCs, which are preferentially enriched in these cultures, in more detail. This method has provided valuable information about clinical drug treatments[98,109].

As mentioned previously, data from the TCGA has been used to classify GBM tumors into four major subtypes: proneural, classical, neural and mesenchymal[111]. Gliomasphere cultures, established from patients' tumors have facilitated understanding the genotypic and phenotypic differences between these subtypes. For instance, comparing a mesenchymal GBM-derived gliomasphere culture with other subtypes may elucidate the mechanisms of proneural-mesenchymal transition (PMT) in GBM[112]. This information might be useful since in variety of other cancers, as upregulation of

mesenchymal genes is often correlated to more aggressive phenotype[113]. Interestingly, each GBM tumor subtype expresses distinct profiles of ECM receptors. Therefore, it is not farfetched to hypothesize that each subtype contains a unique ECM. Finally, it is worth mentioning that although these subtypes capture the primary GBM tumor spectrum, their characteristics most likely exist in a continuum in each patient[113].

Despite their advantages over adherent cultures, gliomasphere cultures have their own disadvantages. First, gliomasphere cultures are highly enriched in GSCs, which are relatively low in abundance in primary GBM tumors[114]. Second, formation of gliomaspheres is strictly an *in vitro* phenomenon whereas *in vivo*, GSCs reside in their niche such as the perivasculature niche[98]. To improve on gliomasphere cultures, Hubert, *et al.,* 2016, successfully generated 3D, GBM organoids with millimeter-range sizes (gliomaspheres are typically 100–200 μm)[115]. In this organoid model, a hypoxic gradient was present throughout, inducing phenotypical difference between cells residing at the core versus cells residing at the periphery. Furthermore, the organoids also contained GSCs, resistant to radiotherapy, at the core, indicating a better resemblance to a human GBM tumor. Finally, when xenografted in mice, tumors formed from these organoids better matched histologically to a clinical GBM tumor. Although this organoid model has the advantage over gliomasphere culture of better mimicking clinical tumors, it requires months of culture, whereas gliomasphere cultures only need weeks to obtain[115].

***In vivo* rodent models**

In vitro models, although they enable researchers to perform more experiments in a shorter time frame, cannot account for many microenvironmental features of GBM such as stromal and immune cell interactions. Considering this, *in vivo models* have provided

unique useful results. Currently, mice are the most common animals used for *in vivo* studies of GBM. These models include orthotropic xenografts of patient-derived gliomaspheres, syngeneic transplants of mouse GBM cells and genetically engineered mice that spontaneously generate GBM tumors. In the past decade, orthotropic xenografting of patient-derived GBM cells into immunodeficient mice have become the gold standard specially for evaluation of drug efficiency[108,109]. These intracranial xenografts generate tumors that can recapitulate invasive phenotypes and histopathological features of patients[105,109]. Despite these advantages, xenografts established from gliomaspheres, which is the most common method, suffers same disadvantages of gliomasphere cultures (e.g., loss of heterogeneity and phenotypical drift). Another drawback of xenografts is the need for immunodeficient mice to establish human tumors. The use of nude or NOD-scid mice means that important immunological events, such as interactions of GBM and T- cells, are not present[116].

Similar to other cancers, GBM tumors originating from different patients bear different genomic features. Hence, it is essential to develop methods that consider patient-to-patient variability. Recently, researchers have developed 'AVATAR' models in which patient GBM cells are transplanted in a NOD-scid mice freshly (within 12 hours of isolation)[116,117]. Unlike previous methods, transplanted cells in AVATAR models are never cultured *ex vivo*. AVATAR models preserve genomic features, subtype profile and histopathological features of the parental patient tumor[117]. AVATAR models hold promise for finding patient-specific biomarkers and develop patient-specific treatment. However, AVATAR models are not able to consider immunological factors due to the use of

immunodeficient mice. In addition, a general caveat for all mice models is that the human brain microenvironment is considerably different from the murine brain.

Immunocompetent models of GBM are developed based on syngeneic transplantation of mouse GBM cells into species-matched mice[104,118]. Most commonly, C57/B16-background mice are used. For example, a model where cells from a GL261 mouse GBM cell line are transplanted in C57/B16 mice[118,119]. Although this method is able to consider immuno-interactions, long experimental timeline as well as expense and animal use are some of this method's disadvantages.

A disadvantage of both xenograft and syngeneic models is that tumor initiation and development cannot be studied. Therefore, researchers have developed a model based on genetically engineered mice, where the role of specific genes and mutations can be studied during the tumor development[119,120]. In addition, targeted gene manipulations (such as mutation, silencing or overexpressing) can be done temporally[119–121]. Another advantage of GEM models is that tumors are initiated in immunocompetent mice, hence immunological interactions can be studied. In addition to differences between mice and humans, the main drawback of GEM models is lack of control on tumor initiation timing which hurts experimental reproducibility[118,120,121].

Bioengineered models to mimic the GBM microenvironment

While rodent models enable researchers to study GBM in the native brain microenvironment, the cost, lengthy experiments and lack of reproducibility present noteworthy disadvantages. While *in vitro* models can address these challenges, lack of relevancy to clinical data due to absence of microenvironment, makes these models less desirable. To address these challenges, researchers have developed numerous

bioengineered models where physical and chemical features of GBM microenvironment can be addressed accurately. Most of these models are based on hydrogel biomaterials. Hydrogels are sponge like materials that exhibit tissue-like water content and mechanical properties which can be engineered to support cell culture in 3D[122]. The advantage of hydrogels is that their tunability on mechanical and chemical properties. This tunability enables researchers to investigate the role of matrix individual mechanical and chemical properties in GBM progression. In the following sections, I discuss the evolution of engineered biomaterials with their advantage and disadvantages.

2D bioengineered models

To mimic microenvironmental features of tumors, researchers have cultured GBM cells on modified surfaces that represent the GBM ECM both mechanically and chemically. Most early studies used polyacrylamide hydrogels, as they can be readily modified to present various mechanical properties, topographical features and bioactive molecules[66,68,69,123,124].

Whether due to ECM stiffening, or increase in interstitial pressure or both, it is generally believed that cells residing in GBM microenvironment experience higher mechanical forces[64,66,73,74]. To explore the role of these mechanical cues, researchers have cultured GBM cells on different materials such as silicon rubber[125], polyacrylamide[123,124] and HA[62,70], with varying mechanical properties. Most studies reported increaser GBM migration, actin stress fiber formation and focal adhesions when cultured on more rigid surfaces. While the majority of these studies were performed using immortalized, glioma cell lines (e.g. U87MG and U373MG), one study reported that migration phenotype on 2D was unique the patient from which the tumor cells were

derived; while some of the patients' cells migrated faster on rigid surfaces, some were unaffected[126].

As discussed previously in this chapter, an increase in substrate stiffness activates migratory signaling pathways also influenced by integrins and EGFR[66]. On 2D, close localization of focal adhesions and EGFR provided more evidence toward coordinated mechanical response between EGFR and integrins[127]. CD44 also has been shown to act as a mechanosensitive receptor where on a stiffer HA substrate, engagement of CD44 with HA resulted in faster migration[62]. Culturing GBM cells in a confined microenvironment or on a substrate with topographical features also caused similar response to cultures on stiff substrates. Cells in confined microchannels[69] or on a surface with aligned nano-fibers[128,129] exhibited cell polarity and faster migration.

2D engineered surfaces have enabled researchers to conjugate bioactive molecules in a more controlled manner compare to simple absorption, as in traditional ECM-coated culture substrates[70,124]. Moreover, biomaterials can be modified to present combinations of ECM-peptides or whole proteins to better mimic the brain microenvironment. For example, HA-based hydrogels, modified with adhesion peptides are used to investigate interactive role of CD44 and integrins in GBM migration[62,66,70,130]. Furthermore, on a 2D surface, incorporation of HA increased migration speed of U87MG and U373MG cells[130].

Three-dimensional (3D) models

2D models, although they have provided researchers with valuable insight into GBM, do not necessarily mimic the physiological conditions. For instance, punctate focal adhesions that are usually observed in 2D substrates[62,66,123] are not observed in 3D

scaffolds or in a patient tissue[131,132]. Diffusion of nutrients, oxygen and metabolic waste is another feature that is better mimicked in a 3D scaffold compared to a 2D substrate. In the GBM microenvironment, cells experience hypoxic conditions which is shown to cause more tumor malignancy[133]. In addition to diffusion, 3D porous structure directly affects ECM degradation and GBM cells invasion[134,135]. Overall, 3D culture systems will be key to preserving crucial features of GBM tumors in an *in vitro* setting.

GBM cell-ECM interactions are highly complex and heterogenous. Thus, A relevant 3D system, in which ECM properties can be tuned orthogonally can help researchers to disentangle these complex interactions and study them individually. One of the most common 3D systems is hydrogels. Hydrogels are more similar to native brain tissue in water content and can be designed to mimic the mechanical and chemical landscape of the brain more closely than any other system. Hydrogels can be formed using gentle aqueous chemistry which enables cell encapsulation without any harm to the cells. In addition, hydrogels are usually transparent which makes them an ideal model for cell migration studies through various microscopy techniques[136].

Hydrogels are formed either by covalent or physical cross linking of hydrophilic polymer chains into an insoluble network. Covalent crosslinking requires functional groups that can readily react when in close proximity. Condensation, Michael-type and Diels-Alder reactions are some of the most common methods to fabricate hydrogels. Commonly, a Michael-type reaction is used to form crosslinks from thioester bonds formed between a thiol (SH) and an acrylate, maleimide or vinylsulfone moeity[136,137]. Another method for forming covalent bonds is using photochemical methods. Photochemical methods have the advantage of precise spatial and temporal control due

to the fact that crosslinking does not occur until light-exposure happens. Traditionally, photo-crosslinked hydrogels were fabricated through chain-growth polymerization of acrylates[38,39]. More recently, step-growth thiol-ene (e.g. between thiols and norbornenes) photo-reactions have gained more attention[138,139] as the reaction results in a more defined hydrogel network with fewer defects when to chain-growth reactions[140].

For a photochemical reaction to occur, a photoinitiator is necessary. Upon light exposure, the photoinitiator breaks down into radical species which, in turn, initiate crosslinking of polymer chains. Traditionally, the ultraviolet (UV)-activated initiator, Irgacure© 2959 (1-[4 (2-hydroxyethoxy)-phenyl]-2-hydroxy-2-methyl-1-propane-1-one) has been used due to its fairly high water solubility and biocompatibility[141]. More recently, phenyl-2,4,6-trimethylbenzoylphosphinate (LAP) has gained popularity as the photoinitiator due its higher UV absorption, improved water solubility and excellent cytocompatibility (compared to Irgacure© 2959)[142].

Most commonly, non-covalently crosslinked hydrogels are made through temperature or pH-induced formation of hydrogels. Most notable are thermally crosslinked hydrogels, such as those based on collagen I or laminin I which at physiological temperatures[71,126,135,137,143]. Alginate-based hydrogels are also formed from non-covalent crosslinks formed in the presence of a divalent ion like calcium (Ca^{2+})[67,144].

Role of mechanical properties in 3D

The mechanical properties of the ECM surrounding GBM cells affect their behavior. Thus, it is of paramount importance to control the mechanical properties of a culture model. In general, one can increase mechanical properties of a 3D system by increasing the crosslink density or the concentration of the backbone polymer (**Figure 1.**

3). In Michael-type reactions, changing molar ratio of the donor (e.g., thiol) to acceptor (e.g., maleimide) can be used to change crosslink density. In photochemical methods, increasing the concentration of reactant groups (e.g., thiol and norbornene), increasing light intensity or exposure duration, or increasing the amount of the photoinitiator can yield stiffer hydrogels. Similarly, in non-covalent hydrogels, increasing the concentration of the backbone polymer (e.g., collagen I) or adding more Ca^{2+} (in alginate systems) will increase the stiffness of the resulting hydrogels.

In contrast to 2D, GBM cells (U87MG, U87R, U118 etc.) encapsulated in hydrogels showed more migratory phenotypes in softer hydrogels[23,145,146]. However, there are conflicting reports. For example, some studies reported an increase in MMP-9 secretion in stiff HA hydrogels,[38,39] whereas other reported the opposite[147]. These contradictory data might be due to an inability to decouple effects of mechanical properties from ECM. In hydrogels formed from bioactive backbones (e.g. HA or collagen), increasing the stiffness via increasing the backbone polymer means more bioactive molecules available with which cells can interact. Alternatively, mechanical properties can be tuned by changing crosslink density. Regardless, both methods can affect the hydrogel pore size which potentially can alter cell migration as well as diffusion properties of the hydrogel.

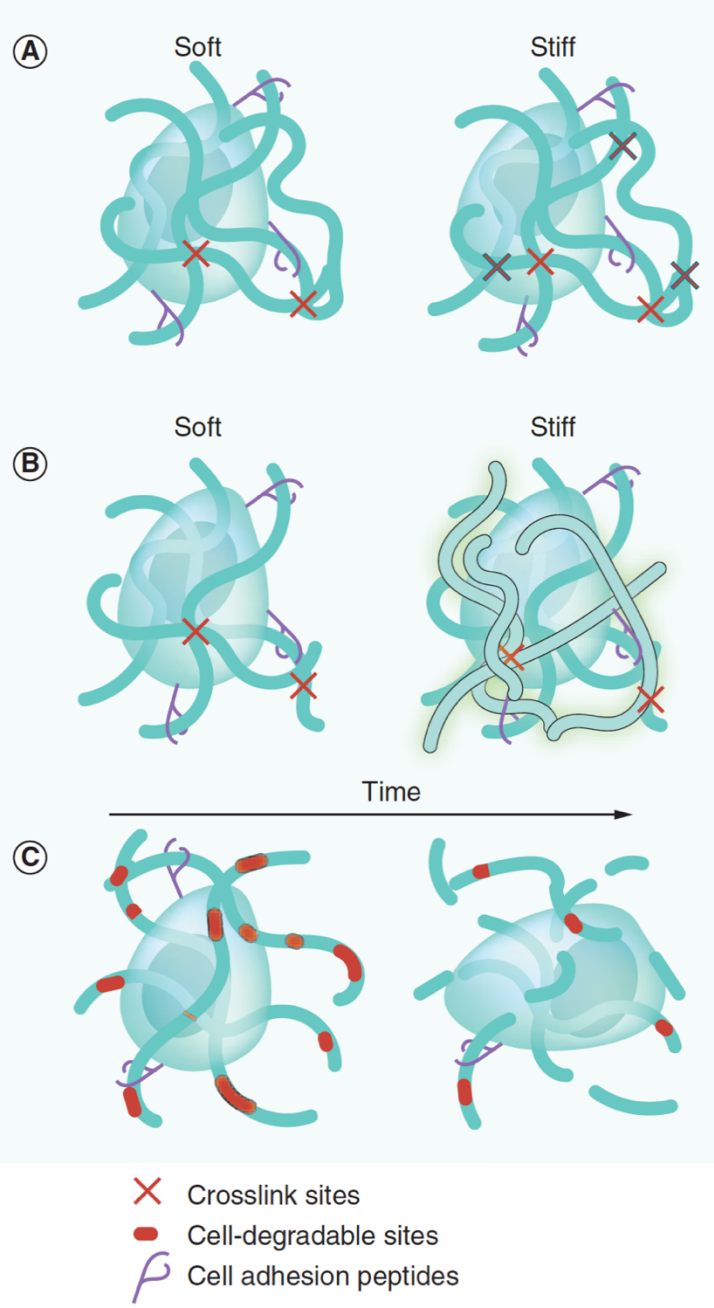

Figure 1. 3: Controlling hydrogel mechanical and chemical properties in 3D: To change mechanical properties of a hydrogel, one can A) change crosslink destiny or B) concentration of the backbone polymer. C) incorporation of degradable sites (e.g., MMP-degradable linkers) can help cell migration via cell-induced degradation of these linkers. (Figure adopted from Xiao et al., 2017)

Biochemical composition of 3D scaffolds

Similar to 2D models, biochemical features of a 3D model substantially affect GBM cells encapsulated within. To mimic the brain microenvironment, researchers have fabricated hydrogels using various ECM-derived biopolymers such as HA[38,39,124,138,139,143], chitosan[135,148], CS[137] and collagen/gelatin[39,128,135,143,149]. As brain ECM contains high amounts of GAGs and few fibrous proteins (e.g., collagen I)[150], HA has been extensively used to fabricate 3D hydrogels for GBM studies. To use these GAGs as hydrogel backbones, they must be chemically modified with functional chemical handles for crosslinking, like thiols and acrylates. Increasing amounts of HA or CS induce GBM cells to be more migratory[134,151], less proliferative[39], and high expressors of genes associated with GBM progression. Example of genes associated with GBM progression include HA synthases[143], hyaluronidases[143], MMP-9[38,39], MMP-2[39], VEGF and HIF1-α[38,39].

In addition, patient-derived GBM cells cultured in 3D hydrogels (such as HA) better mimic chemo and radio resistance observed in vivo than when cultured as gliomaspheres[152]. A HA is not cell adhesive, full proteins like acrylate-modified gelatin[38,39], or collagen I[135,143] are added to the hydrogel network to provide cell adhesion sites. Besides whole proteins, ECM-derived, cell adhesion peptides have been used extensively. The most common peptide used in 3D hydrogels is integrin-binding RGD[62,138,147]. One way to incorporate peptides is to add a functional group (e.g. thiols through a cysteine amino acid) that can react with hydrogel functional groups[152–154]. In addition, it is easier to control peptide functionality.

Modeling GBM invasion in 3D

For cells to migrate, they must either squeeze through open pores in the ECM or actively degrade the ECM. Unlike in 2D, 3D systems can model these aspects of GBM progression. However, in most of the studies, effects of stiffness, polymer content and porosity cannot be decoupled. For example, to increase stiffness of a hydrogel, usually concentration of the backbone polymer or crosslink density is increased[155]. Both of these methods decrease the pore size. Hydrogels formed from biodegradable polymers, can facilitate cell migration through adhesion as well as degradation. In this case, increasing the concentration of backbone polymer increases both adhesion and degradation sites[135]. Collagen-I has been used extensively to study GBM migration. Collagen-I fibers provide a physical structure along which GBM cells tend to migrate[156]. In addition, GBM-secreted MMPs can degrade collagen-I, facilitating GBM migration. For example, Jiglaire et al., 2014, showed that GBM cell (U87MG) migration in a 3D collagen hydrogel depended on MMP-1 secretion, while same cell line's migration on a 2D collagen mat was independent of MMP secretion. Despite wide-spread use of collagen-I in GBM studies (since collagen-1 ins upregulated in the tumor), it is unclear how these results are comparable to clinical data as brain ECM contains negligible amount of fibrous proteins[10,136,157].

A major physiological hallmark of GBM migration is overexpression of MMPs. To create a more controlled degradation model of GBM invasion in 3D, researchers have incorporated MMP-degradable sites in the hydrogel network (**Figure 1. 3-C**). This is usually done by synthesizing a bi-functional MMP-degradable peptide where the degradable sequence is positioned between two functional groups (e.g thiols)[135,144]. Alternatively, HA-containing hydrogels can support degradation through hyaluronidase,

which degrades HA and is also overexpressed by GBM cells[134,158]. Moreover, some studies suggest that the presence of HA can upregulate expression of MMPs in 3D hydrogels[38,39,143].

Only a few recent studies have tried to decouple effects of stiffness, porosity and biochemical presence in 3D. Kumar et al., 2010 [71], fabricated interpenetrating networks from collagen-I and agarose in a way that hydrogel stiffness was increased by increasing the concentration of relatively cell-inert agarose. This study found that softer hydrogels promoted more GBM cell (U87MG, U373MG and U251MG) migration. Although they could decouple mechanics from biochemical factors, adding more agarose in stiffer gels could change hydrogel porosity. One possible method to decouple stiffness from porosity could be using PEG-based microribbons[159]. Alternative, one could use covalently adaptable networks where crosslinks can work as a 'gate' where cells can break crosslinks while passing and crosslinks can reform afterwards[160]. Finally, Griffin et al., 2015, fabricated hydrogels of microporous annealed particles (MAP) in which micro-hydrogels are covalently annealed together to from a macro-hydrogel. In this system, adjusting mechanical properties of particles does not alter the porosity of the hydrogel[161].However, the surface geometry and (i.e. small curved surface) is vastly different in MAP gels and could affect cell phenotype[162,163].

Modeling cell-cell interaction in 3D

In the physiological microenvironment, GBM cells dynamically interact with surrounding cells (e.g., ECs, astrocytes etc.) (Error! Reference source not found.). While s everal studies previously used conditioned media (media with non-cancerous cells secretion like ECs) to culture GBM cells in 2D systems, they cannot provide information

about the crosstalk between GBM tumor and other cell types residing the GBM microenvironment. Transwells[53,164] and Boyden chambers are among methods used to study paracrine signaling among cells; however, these methods cannot study the direct crosstalk between GBM cells and their neighboring non-tumor cells. GBM cells and their neighboring non-tumor cells reside in a 3D microenvironment and communicate directly or indirectly through this 3D microenvironment. Therefore, 3D models have been necessary to study these interactions.

To study the interaction of GBM cells with endothelial cells, Chen et al., 2009, seeded transformed ECs (HUVECs) on dextran beads. These beads later were encapsulated in a 3D fibrin hydrogel and GBM cells were cultured on top of the hydrogel. GBM secreted paracrine caused more angiogenesis in ECs[165]. This method could only study paracrine signaling. In an improved study, Yang et al., 2014, cocultured a GBM cell line (U251) with an immortalized astrocyte (TNC-1) with in 3D hydrogels. Their results suggest that the presence of astrocytes protected GBM cells from TMZ-induced apoptosis[166]. Recently-developed organ-on-chip devices like AngioChip® may provide a platform technology for more precise coculture systems[26]. For example, using this technology, astrocyte-endothelial cocultures showed BBB-like properties[167,168]. Methods like these can be used to investigate interactions of GBM cells with the perivascular niche.

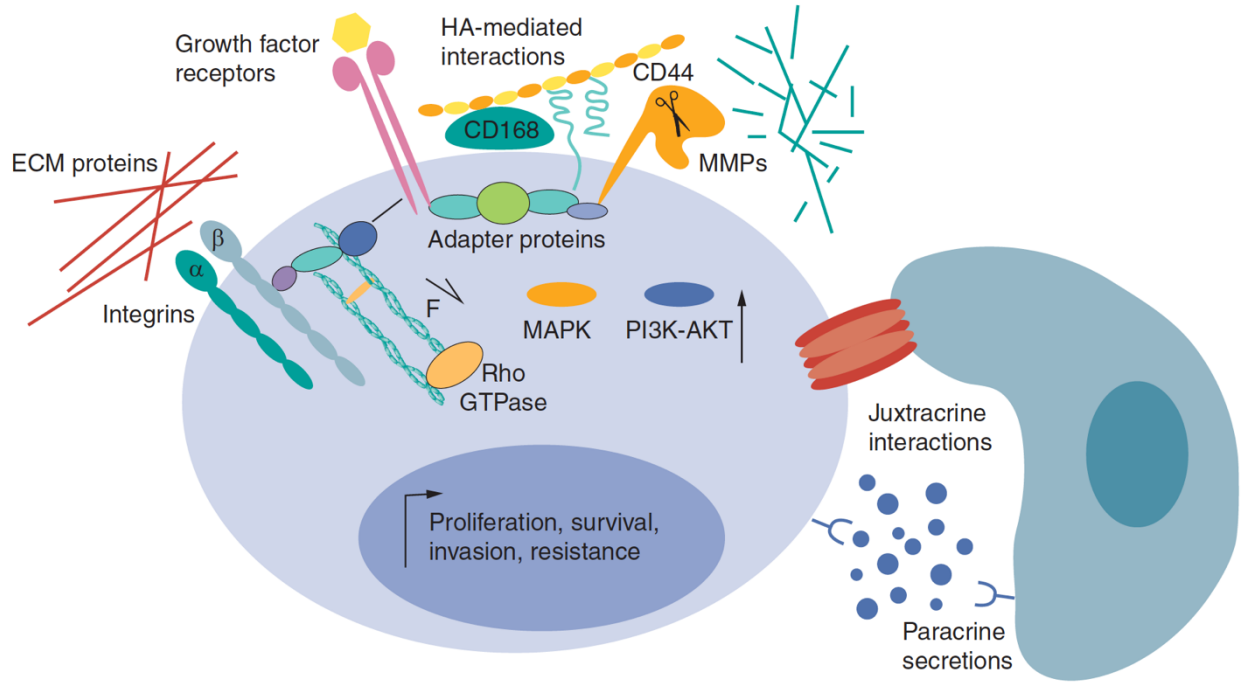

Figure 1. 4: Cell-ECM and Cell-Cell interactions at the level of a single cell. Cell-cell interactions happens directly through gap or cadherin-mediated adherens (juxtracrine interactions) or indirectly though secreted soluble factors by neighboring cells (paracrine signaling) (adopted from Xiao et al., 2017)

Chapter 2: Role of microvasculature in glioblastoma invasion

Introduction:

The glioblastoma (GBM) perivascular niche (PVN) is mostly characterized by a hyper-proliferative and hyper-permeable neovasculature that supports the tumor and, in particular, glioma stem cells (GSCs). GSCs actively seek out these vessels[169], migrate alongside them and maintain close association with vasculature's endothelial cells (ECs) and pericytes [28,98,170]. The GBM PVN is thought to be similar to the neural stem cell (NSC) PVN, which normally promotes NSC proliferation and survival[171,172]. Throughout the body, stem cells normally are maintained within similar protective niches[173]. New vasculature developed in and around GBM tumors contributes to formation of an hypoxia microenvironment[14], which, in turn, promotes addition tumor creating a forward feedback that maintains multipotent GSCs [174].

In addition to GSCs and ECs, the GBM tumor PVN includes microglia, astrocytes, and pericytes, forming a very complex microenvironmental landscape[175]. For example, infiltrating immune cells contribute to inflammatory angiogenesis and tumor cells proliferation through cytokine signaling[176,177]. Astrocytes, whose end-feet cover approximately 99% of vessel surfaces in the brain, are essential to blood brain barrier (BBB) function[178,179]. However, in rodent models xenografted GBM cells have been observed to disrupt these astrocytic end-feet while migrating alongside the vessels, degrading the basement membrane and possible increasing "leakiness" of tumor vasculature[28,170,180].

Interestingly, Calabrese et al., 2007, have demonstrated that ECs derived from patient GBM tumors (TECs) secrete factors that promote GSC self-renewal and

proliferation *in vitro* and tumor growth in xenografted models[98]. This example clearly shows the need for more profound comprehension of signaling pathways in which GBM tumor interacts with neighboring vessels around them.

Recently, the Kornblum lab (UCLA) has developed a list of angiocrines based on comparing the transcriptomes of human TECs derived obtained from GBM resection surgeries and non-cancerous ECs derived from human brain tissue obtained in the course of epileptic resection surgery (The interactome). The interactome provides us with a list of proteins that are differentially overexpressed in tumor derived ECs when compared with "healthy" brain ECs. In addition, the interaction highlights the candidate GBM receptors that interact with the proteins expressed from ECs. To investigate the role of interactome's protein list on GBM migration, we decided to use the HA hydrogel platform, designed in our lab, in combination with a curated list of targets from Kornblum lab. The HA hydrogel platform allowed us to culture patient-derived GBM gliomaspheres in a 3D microenvironment and track GBM cell migration in response to the addition of target proteins.

Materials and methods:

HA Thiolation

High molecular weight HA was thiolated according to established protocols[152]. In all cases, molar ratios are reported with respect to HA carboxyl groups. Briefly, sodium hyaluronate (M_W = 700 kDa, Life core) was dissolved in deionized water (DI-H_2O). Then, 1-ethyl-3-[3-dimethylaminopropyl]carbodiimide (EDC, Thermo Scientific Pierce) was dissolved in DI-H_2O and added to the solution at a 0.125 molar ratio. N-hydroxysuccinimide (NHS, Acros Organics) was then added to the HA solution at a 0.062

molar ratio. The solution beaker was stirred continuously at room temperature (RT) while pH was adjusted to 5.50 using 1 M HCl for 45 minutes. Then, cystamine dihydrochloride (Sigma-Aldrich) was added to the reaction at a molar ratio of 0.125 and pH was adjusted to 6.25 using 1 M NaOH. The reaction was continuously stirred at RT overnight. The next day, dithiothreitol (DTT, Sigma-Aldrich) was added (0.5 molar ratio), the solution pH adjusted to 8.50 using 1 M NaOH and the solution was stirred at RT for 2 hours. The reaction was quenched by adjusting the pH to 4.00. The solution was then dialyzed (MWCO 14 kDa, regenerated cellulose, ThermoFisher Scientific) against pH 4.00 DI-H_2O for 3 days while protected from light. Dialysis water was refreshed twice daily. Purified HA was passed through 0.22 μm filters (EMD Millipore), flash frozen using liquid nitrogen and lyophilized. The dried product was vacuum sealed and stored at -20°C. Thiolation percentage was measured using ^{1}H-NMR spectroscopy and an Ellman's assay for free thiols[152].

Hydrogel fabrication and characterization

Hydrogel precursor solution was prepared by dissolving HA-SH (0.5% w/v), 4-arm thiol terminated polyethylene glycol (PEG-SH) (Laysan Bio), 8-arm norbornene terminated polyethylene glycol (PEG-Norb) (Jenkem), 0.025% w/v lithium phenyl-2,4,6 trimethylbenzoylphosphinate (LAP, Sigma-Aldrich) and 0.25 mM thiolated peptides (*Table 2. 1*) (JenKem, USA) in 20 mM HEPES buffer (pH=7). The hydrogel precursor solution was cast into 4 mm diameter silicone rubber molds (Grace Biolabs) and irradiated with long-wave UV (365 nm, 4.2 mW/cm^2) (Blak-Ray^{TM} B-100A UV lamp, UVP^{TM}) for 15 seconds. Hydrogel storage moduli (G') were measured using a discovery hybrid rheometer-2 (DHR-2, TA Instruments) at 37 °C. Frequency sweeps were performed under

1% constant strain in the range of 0.1 to 1.0 Hz. Storage modulus of each sample was calculated as the average value of the linear region of the storage curve from the frequency sweep plot. For statistical analysis, 3 separate measurements were taken in which 5 samples from each condition were measured.

Table 2. 1: Peptides' sequence used in hydrogel fabrication.

Peptide	Sequence
RGD	GCGYGRGDSPG
IBSP	GCGYGGGGNGEPRGDNYRAY

Cell culture and encapsulation

Patient-derived GBM cell lines, HK217 (proneural), HK301 (proneural) and HK280 (mesenchymal) were collected with strict adherence to UCLA Institutional Review Board protocol 10-000655. Cell cultures routinely tested negative for mycoplasma contamination (Life Technologies, C7028). Cells (50,000/mL) were cultured in DMEM/F12 with 1xG21 (Gemini Bio), 1% noromycin (Invivogen), 50 ng/ml EGF (Peprotech), 20 ng/mL FGF-2 (Peprotech), and 25 mg/mL heparin (Sigma-Aldrich). Sizes of GBM spheroids were standardized by seeding approximately 600K cells per well into Aggrewell™ well plates (Stemcell Technologies) one day prior to encapsulation. The following day, spheroids were harvested from the wells, centrifuged briefly (200xG, 1 min.) and resuspended in the hydrogel precursor solution. Spheroid-laden hydrogels were formed as described in the above hydrogel fabrication section. Cell migration was observed periodically (Imaged at Day 1,3,6 and 9) by acquiring phase contrast images

on a Zeiss Axio.Z1 Observer microscope with a Hamamatsu Orca Flash 4.0 V2 Digital CMOS Camera and Zeiss ZEN 2 (Blue Edition) software. Cell migration was quantified using shape factor (circularity) and length of migration from sphere edge. To calculate circularity, perimeter of each sphere was marked in ImageJ software and circularity ($4\pi A/P^2$, A=area, P=perimeter) was calculated using ImageJ shape description. For migration distances, in ImageJ, 5 longest migration distances from the edge of a sphere were measured for 10 spheres. For statistical analysis, 3 separate experiments were done where migration was analyzed for 10 spheres per condition. At the end of an experimental period, hydrogels were fixed using 4% paraformaldehyde (PFA)[152] and stained with Hoescht (nuclei) and Cell Mask™ (cell membrane). These gels then were imaged using a Leica SP5 confocal microscope.

To block GBM integrin αV, GBM spheroids were incubated with 10 μg/ml Integrin alpha V antibody (abcam, ab16821) a day prior to encapsulation. In addition, after the encapsulation, hydrogels were incubated in GBM media containing 10 μg/ml of same antibody over the course of the experiment.

GBM cell /EC co-encapsulation

GBM tumor-derived endothelial cells (TECs) were isolated from freshly patients' tumor resection using magnetic activated cell sorting (MACS) against CD31. Human brain microvascular endothelial cells (HBMVECs) were purchased from Sciencell, thawed and expanded for 2 passages before cryo-preservation. Endothelial cells were cultured using standard EC media (Sciencell, Cat#1001). Integrin binding sialo protein (IBSP)knock-down in TECs were achieved using GIPZ IBSP shRNA Viral Particle Starter Kit (Horizon Discovery). These cells were passaged once before encapsulation. All endothelial cells

were used in early passages (<P5). In order to distinguish GBM cells from ECs, GBM cells were infected with a lentiviral vector encoding for blue fluorescent protein (BFP). These GBM cells were passaged once before being used in the experiment. We used the Aggrewell™ (above) to obtain spheroids of relatively uniform sizes. Gliomaspheres of 100-150 μm were used.

Co-cultures of ECs and GBM cells were established in two steps. First, GBM spheroids were resuspended in HA-cysteine hydrogel precursor, casted in 4 mm diameter, silicone rubber molds and hydrogels were crosslinked as described above. In the second step, GBM spheroid-laden hydrogels were transferred into 8 mm diameter molds and a solution of HA-RGD (500μM RGD) containing ECs (10^7 cell/ml) was casted around the initial hydrogel and formed under UV. Final hydrogels were transferred to EC medium and imaged periodically (timepoints similar to previous part) as described above. At the end of experiments (Day 9), hydrogels were fixed using 4% PFA and imaged using a Leica SP5 confocal microscope.

Western blot

EC's protein content was extracted using established method[181]. From each EC type, 300k cells were isolated, centrifuged at 250XG for 5 minutes to get the cell pellet. Media was removed and cells were lysed using RIPA buffer on ice for 15 minutes. Then the solution was centrifuged at 17,000 XG for 15 minutes at 4 °C. Supernatant was separated and kept at -80 °C.

To prepare western blot samples, protein solutions were mixed with Laemmli buffer (2X, contain 5 %v/v β-mercaptoethanol, bio-rad) in 1:1 ratio and heated at 97 °C for 5 minutes. Samples were loaded in a Nupage™ 4-12% bis-Tris protein gel (Thermo

Scientific). Gels were run in MOPS-SDS buffer (20X, thermo fisher) at 60V for 15 minutes the 165V for 1 hour. Later proteins were transferred onto a PVDF membrane (Thermo Scientific Pierce™) in tris/glycine(10X, Bio-Rad) buffer containing 20%v/v methanol.

IBSP detection was done using a human IBSP polycolonal antibody (Rabbit, Thermo Fisher Scientific) as the primary antibody and then a goat anti-rabbit IgG (HRP linked, cell signaling). For the housekeeping gene, GAPDH was stained using a GAPDH loading control antibody (mouse, Fisher Scientific) and then a goat anti-mouse IgG secondary antibody (HRP, Novus biological). Finally, protein bands were developed using the Clarity™ western ECL substrate (Bio-Rad). Protein bands were visualized using MYECL gel imager (Thermo Scientific).

Statistical analysis

Normality of each data set was analyzed using D'Agostino & Pearson omnibus normality test. For normally distributed population, one-way ANOVA and then t-test were used to determine the statistical differences among the groups. For non-normal distributions, the Mann-Whitney non-parametric test was used.

Results:

We chose to use high molecular weight hyaluronic acid (MW=750 kDa) as the hydrogels' main component. To do so, we first introduced thiol functional groups to 5-6% of carboxylates on N-glucuronic acid of HA disaccharide building blocks using EDC/NHS chemistry. The extent of modification was quantified using ^{1}HNMR (**Figure 2. 1**).

We utilized thiol-ene photo-click chemistry to fabricate hydrogels (**Figure 2. 2**). The advantage of photo-click chemistry over other methods is the on-demand gel formation and higher control over the hydrogel structure since gelation only happens when gel pre-

cursor solution is illuminated by a light source. Hydrogels mechanical properties was modulated by tuning the crosslinking functional group concentration (**Figure 2. 2)**. For cell studies, we chose to work with the 0.93 mM thiol content hydrogels as their mechanical properties best approximate healthy brain tissue[182].

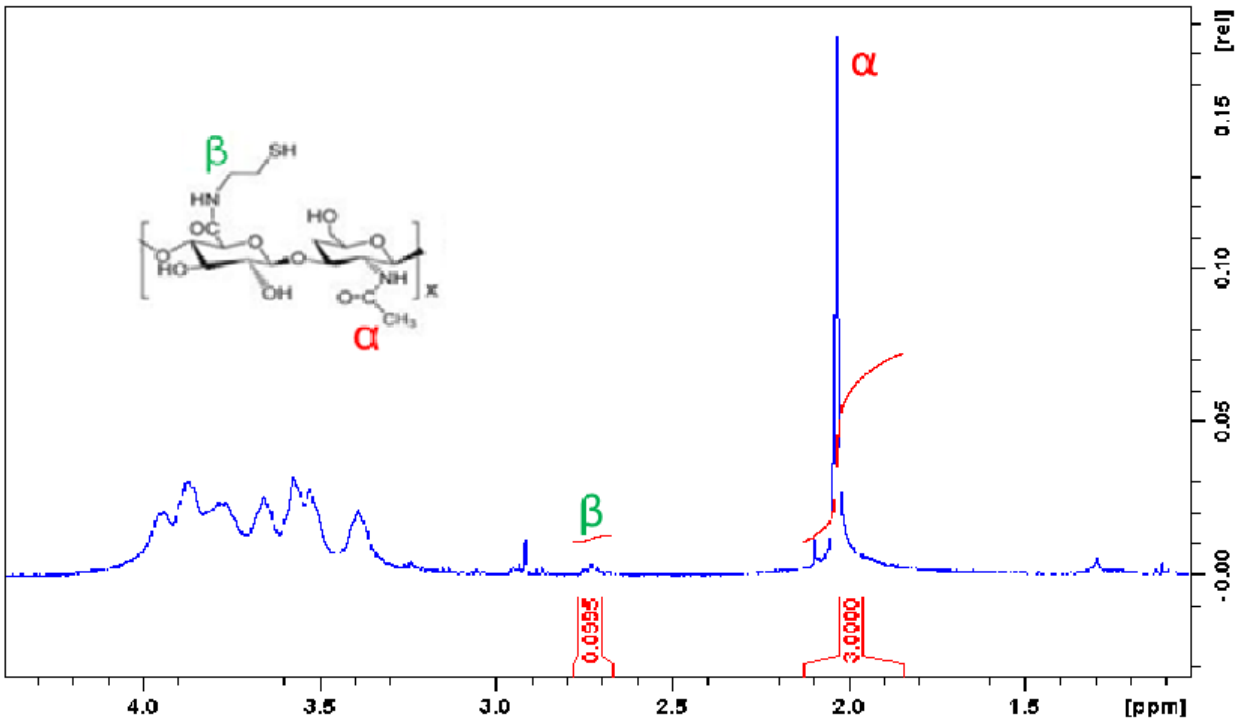

Figure 2.1: High molecular weight HA was modified to introduce thiol functionality. Representative ^{1}HNMR shows successful introduction of thiols to approximately 5% of disaccharide units.

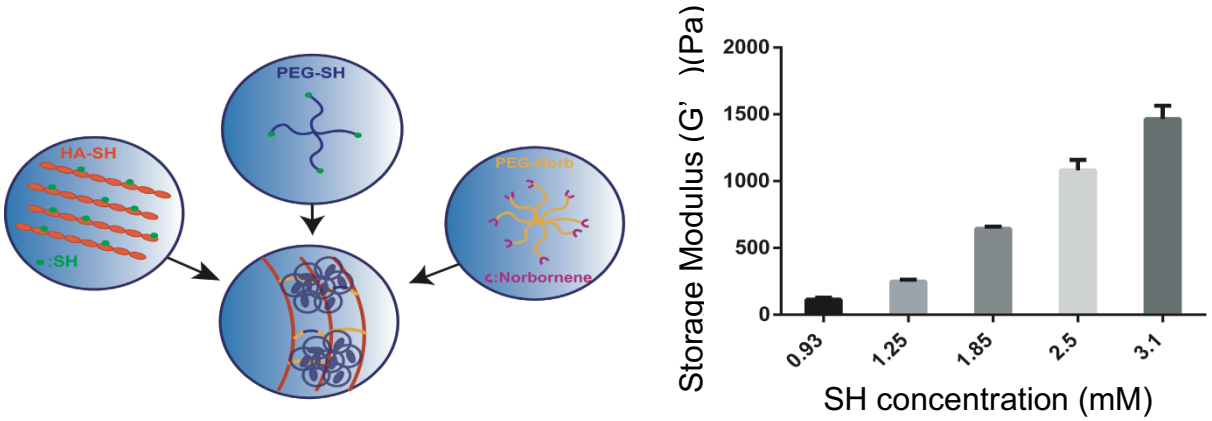

Figure 2.2: (left) HA hydrogels fabricated using thiol-ene photo-click chemistry. Thiolated HA is used as the main component while PEG-norb is the crosslinker and PEG-SH is added for mechanical tunability. Hydrogel forms when pre-cursor solution is illuminated with UV light and generate free radicals from LAP. (right) Mechanical properties of hydrogels were modifies by altering the concentration of PEG-SH and PEG-Norb while keeping HA concentration at 0.5 w%.

Based on the GSC:EC GBM/EC interactome generated by the Kornblum lab, we chose to investigate the potential role of some of the highest differentially expressed proteins (including lumican, Wnt5A, inhibin-beta A and IBSP) in GBM invasion using our *in vitro* 3D culture model (**Figure 2. 3)**. GBM gliomaspheres were encapsulated in HA hydrogels with 250 μ M RGD peptide as the base condition. We added the target proteins at 10 μg/ml to the incubation media. Only addition of IBSP induced extensive cell migration in GBM spheroids.

To confirm these results, we focused on IBSP and studied GBM migration in three cell lines from two main GBM subgroups (proneural and mesenchymal). For this experiment, we used and IBSP peptide to compare it directly to a generic RGD peptide. Interestingly, in all three cell lines, GSCs in IBSP hydrogels exhibited stronger migratory phenotypes. Finally, as the interactome suggested that GBM cells have high expression of integrin alpha V (INTaV), we used an INTaV antibody to compete with off IBSP-derived peptide bound to INTaV on GBM cells. Results for all three GBM lines clearly showed that binding disruption completely abrogated GSC migration (**Figure 2. 4).**

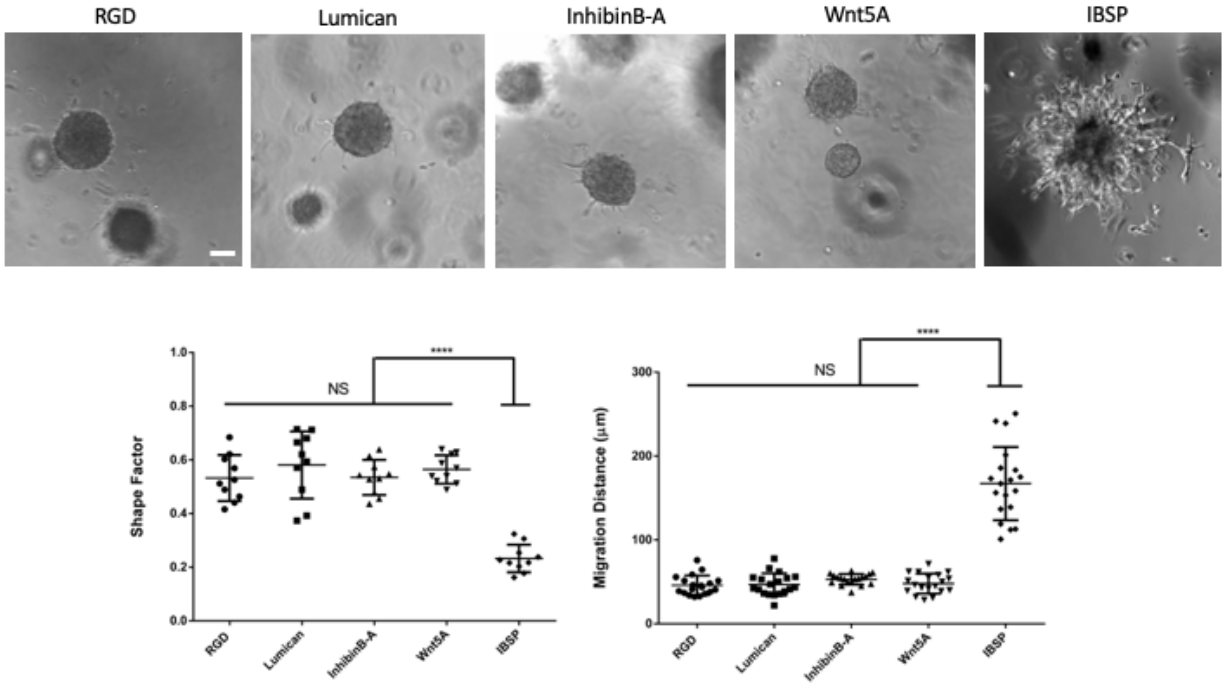

Figure 2.3: Migration of GBM cells were studied in HA hydrogels while the interactome proteins were added to the hydrogel. Compared to a generic RGD sequence, only IBSP induced significant migratory phenotypes. (Scale bar = 100 μm) Shape factor and average migration distance clearly shows the effect of IBSP in GBM migration. statistical analysis was done using Mann-Whitney non-parametric test (****: P<0.0001).

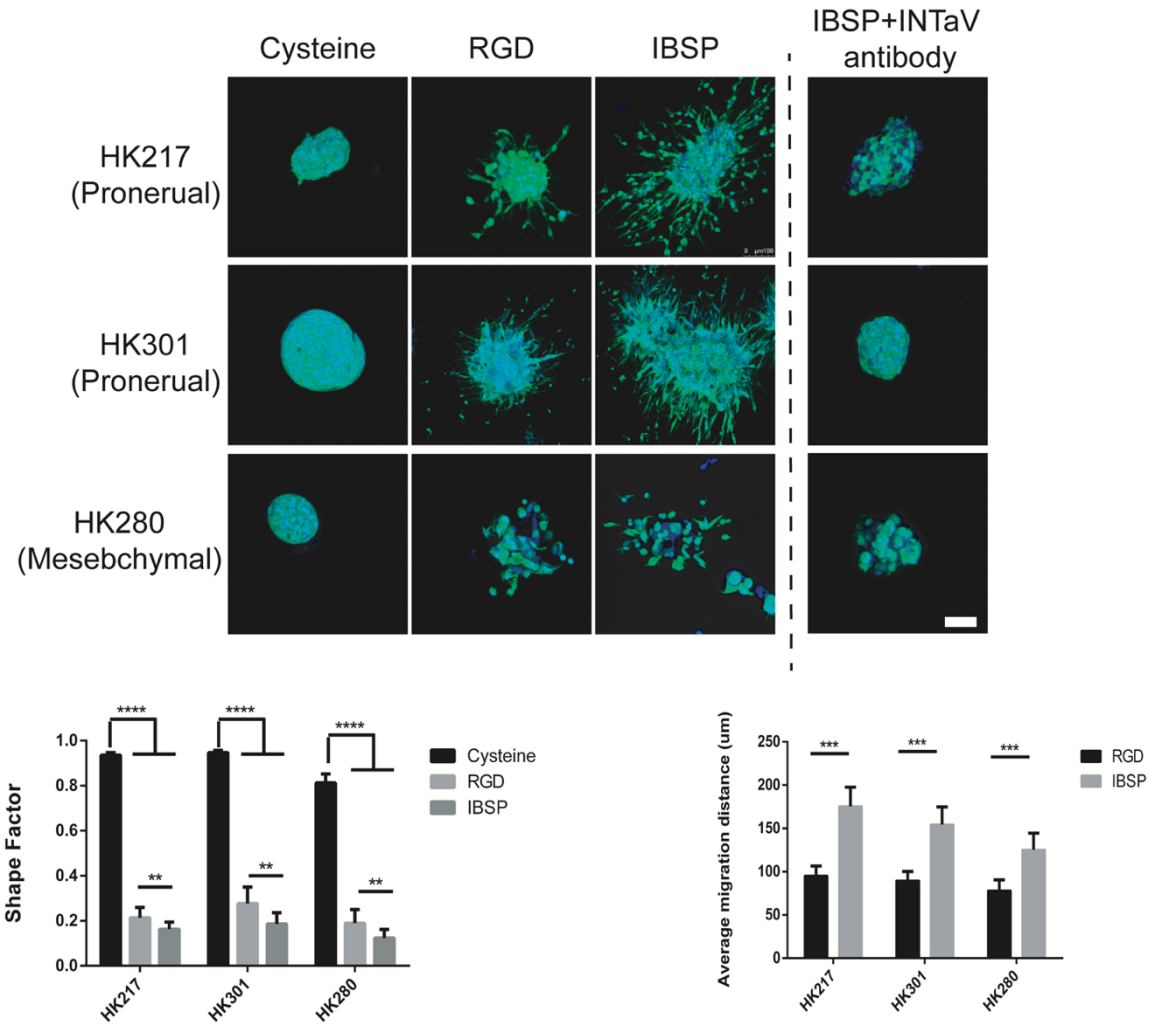

Figure 2.4: Comparison of GBM migration in HA-IBSP hydrogels against HA-RGD gels. IBSP induced significantly more migratory behavior in GBM gliomaspheres across all three cell lines. In addition, interfering the interaction of GBM cells with IBSP through blocking ITNaV stopped cell migration. (Blue: Hoechst 33342 stain of nuclei, green: cell mask$^{TM)}$. (Scale bar= 100μm). Cell migration from gliomaspheres were characterized at the final day using shape factor and average migration distance. Both metrics exhibit higher migratory phenotypes in HA-IBSP hydrogels. (****: p<0.0001, ***: p<0.001)

Together, these data we show that higher IBSP expression in TECs, compared to normal ECs, could potentially cause more migratory activity in GBM cells. To validate these results, we developed an interfacing hydrogel system in which GBM spheroids were encapsulated in the inner HA-cysteine hydrogel, while TECs were encapsulated in the outer HA-RGD hydrogel (**Figure 2. 5).**

GBM spheroids co-encapsulated with TECs showed extensive migration. Here, brain-mimetic culture scaffolds allowed us to evaluate the GBM/TEC crosstalk in a 3D microenvironment which is superior to previous methods. To investigate the role of IBSP in GBM migration, we knocked down IBSP expression in TECs using shRNA encoded by a lentiviral vector. IBSP knockdown was confirmed using western blot (**Figure 2. 6)**. We also verified IBSP expression in wild-type TECs with different passages that were used in the experiments. IBSP-knock down TECs were co-encapsulated with GBM spheroids using same interfacing hydrogel method. Knocking down IBSP in TECs significantly reduced GBM migration. As negative controls, we knocked down GAPDH in TECs as well as an IBSP scramble knock down. Neither of these conditions affected GBM migration (**Figure 2. 7).**

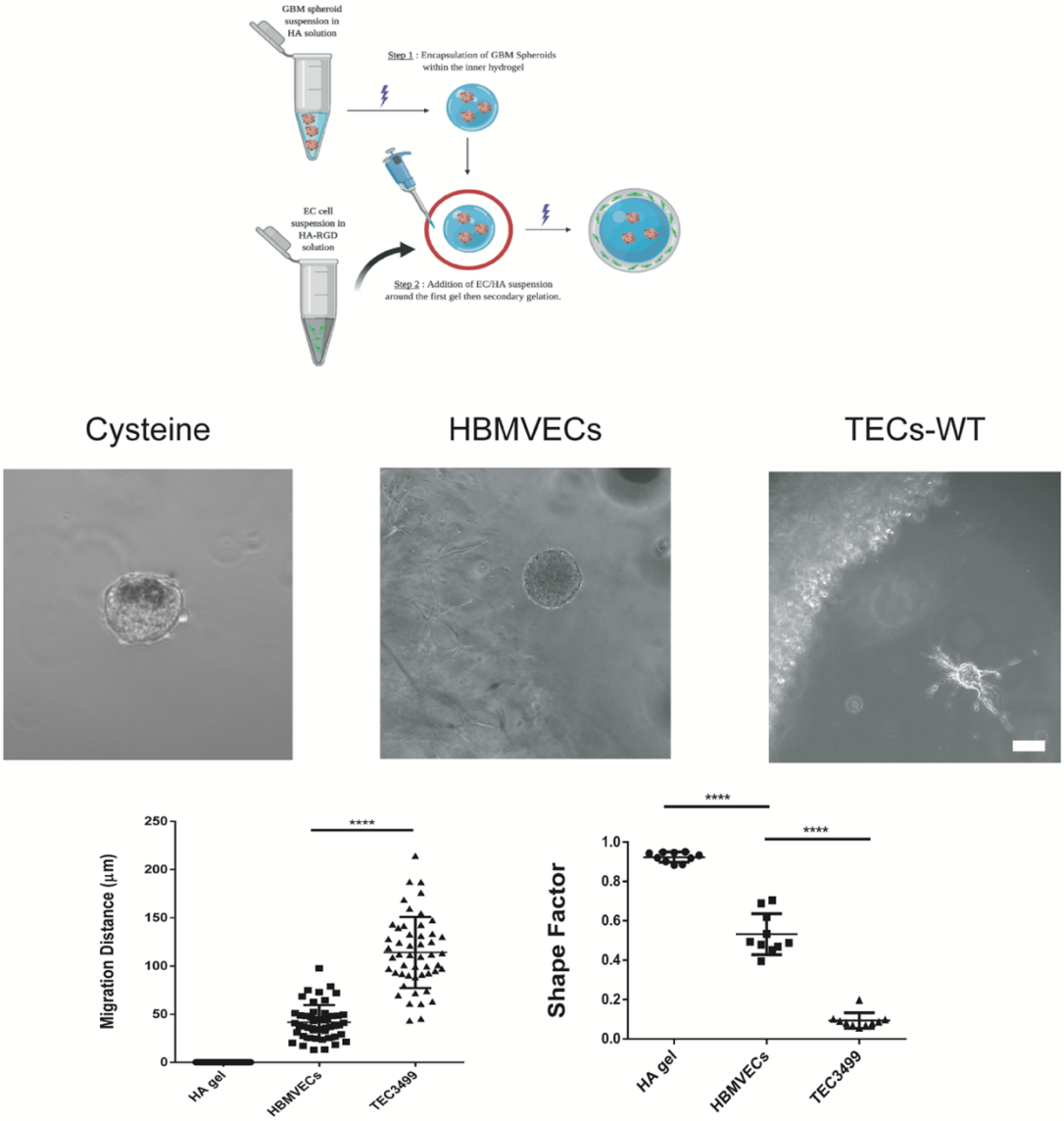

Figure 2.5: (Top) schematic representation of an interfacing hydrogel fabrication process. First solution of HA-cys containing GBM gliomaspheres is injected into inner mold and exposed to UV light to form the hydrogel. The inner hydrogel is moved to a bigger mold where solution of HA-RGD containing ECs is injected around it and exposed to UV to form the outer layer. (Middle) GBM gliomaspheres do not show any migration in cysteine condition (negative control) and minimal migration when co-encapsulated with human brain microvasculature endothelial cells (HBMVECs), whereas co-encapsulation with TECs resulted in an extensive GBM migration (scale bar= 100 µm). (Bottom) Shape factor and migration distance analysis clearly show the effect of TECs on GBM migration. (****: $p<0.0001$)

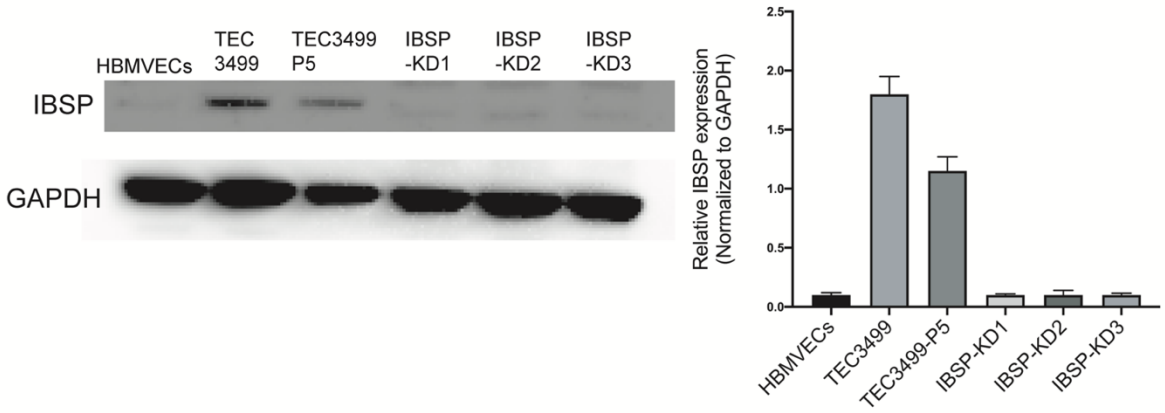

Figure 2.6: In order to verify the role of IBSP in GBM migration, IBSP expression in TECs were knocked down using viral vectors. Western blot analysis confirmed expression of IBSP in wild type TECs at passage 1 and passage 5. Moreover, viral infection successfully knocked down IBSP expression. As a control we compared TECs with HBMVECs which do not express IBSP.

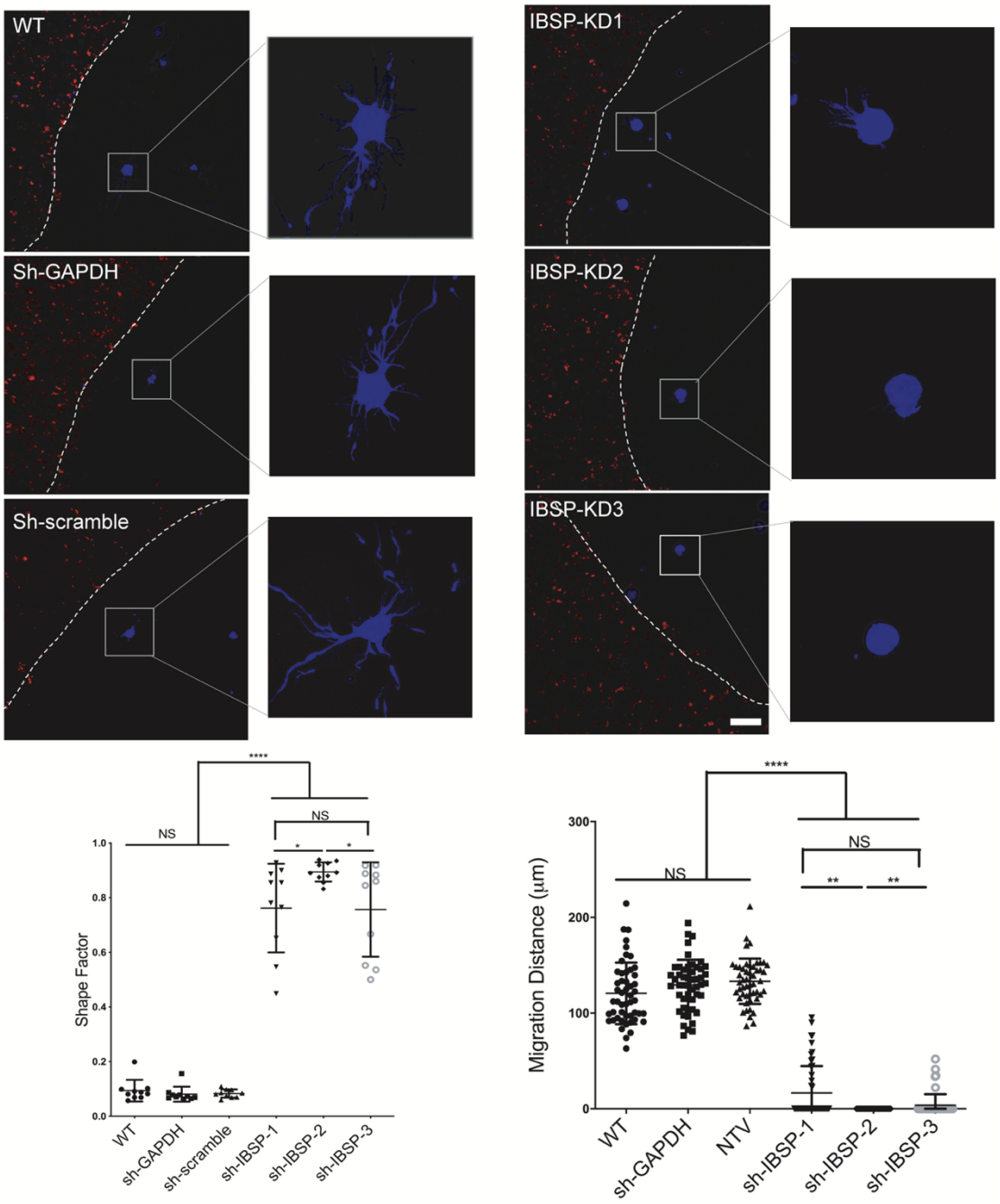

Figure 2.7: GBM/ECs co-encapsulation in interfacing hydrogels. GBM cells were transfected with a BFP plasmid for tracking purposes. Wild-type ECs were transfected with a m-cherry plasmid. Other transfection had a m-cherry subunit in the plasmid construct. (Scale bar = 250 μm). Shape factor and migration distance quantification show the reduction of GBM migration when IBSP is not expressed by endothelial cells. (****: p<0.0001, **: p<0.01, *: p=0.05)

Discussion:

In this chapter, we investigated how the PVN affects GBM cell migration. To do so, we fabricated a biomimetic HA based hydrogel platform (**Figure 2.1 and Figure 2.2**) to encapsulate patient derived primary gliomaspheres. We chose HA since it is one of the main components of the brain ECM. Unlike other methods, such as orthotropic murine implant, this *in vitro* platform allowed us to tune chemical compositions of the microenvironment to mimic the GBM/PVN interaction. We combined this platform with data obtained from the Kornblum lab Interactome to study how proteins, overexpressed in GBM vasculature, contribute to GBM invasive behavior. Results in **Figure 2.3 and Figure 2.4 (**with the IBSP peptide), and **Figure 2.7** (with ECs co-encapsulation) clearly showed that among the Interactome candidate proteins, IBSP induced an aggressive phenotype in GBM cells. IBSP, (also known as bone sialoprotein 2 or integrin-binding sialoprotein) is a component of mineralized tissue such as bone, and dentin[183]. In healthy tissue, IBSP functions as a nucleus for the first apatite formation[184]. In cancer, studies have focused on the role of IBSP in breast[184,185], primary bone[186,187], and cervical cancers[188]. A few recent studies have reported expression of IBSP in GBM but none investigated its role in GBM invasion[189–191]. In this chapter, we showed a clear correlation between IBSP overexpression in GBM vasculature and GBM migratory phenotypes.

This information potentially can be used to develop a novel GBM anti-migratory therapeutics, in which GBM invasion could be controlled through targeting the IBSP expression in GBM vasculature (by knocking down IBSP). It is necessary to mention that this knock-down most likely needs to be targeted to the GBM vasculature to avoid complications that may rise from IBPS depletion in other organs like bone. In addition,

disrupting the IBSP/GBM interaction through integrin αV (using small molecule drugs) is an option to control GBM cell migration. Although a simple treatment in an *in vitro* setting, it is expected that many challenges will be encountered to *in vivo* translation. The complexity of the brain, severe side effects, and impermeable blood-brain barrier makes drug delivery to the brain a daunting task[192]. One example of small molecule drugs, used to interrupt GBM integrin/ECM interaction, is Cilengitide. Cilengitide, an integrin antagonist, is a cyclic form of the RGD peptide with sub-nanomolar activity against αVβ3 receptor and nanomolar activity against closely related receptors such as αVβ5 and αVβ1[193]. Although effective in phase I and II clinical trials in the US, Cilengitide failed phase III studies, which found that addition of Cilengitide to temozolomide (TMZ), the standard chemotherapy, did not increase the median overall survival of GBM patients[194]. The failure of Cilengitide in phase III clinical studies may be due to factors independent of its mechanism of action; for example, its short half-life (4-5 hours), inadequate penetration through blood-brain barrier (BBB), and rapid clearance from tumor tissue[195,196]. Together, these factors likely prevent achieving consistent therapeutic levels in the tumor. One way to tackle these issues would be to use nano-carriers. For instance, Zhao *et al.*, 2016, showed that Cilengitide encapsulated in heparin-poloxamer nanoparticles was successfully delivered across the BBB and accumulated in GBM tumors in a rat model[197]. Despite the failure of Cilengitide, integrins are still important targets in GBM and a deeper comprehension of GBM/ECM interaction is crucial to design more effective agents. We believe the HA hydrogel platform is highly suitable for more thorough investigations on GBM/ECM interactions.

Chapter 3: Role of tumor mechanical properties on glioblastoma progression

Introduction:

Similarly to many other solid tumors, GBM tumors stiffen (increase in bulk mechanical modulus) when compared to the healthy brain tissue[75]. This increase in stiffness has been attributed to increased ECM deposition and compaction, along with elevated fluid pressure, in the tumor microenvironment[198]. Glioma stiffness increases with tumor grade, where the most malignant grade, GBM or grade IV glioma, is stiffer than lower tumor grades[199]. GBM has inhomogeneous mechanical properties. The tumor core is hyper-cellular core and approximately 10X stiffer than the surrounding, non-cancerous tissue, whereas necrotic regions of a GBM tumor are very soft[200].

GBM cell migration and proliferation are directly influenced by the mechanical properties of the ECM[123,125]. For instance, high substrate stiffness facilitates CD44-mediated migration of GBM cells seeded onto a HA substrate[62]. At the same time, epidermal growth factor (EGFR) signaling and proliferation rates increase with ECM stiffness[66]. This increase in tissue stiffness generates a positive feedback loop, where GBM cell proliferation and ECM deposition cause an increase in tissue stiffness, which in turn, promotes cell proliferation and matrix deposition[75]. In addition, growing tumors exert mechanical pressure onto healthy brain tissue, which causes cell death in adjacent, non-cancerous brain tissue[201].

Metabolic alteration is a common in cancers. Over the last decade, tumor metabolism has gained immense attention from cancer researchers and altered energy metabolism is now considered a fundamental core hallmark of cancer cells[202]. In eukaryotes, energy is produced by oxidative phosphorylation (OXPHOS), where a

glucose molecule is converted to a pyruvate which can be further metabolized to acetylCoA and fuel the tricarboxylic acid (TCA) cycle, an oxygen-dependent process[203]. Alternatively, pyruvate can be metabolized to cytosolic lactate by lactate dehydrogenase (LDH). Historically, it was believed that the direct conversion of glucose to lactate only occurs in the absence of oxygen. Paradoxically, in 1924, Otto Warburg demonstrated that cancer cells dominantly use glucose to produce lactate, even in the presence of oxygen[204]. Although counter intuitive, it has been shown that by increasing their glycolytic flux, cancer cells cope with higher energy demands as well as biosynthetic needs[205]. Glucose consumption is the principle behind the use of 2-[18F]-fluoro-2-deoxy-D-glucose in positron emission tomography (PET) imaging, where tumor are identified by higher glucose uptake[206].

Similar to the other cancer stem cells (CSCs), glioma stem cells (GSCs) have been found to rely on glycolysis for their maintenance[207]. As mentioned above, production of pyruvate from glucose is the first step in fueling the TCA cycle through conversion of pyruvate, which is converted to acetyl coenzyme A (AcetylCoA) by pyruvate dehydrogenase (PDH) after shuttling into in mitochondria. Pyruvate can also be used to start the non-oxidative path (glycolysis) by conversion to lactate (through lactate dehydrogenase, LDH). In GSCs, activation of pyruvate dehydrogenase kinase (PDK), which phosphorylates and inactivates PDH, as well as activation of LDH-A through HIF-1α, have been reported[208]. Together, these results provide strong scientific foundation for the hypothesis that GSCs primarily utilize glycolysis to produce energy. In contrast, a study by Marin-Valencia *et al.,* 2012*,* contradicted this finding, reporting that GBM cells use both glycolysis and OXPHOS[209]. Collectively, these results suggest that GSCs utilize

both non-oxidative and oxidative pathways to produce energy and biosynthetic precursors.

The majority of studies to date have focused on the role of oxygen and nutrient availability around GSCs, as directly controlled by the tumor vasculature. The GBM tumor microenvironment is often hypoxic due to aberrant presence of vasculature in GBM[210]. Hypoxia is mainly regulated through HIF family of transcription factors, which regulates the expression of a large group of genes including those relevant to metabolism. HIF-1α activates transcription of glucose transporters, like GLUT1 and GLUT3, which increases glucose availability in GSCs. Furthermore, HIF1-α activates transcription of specialized enzymes required for glycolysis, such as hexokinase (HK), pyruvate kinase M2 (PKM2) and LDH-A[210].

Cancer cell metabolism may reflect a symbiotic relationship among cancer cells and stromal cells in the PVN. Sonveaux, *et al.,* 2008*,* suggested that perivascular cells would spare glucose for the hypoxic cancer cells[211]. Hypoxic cancer cells then would convert glucose to lactate via glycolysis, which could be transported back into perivascular cells and converted to pyruvate used in OXPHOS[211]. In a review, Lisanti et al., 2014, brilliantly summarized that the stromal cells, in particular cancer-associated fibroblasts, increase their aerobic glycolysis to generate excessive lactate and pyruvate which are then secreted. Associated tumor cells then absorbed these metabolites for use in OXPHOS[212]. Such symbiotic relationships between glycolytic and oxidative cells has been dubbed the “reverse Warburg effect”, where metabolic waste of a group of cells are used as the metabolic fuel for a group of neighboring cells[213].

There are few studies (even fewer in GBM) that connect the mechanical landscape of a tumor to its metabolism. Bertero *et al.*, 2019, using orthotropic xenograft mice model of sarcoma, defined a crucial role of matrix stiffening in tumor and mechanosignal transduction through YAP/TAZ which caused an upregulation in LDH-A expression[214]. This finding suggests that increased tumor stiffness induces a metabolic switch towards increased glycolytic activity[214]. Similarly, Liu. *et al.,* 2020*,* described mechanically induced, metabolic reprogramming of hepatocellular carcinoma, where a stiffer matrix accelerated cell migration through an increase in aerobic glycolysis[215]. Finally, Sullivan et al., 2018, demonstrated a mechanistic correlation between extra cellular remodeling and breast cancer cell metabolism regulation[216]. In particular, they showed that degradation of hyaluronic acid (HA) by hyaluronidase was triggered by an increase in glycolysis.

In this study, the goal is to identify the role of tumor stiffness in GBM progression. Specifically, we focus on the influence of matrix stiffness on GBM metabolism. First, using atomic force microscopy (AFM), we measured the mechanical stiffness of patient derived GBM tumors orthotopically xenografted in mice. Using 3D, HA-based hydrogels, we generated hydrogels approximately stiffness of GBM tumors and normal brain. In hydrogel cultures, we use RNA-sequencing and fluorescence-lifetime imaging (FLIM) to investigate how stiffness reprograms GBM cellular metabolism. Finally, using small molecule inhibitors, we draw a connection between stiffness, mechanosignaling, ECM receptors (in particular CD44 and integrins), and metabolic reprogramming.

Material and Methods:

Animal experiments

Mice were prepared for aseptic surgery in accordance with protocols set by UCLA's Division of Laboratory Animal Medicine. HK408 cells (proneural) expressing firefly luciferase and GFP were dissociated with TrypLE (Thermo Fisher) and resuspended to 10^5 cells per 3 μL in growth medium. 3 μL of cell suspension was implanted into the right striatum of NSG mice at 0.5 mm anterior and 1.0 mm lateral of bregma, and 2.5 mm deep. Tumor growth was monitored by luminescence imaging on an IVIS Illumina II system at the Crump Institute's Preclinical Imaging Technology Center. 100 µL Dylight-594 tomato lectin (Vector Laboratories) (1mg/ml in PBS) were injected into the tail vein 30 minutes prior to euthanasia. Mice brains were freshly sectioned into 100 µm slices using a Leica VT1200S Vibratome. Brain slices were adhered to glass slides using Cell-Tak™ cell and tissue adhesive (Corning)[217].

Atomic force microscopy (AFM) measurements

AFM measurements were done on a Bruker Nano wizard 4 atomic force microscope using a silicon nitride cantilever equipped with 2.5 µm (diameter) silicon dioxide particles (NovaScan, nominal spring constant of 0.01 N/m). All measurements were done in PBS at 37 °C. Post-installation, the probe was allowed to thermally equilibrate in the PBS buffer for 1 hour. For every experiment, AFM sensitivity was measured using a generated force-curve on the glass slide. In addition, probe's spring constant was measured using the manual thermal calibration. Measurements were done at 0.2 μm/s indentation speed while 1 μm indentation was used. For each region of interest, a matrix of 32X32 μm with 4 μm interval was measured (8X8 grid). Data analysis

was carried out in JPKSPM data processing software using the Snodden model for spherical probes.

Hydrogel Formation

Hydrogel precursor solution was prepared by dissolving HA-SH (0.5 %w/v), 4-arm thiol terminated polyethylene glycol (PEG-SH) (Laysan Bio), 8-arm norbornene terminated polyethylene glycol (PEG-Norb) (Jenkem), 0.025 %w/v lithium phenyl-2,4,6 trimethylbenzoylphosphinate (LAP, Sigma-Aldrich), 0.25 mM thiolated RGD (GCGYGRGDSPG, Genscript), in 20 mM HEPES buffer (pH=7). After dissolving, the hydrogel precursor solution was cast into 4mm silicone molds (Grace Biolabs) and irradiated with long-wave UV (365 nm, 4.2 mW/cm^2) (Blak-Ray^{TM} B-100A UV lamp, UVP^{TM}) for 15 seconds.

Hydrogel characterization

AFM measurements were done as mentioned in the previous section. Hydrogel storage moduli (G') were measured using a discovery hybrid rheometer-2 (DHR-2, TA Instruments) at 37 °C. Rheology frequency sweep experiments were performed under 1% constant strain in the range of 0.1 to 1.0 Hz. Storage modulus of each sample was calculated as the average value of the linear region of the storage curve from the frequency sweep plot. For statistical analysis, 3 separate measurements were taken in which 5 samples from each condition were measured. For diffusion measurements, we used fluorescence recovery after photo-bleaching (FRAP). Hydrogels were incubated with fluorescein isothiocyanate-dextran (FITC-Dextran) solution (0.33 mg/ml in PBS) overnight. 5 pre-bleach images were taken at 10% power of 488 laser under a SP5 laser scanning confocal microscope (Leica). In order to bleach, 30 μm region of hydrogels were

exposed to full power 488 laser (600 μm pinhole) for 20 seconds. 1000 frame of images were taken as post bleached images. t_d values (time for half recover) were calculated from fluorescence recovery graphs. Diffusion coefficients (D_e) were calculated using simplified Fick's law[218].

Cell culture and encapsulation

Patient-derived GBM cells, HK177 (mesenchymal) and HK408 (proneural), were generously provided by Dr. Harley Kornblum at UCLA. All cell lines were collected with strict adherence to UCLA Institutional Review Board protocol 10-000655. Cell cultures routinely tested negative for mycoplasma contamination (Life Technologies, C7028). GBM cells (50,000/mL) were cultured in DMEM/F12 with 1xG21 (Gemini Bio), 1 v/v% noromycin (Invivogen), 50 ng/ml EGF (Peprotech), 20 ng/mL FGF-2 (Peprotech), and 25 mg/mL heparin (Sigma-Aldrich).

As sphere size can potentially alter spheroid behavior in hydrogels[219], GBM spheroid sizes were standardized by using Aggrewell™ well plates (Stemcell Technologies) one day prior to encapsulation. To do so, Aggrewell wells were filled with 1 ml pluronic F-127 solution (5 %w/v), centrifuged at 3000 G for 5 minutes and incubated for 30 minutes at room temperature. Then, wells were washed with 1ml complete media, cells were added, and wells were filled to 1 ml with GBM media. Finally, the plate was centrifuged at 300 G for 3 minutes.

The following day, spheroids were harvested from the wells, centrifuged briefly (200G, 1 min) and resuspended in the hydrogel precursor solution. Hydrogels were formed as described above. Post-formation, spheroid-laden hydrogels were transferred

to 24-well well plates and cultured in 500 μl. Half of media volume (250 μl) was replaced by fresh media every other day.

Immunofluorescent staining

Spheroid-laden hydrogels were fixed in 4% paraformaldehyde (PFA) for 15 minutes at 37 °C. Then, incubated with PBS solution containing 5% sucrose for 1 hour at room temperature followed by PBS solution containing 20% sucrose overnight at 4 °C. The next day, hydrogels were incubated in optimal cutting temperature solution containing 20% sucrose for 3 hours at 4 °C. Finally, blocks were frozen at -30 °C (dry ice+2-methylbutane mixture) and stored at -80 °C. Cryosectioning was performed on a Leica cryostat 3050S to obtain 10–12 μm sections.

Immunofluorescent staining was done using an established protocol. Cryosections were air-chilled for 20 minutes, fixed with 4% PFA for 15 minutes at room temperature, washed 3X5 minutes with Tris buffer saline containing 0.1 % (v/v) Tween-20 (TBST). In case of cytoplasmic/nuclear staining, sections were permeabilized with Tris-bufferred saline containing 0.5% (v/v) triton X-100 for 15 minutes at room temperature. Blocking was carried out using a 2% (w/v) bovine serum albumin (BSA)+4% (w/v) normal donkey serum/normal goat serum (depending on the secondary) for 1 hour at room temperature. Primary antibody incubation was done in blocking solution overnight at 4 °C. The next day, sections were washed for 3X5 minutes in TBST, then incubated with secondary antibody solution (in blocking solution) for 1 hour at room temperature. Finally, sections were washed again for 3X5 minutes using TBST.

RNA-sequencing

At the end of each experiment, 6 hydrogels per condition were combined for RNA extraction. RNA extraction was performed based on previously established protocol using Qiagen Rneasy Micro kit. Hydrogels were incubated in lysis buffer (RLT) and disintegrated using a 1ml syringe equipped with a 20G needle[181]. The lysate was flown through Qiagen Qiashredder column at 17,000 G for 2 minutes. Lysate were transferred to the Rneasy micro column and RNA was extracted based on the manufacturer protocol.

RNA sequencing was performed at UCLA Technology Center for Genomics & Bioinformatics (TCGB). RNA concentration and quality were checked using a Nanodrop spectrophotometer (Thermofisher). Libraries for RNA-Seq were prepared with KAPA Stranded mRNA-Seq Kit. The workflow consists of mRNA enrichment and fragmentation, first strand cDNA synthesis using random priming followed by second strand synthesis converting cDNA:RNA hybrid to double-stranded cDNA (dscDNA), and incorporates dUTP into the second cDNA strand. cDNA generation is followed by end repair to generate blunt ends, A-tailing, adaptor ligation and PCR amplification. Different adaptors were used for multiplexing samples in one lane. Sequencing was performed on an Illumina NovaSeq6000 for PE 2x150 run. Data quality check was done on Illumina SAV. Demultiplexing was performed with Illumina Bcl2fastq v2.19.1.403 software. The reads were mapped by STAR 2.27a[220] and read counts per gene were quantified using human Ensembl GRCh38.98 GTF file. In Partek Flow, read counts were normalized by CPM +1.0E-4. All results of differential gene expression analysis utilized Partek's statistical analysis tool, GSA. For differentially expressed gene list, p-values and fold change (FC) filters were applied. The filter was $p<0.05$ and $FC>2$ for all differential gene expression

results. Ingenuity Pathway Analysis software (IPA, Qiagen)[221] was used for pathway analysis. Using the list of significantly ($p<0.05$) differentially expressed (FC>2) genes, the Canonical Pathway analysis, Disease & Function analysis, and networks analysis were performed by IPA.

NADH fluorescence lifetime imaging (FLIM)

NADH fluorescence lifetime images were acquired with an LSM 880 confocal microscope (Zeiss) with a 40x 1.2NA C-Apochromat water-immersion objective coupled to an A320 FastFLIM acquisition system (ISS). A Ti:Sapphire laser (Spectra-Physics Mai Tai) with an 80 MHz repetition rate was used for two-photon excitation at 740 nm. The excitation signal was separated from the emission signal by a 690 nm dichroic mirror. The NADH signal was passed through a 460/80 nm bandpass filter and collected with an external photomultiplier tube (H7522P-40, Hamamatsu). Cells were imaged within a stage-top incubator kept at 5% CO_2 and 37^{o}C. FLIM data were acquired and calibrated with the SimFCS 4 software developed at the Laboratory for Fluorescence Dynamics at UC Irvine. Calibration of the system was performed by acquiring FLIM images of coumarin 6 (~10 μM), which has a known lifetime of 2.4 ns in ethanol, to account for the instrument response function.

Phasor FLIM NADH fractional analysis

NADH assumes two main physical states, a closed configuration when free in solution, and an open configuration when bound to an enzyme[222]. These two physical states have differing lifetimes, 0.4 ns when in its free configuration, and 3.4 ns when in its bound configuration[223,224]. To quantify metabolic alterations, we perform fractional analysis of NADH lifetime by calculating individual pixel positions on the phasor plot along

the linear trajectory of purely free NADH lifetime (0.4 ns) and purely bound NADH lifetime (3.4 ns). We quantify the fraction of free NADH by simply calculating the distance of the center of mass of a spheroid's cytoplasmic NADH FLIM pixel distribution to the position of purely bound NADH divided by the distance between purely free NADH and purely bound NADH on the phasor plot. To ensure avoiding contribution from background fluorescence which may be present in the media, we perform a three-component analysis post-background calibration to linearly unmix its contribution. We also use an empirically determined intensity threshold for each file to exclude any low-intensity background signal arising from the surrounding ECM and media. These segmentation and phasor analysis methods are described in detail elsewhere[224].

Receptor inhibition

To interfere GBM cell interaction with RGD and HA, Cilengitide (CRGD) and ezrin inhibitor was used respectively. Post-encapsulation, spheroids were treated with Cilengitide (Sigma Aldrich) and NSC668394 (Ezrin inhibitor, Sigma Aldrich). Cilengitide stock solution was prepared at 5 mM in PBS. NSC668394 stock solution was prepared at 10 mM in DMSO. For inhibition experiments, final concentration of 25 μM Cilengitide and 10 μM NSC668394 were used.

Statistical analysis

Normality of each data set was analyzed using D'Agostino & Pearson omnibus normality test. For normally distributed population, one-way ANOVA and then t-test were used to determine the statistical differences among the groups. For non-normal distributions, Mann-Whitney non-parametric test was used. All statistical analysis were done in Prism 8 software.

Results:

GBM mechanical properties

To investigate the biophysical properties of a GBM tumor, patient-derived, GFP+ tumor cells were orthotopically xenografted into mice. Unlike other studies, where mice brains were extracted at a certain time point, each mouse was sacrificed only when euthanasia criteria (weight loss, loss of function, etc.) were met. This way, we were able to correlate the stiffness of each tumor to the generated Kaplan-Meier survival curve (**Figure 3. 1. A**). Post-extraction, each brain was sectioned to 150 μm slices using a vibratome (**Figure 3. 1.B**). These slices were adhered to glass slides for AFM measurements. **Figure 3. 1.B** shows three representative slices obtained from three individual mouse brains. For each slice, stiffness of the tumor core (C), tumor edge (E) and adjacent brain tissue (AB) were measured (**Figure 3. 1.C**). **Figure 3. 1.D** shows cumulative stiffness measurements for the three regions of interest. Measured Young's moduli of tumor core, edge, and healthy tissue were 3375±2716 Pa, 1153±1118 Pa, and 311.5±261.5 Pa, respectively (meidan± standard deviation). In addition to the absolute values, cumulative stiffness fold changes (normalized to healthy tissue) are reported in **Figure 3. 1.E.** Based on our data the tumor core is 8.929±6.6 fold and tumor edge is 2.89±2.8 fold stiffer than the adjacent healthy tissue.

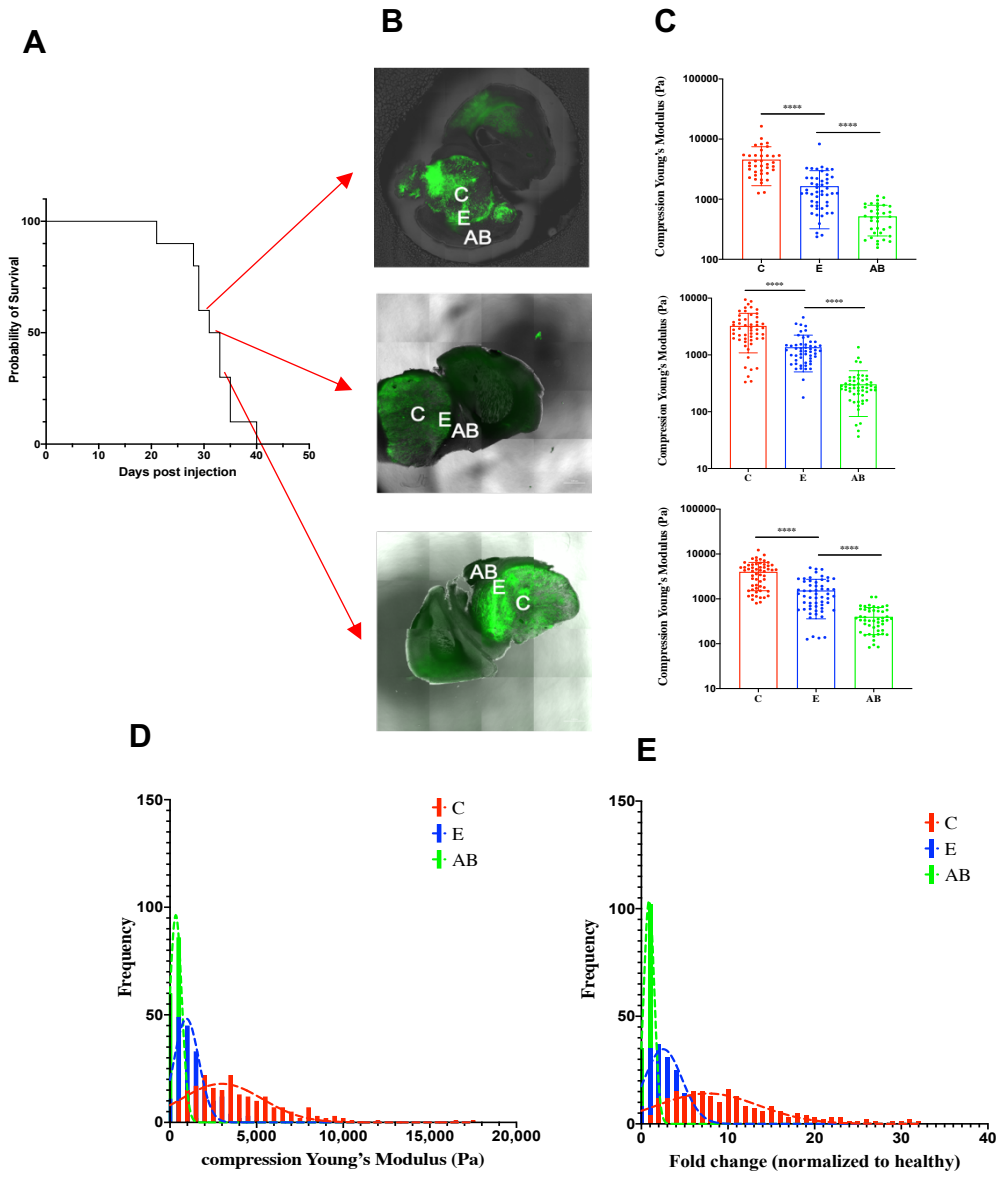

Figure 3. 1: Human GBM cells xenografted in murine brain for AFM measurements. A) Kaplan-Meier survival curve of murine test subjects. B) Representative images of mice brain slices. GBM cells express GFP endogenously. Tumor core, edge and adjacent brain tissue are denoted by C, E, and AB respectively. C) Micro-compression measurements of each representative brain slice show a stiff core with softer periphery, yet both are stiffer than adjacent healthy tissue. D) Cumulative micro-compression moduli distribution of 5 mice brains. E) Fold increase of tumor core and edge normalized to healthy tissue. (****: P<0.0001)

3D, hyaluronic acid-based hydrogels to mimic the mechanical landscape GBM

Using AFM stiffness measurements of GBM xenografts, we designed an HA-based hydrogel platform in which, hydrogel mechanical properties could be tuned orthogonally to mimic the tumor core and adjacent brain tissue (**Figure 3. 2.C**). We utilized a thiol-ene photochemical technique to take advantage of chemical reaction between thiol (SH) functional groups on modified HA, and norbornene functional groups (Norb) on an 8-arm PEG-norbornene. This reaction only occurs in the presence of a photoinitiator (here, LAP) and a light source (here, 365 nm) as depicted in **Figure 3. 2.A.** Using this technique, we were able to obtain a wide range of hydrogel stiffnesses by tuning the crosslinker concentration (4-arm PEG-SH and 8-arm PEG-Norb) while keeping the HA concentration constant (0.5 wt%) (**Figure 3. 2.B and C**). Soft hydrogels (mimicking the healthy tissue) swelled about 50% more than the stiff ones (mimicking the tumor core) (**Figure 3. 2.D**). Finally, since stiffer hydrogels were formed by increasing the crosslink density, we investigated the diffusion profile of two large molecules (FITC-Dextran, 20 and 70 kDa) which cover the size of most nutrients, and growth factors in the growth media. Based on our FRAP data, there is no significant differences in diffusion coefficient of dextran molecules in soft and stiff hydrogels (**Figure 3. 2.E**)**.** These data confirm that it is unlikely that differences in diffusion between hydrogel conditions drive effects on GBM cell phenotypical/genotypical changes.

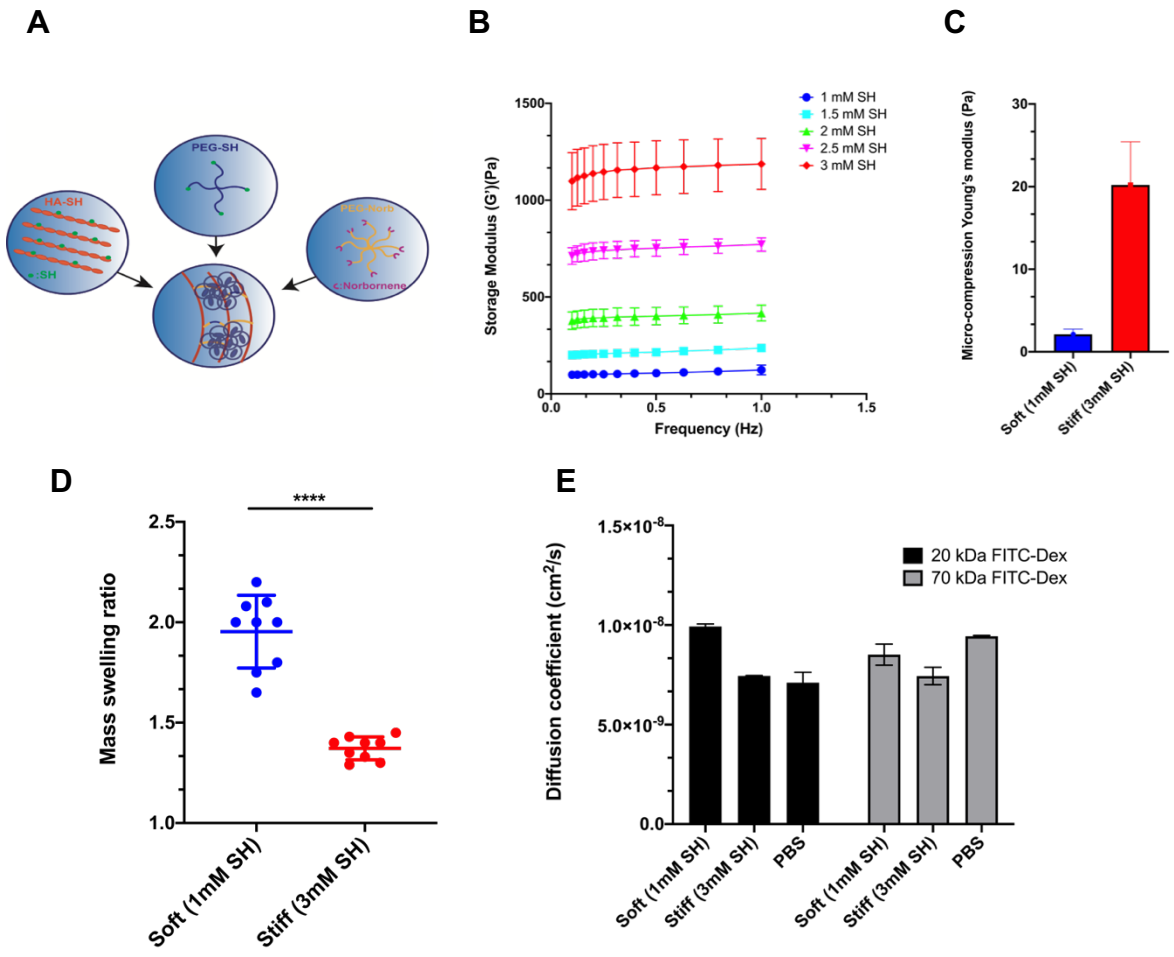

Figure 3. 2: Hydrogel structure and properties: (A) schematic representation of hydrogel fabrication using UV light (365 nm), (B) Storage modulus of hydrogels is tuned by changing total thiol concentration to represent healthy brain or tumor tissue (C) micro-compression modulus of 1mM SH and 3mM SH hydrogels measured with AFM, (D) Mass swelling measurements in soft and stiff hydrogel (E) Diffusion of two different size of dextran (20kDa and 70 kDa) in soft (120 Pa) and stiff (1200Pa) hydrogels were compared to diffusion of respective dextran molecules in PBS.(****: P-Value<0.0001)

GBM spheroid encapsulation in HA hydrogels

Uniformly distributed size of GBM spheroids were formed in Aggrewell™ well-plates. Each well of Aggrewell (Aggrewell 400) has 1200 μ-wells. Since the size of spheroids are directly controlled by the number of cells plated in each μ-well, different number of cells were seeded in each well, and size distribution was studied after 24 hours of incubation. As can be seen in **Figure 3. 3,** each seeding density resulted in a semi-uniform distribution. We used seeding densities of 100, 250, 500, 750, and 1000 cells per μ-well. The resulted spheroid diameters are 72.68±9.88 μm, 103.7±12.83 μm, 133.9±11.12 μm, 161.8± 15.07 μm, and 187.9±15.34 μm, respectively. To avoid hypoxic core formation, we chose to work with 500 cells/μl condition which resulted in sphere size between 100-150 μm.

Next, we sought to investigate the GBM viability in the course of an experiment. Therefore, encapsulated spheroids survival was examined using LIVE/DEAD® viability/cytotoxicity kit at day 1, 3, and 6 post-encapsulation. GBM cells live percentage was not statistically different between soft and stiff hydrogels in each day. On the other hand, survival was lower at the end of the experiment time course (day 6) when compared to the beginning of the experiment (day 1). Live percentages in soft condition were 93.2±4.31, 89.58±4.2, and 85.71±1.66 at day 1, 3, and 6, respectively. In stiff hydrogels live percentages for GBM cells were 93.3±4.78, 90.98±5.4, and 82.42±6.39, respectively (**Figure 3. 4**).

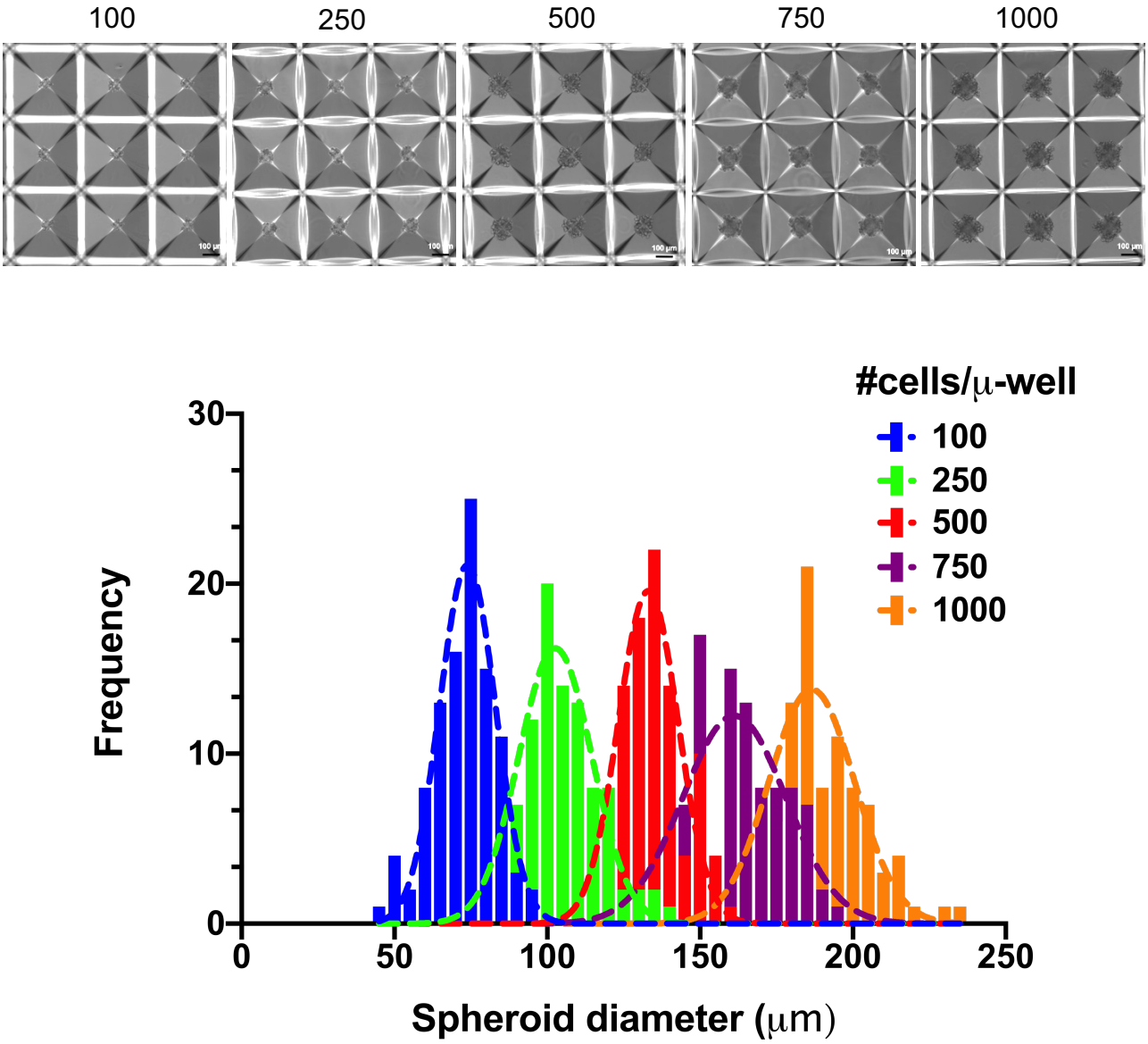

Figure 3. 3: To form uniform size of GBM spheroids, Aggrewell™ plates were used. Spheroid size was controlled by initial seeding density per each micro-well. Size distributions were statistically different from one another (P<0.0001). (Scale bar= 100μm)

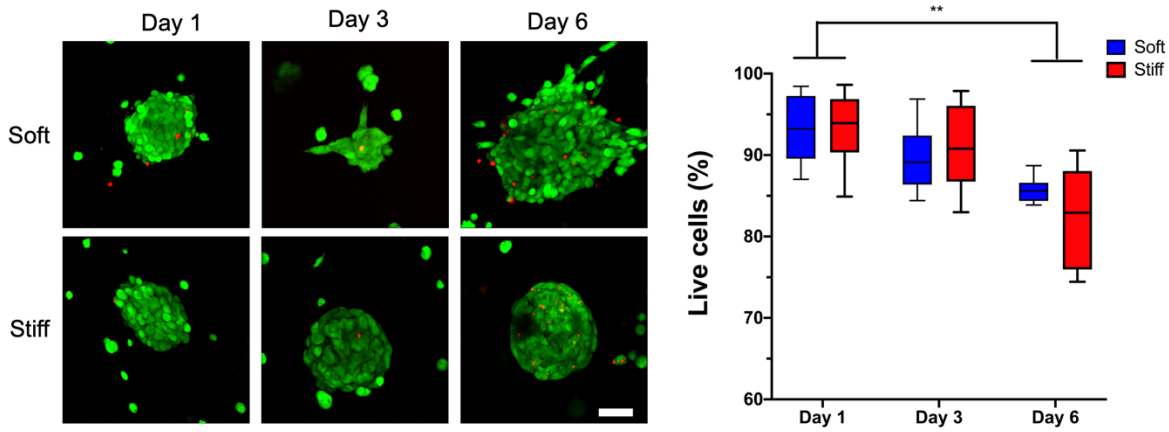

Figure 3. 4: Live/Dead staining of GBM spheroids in HA hydrogels in the course of an encapsulation experiment. There was no difference in GBM cells survival between soft and stiff groups in each day. But cell survival was lower in both hydrogel conditions at day 6 compared to day 1. (Scale bar 100μm) (**: P<0.001)

ECM stiffness alters OXPHOS genes' expression

To investigate how ECM stiffness affects GBM cells, we used bulk RNA-sequencing. At the end of each experiment, we extracted RNA from a pool of hydrogels in each condition. In addition, RNA was extracted from the gliomasphere culture of the same passage. Comparing the RNA-seq results among the repeats for each cell line, and between the two cell lines revealed a group of mitochondrially-encoded genes (denoted by MT-), that are consistently enriched in stiff hydrogels (**Figure 3. 5**). The proteins translated from these genes are all involved in a mitochondria's electron transport chain (ETC). ETC is a series of protein complexes at the mitochondria inner membrane in which synthesis of adenosine triphosphate (ATP) happens[225]. Many of the genes, overexpressed in stiff hydrogels belong to complex I and complex IV of the ETC. These results suggest that mechanical properties of microenvironment could potentially affect GBM cells' metabolism, where in stiff microenvironment, GBM cells utilize the oxidative phosphorylation (OXPHOS) more than glycolysis (GLY).

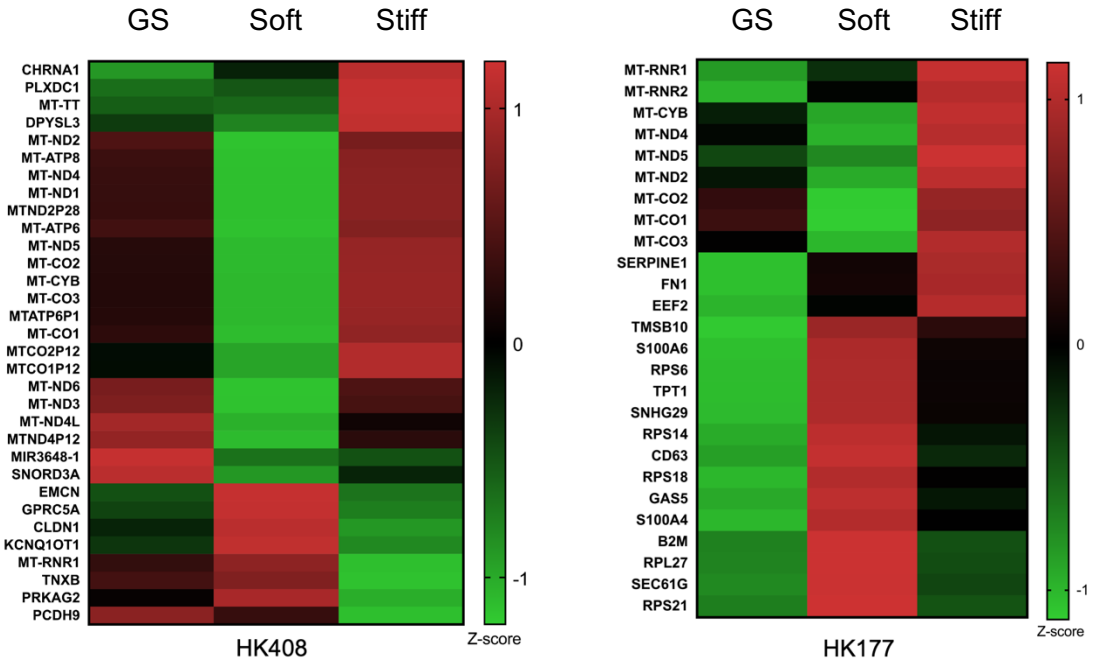

Figure 3. 5: Bulk RNA-sequencing results represented as heatmaps. For both cell lines, Mitochondria-encoded genes (denoted by MT-) are differentially overexpressed in stiff hydrogels when compared to soft. (GS: Gliomasphere)

GBM cells metabolism depends on the ECM stiffness

As discussed in the previous section, based on our RNA-sequencing results, GBM cells overexpress proteins involved in OXPHOS in stiff hydrogels when compared to soft hydrogels (**Figure 3. 5**). To confirm these results, we performed FLIM on GBM spheroids cultured in soft and stiff hydrogels. FLIM is a non-invasive method in which, fluorescence intensity of a fluorophore is measured overtime to calculate the intrinsic fluorescence decay time (lifetime)[226]. Here, we took advantage of Nicotinamide adenine dinucleotide (NADH) autofluorescence properties at 360 nm[227]. This method eliminates the need for any fluorescence staining hence can be used for live-cell imaging. Previously, it has been shown that bound NADH (most likely being used in OXPHOS) has higher fluorescence lifetime (3.4 ns) than free NADH in cytosol (most likely used for glycolysis) (0.4 ns)[228]. From the measured fluorescence lifetime, one can calculate NADH fraction bound to a protein, hence determine whether a cell is using more of OXPHOS or GLY as its metabolism pathway[223].

FLIM analysis showed that cells derived from two distinct GBM tumors have more bound NADH when cultured in stiff, compared to soft, hydrogels. This finding indicates that stiffer substrates induce GBM cells to upregulate OXPHOS activity, while softer substrates induce a shift towards dominant glycolysis (**Figure 3. 6**). Together, results suggest that matrix stiffness can cause a switch in GBM cell metabolism and confirms our observation from RNA-seq studies where genes related to OXPHOS proteins were differentially upregulated in stiff hydrogels.

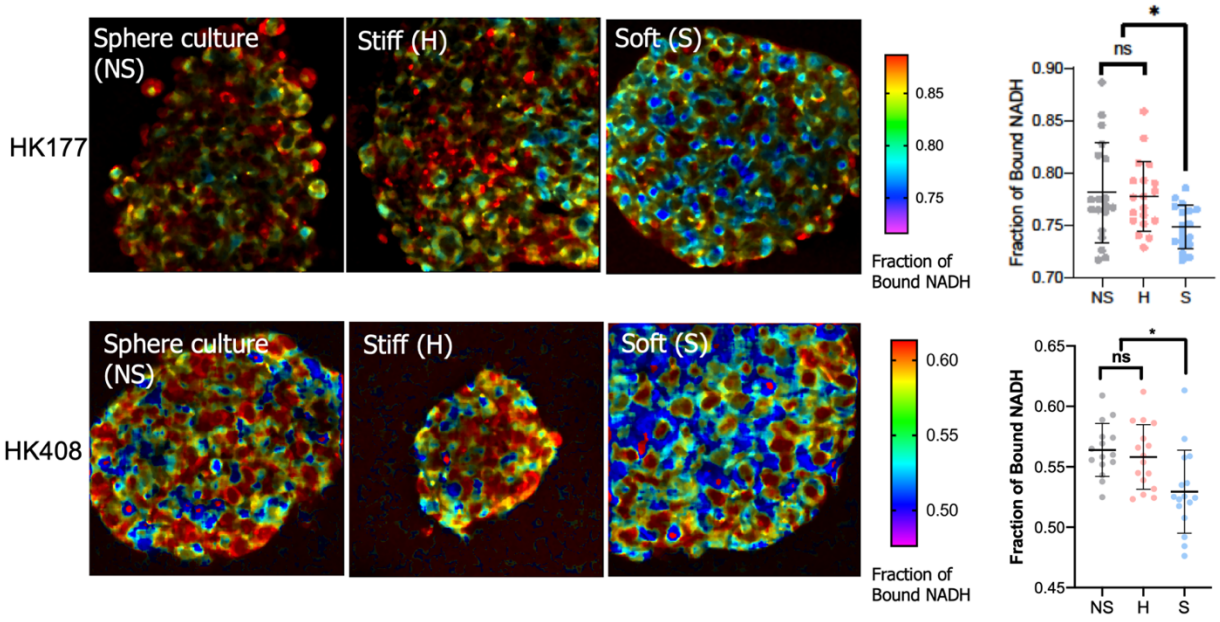

Figure 3. 6: Fluorescence-lifetime imaging (FLIM) used to measure fluorescence-life time of NADH. In both cell lines, less fraction of bound NADH was observed in spheres encapsulated in soft hydrogels, compared to the ones in stiff hydrogels. Lower fraction of bound NADH indicates that GBM cells switch to a more glycolytic metabolism pathway in soft hydrogels.

Integrins and CD44 directly mediate the metabolism switch

GBM cell-ECM in the hydrogel platform interactions occur primarily through integrins (with RGD) and CD44 (with HA). Thus, we sought to understand whether these interactions have a role in mechanical control of metabolism. To inhibit integrin interactions with the hydrogel, GBM spheroids were treated with cilengitide (CRGD). Cilengitide, a cyclic RGD pentapeptide, specifically inhibits the integrin αV family interactions with the RGD motif in many ECM proteins (like vitronectin, fibronectin etc.)[229]. Since CD44 plays many important roles in GBM cell growth, migration, etc., we sought to target the specific CD44 downstream interaction which directly plays a role in the cell migration and mechanical signaling. Hence, we chose to use a small molecule drug inhibiting ezrin/CD44 interaction. Ezrin, an adaptor protein of the ezrin/radixin/moesin (ERM) subfamily, bridges the intracellular domain of CD44 receptors and the F-actin cytoskeletoon[230]. Inhibition of ezrin, using a small molecule drug, have been shown to inhibit invasiveness behavior in other cancers in an in vitro setting[231].

Gliomaspheres, treated with CRGD showed a small shift towards OXPHOS dominance in both soft and stiff hydrogels. When cultured in soft hydrogels, the bound fraction NADH increased slightly from 0.5$\pm$0.01 in control samples to 0.52$\pm$0.03 in CRGD-treated ones ($p=0.0216$). In stiff hydrogels, CRGD treatment caused a more pronounced shift toward OXPHOS, where fraction of bound NADH increased from 0.53$\pm$0.02 in control samples to 0.56$\pm$0.02 in CRGD treated samples ($p<0.0001$). Nevertheless, post-CRGD treatment, similar to the control, GBM cells in soft condition were using more GLY when compared to spheres in stiff condition. In treated conditions, fraction of bound NADH in soft and stiff hydrogels were 0.52$\pm$0.03 and 0.56$\pm$0.02 ($p< 0.01$).

Ezrin inhibition caused a noticeable shift toward OXPHOS in both soft and stiff culture conditions. In soft hydrogels, the fraction of bound NADH increased from 0.5±0.01 in control samples to 0.61±0.01 in treated group ($p<0.0001$). In stiff hydrogels, the fraction of bound NADH increased from 0.53±0.02 in control samples to 0.6±0.008 in treated group with the p-value of <0.0001. However, there were no statistical differences between gliomaspheres in soft and stiff hydrogels with ezrin inhibition (p-value of 0.32). Combinatory treatment of CRGD and NSC668394, worked similarly to ezrin inhibition (**Figure 3. 7**).These data suggest that disruption of ECM-GBM cells interactions, through either integrins or CD44, induce a shift toward OXPHOS metabolism. Furthermore, this effect most affected when CD44 interactions with the F-actin cytoskeleton are disrupted. Moreover, only CD44-F-actin disruption eliminated the difference is metabolic preference between gliomaspheres cultured in soft and stiff hydrogels. Together, data clearly show that the mechanical signaling can induce metabolic changes in GBM cells, as relayed through HA/CD44/F-actin axis.

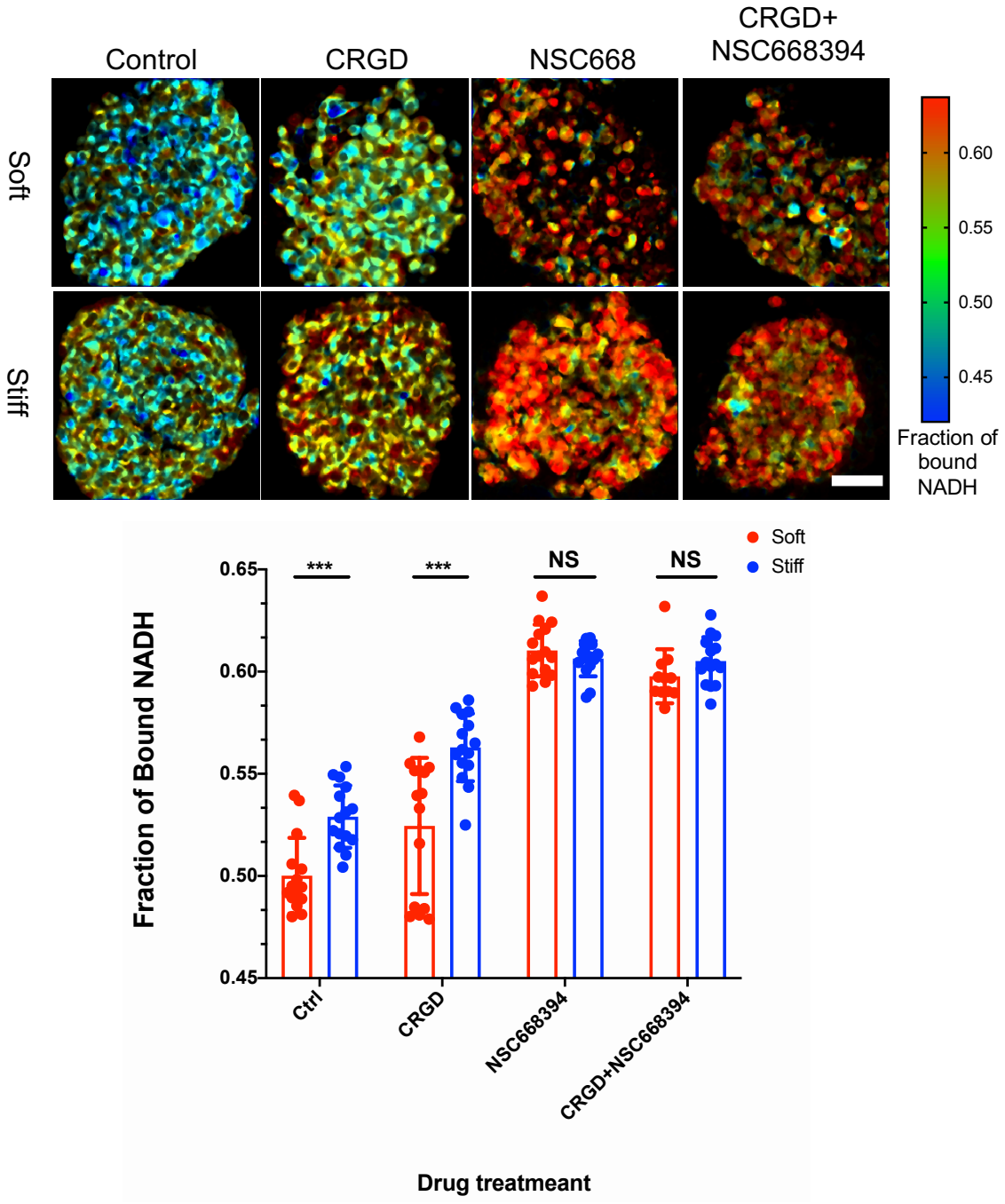

Figure 3.7: FLIM was used to study effect of GVM cell CD44 and Integrins on the metabolism switch. (Top) Representative FLIM images of GBM spheroids. (Bottom) measured fraction of bound NADH as a metabolism switch indicator. (Scale bar = 50 μm) (***: P<0.001).

GBM cell migration and metabolism

In the previous section, we talked about the role of ECM stiffness on GBM metabolism switch. In addition to metabolism, we have data showing that stiff microenvironment inhibits GBM cell migration (**Figure 3.8**). On average, in soft hydrogels GBM cells migrated 165.54±58.65 μm away from their original Gliomasphere whereas in stiff hydrogels no migration was observed. Moreover, our preliminary pH measurements, through phenol red absorption at 560 nm, shows lower 560nm absorbance in media collected from soft gels at day 6, when compared to media collected from stiff gels (**Figure 3.8**). At day 3, the 560 nm absorbances are 0.1367±0.011 and 0.1274±0.013 for soft and stiff conditions respectively ($p=0.1137$). At day 6, the absorbance values are 0.1486±0.007 and 0.1613±0.011 for soft and stiff hydrogels respectively ($p<0.01$). It has been shown that phenol-red lower absorbance at 560nm corresponds with a lower pH[232].

On the metabolism side, our FLIM data suggests that in soft hydrogels, where GBM gliomaspheres preferentially use glycolysis, migratory cells switch their metabolism to OXPHOS (**Figure 3.9**). in soft hydrogels the fraction of bound NADH increased from .5±0.018 in gliomaspheres to 0.55±0.015 in the migratory population ($p<0.0001$).

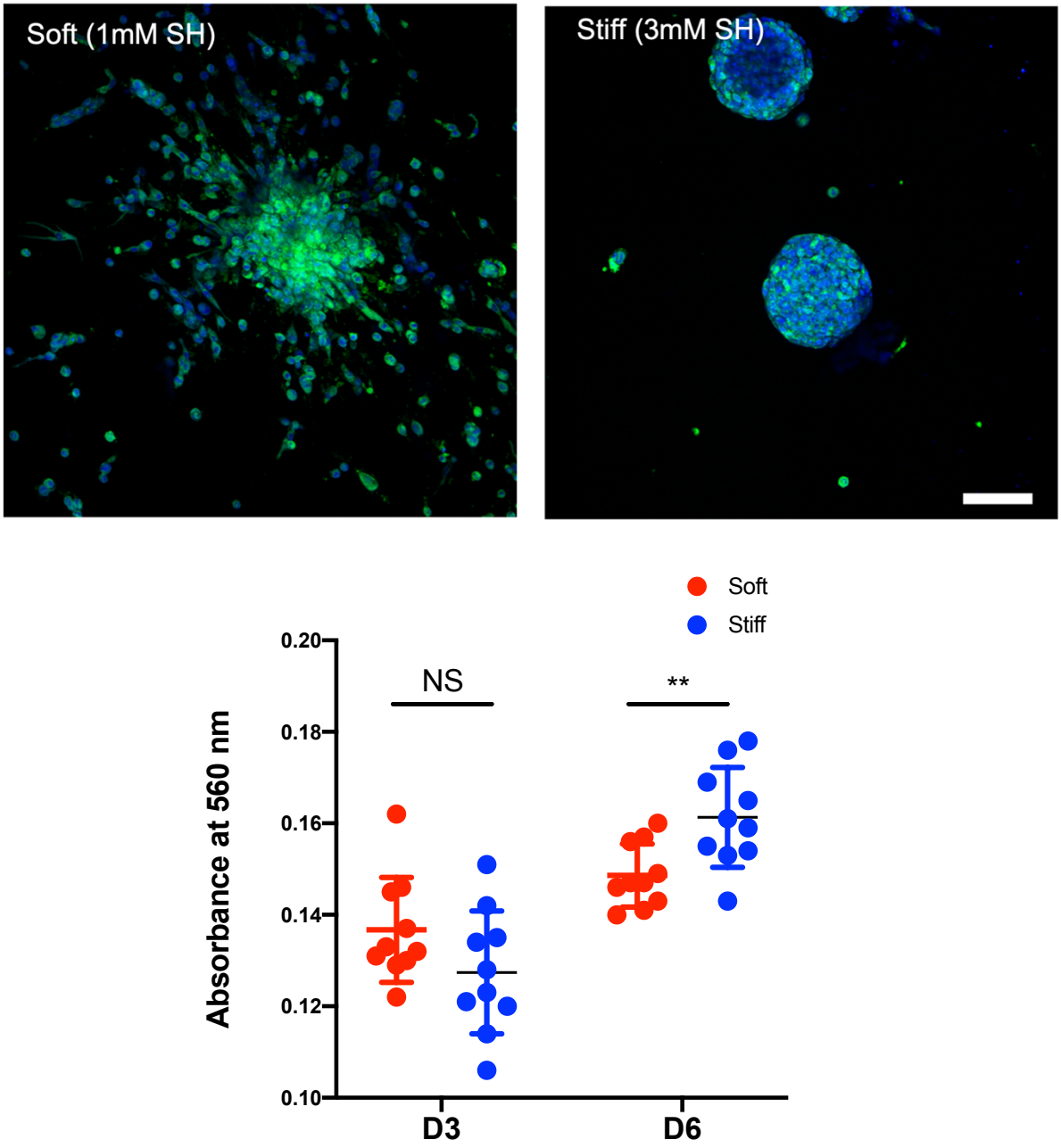

Figure 3.8: (Top) GBM spheroids encapsulated in soft hydrogels exhibit strong migratory phenotype whereas in stiff conditions no cell migration was observed. (scale bar = 100 μm) (Blue: Hoechst staining of nuclei, Green: Phalloidin staining of actin). (Bottom) Phenol-red absorbance measurement at 560 nm shows at day 6, environment is more acidic around soft gels compared to stiff ones.

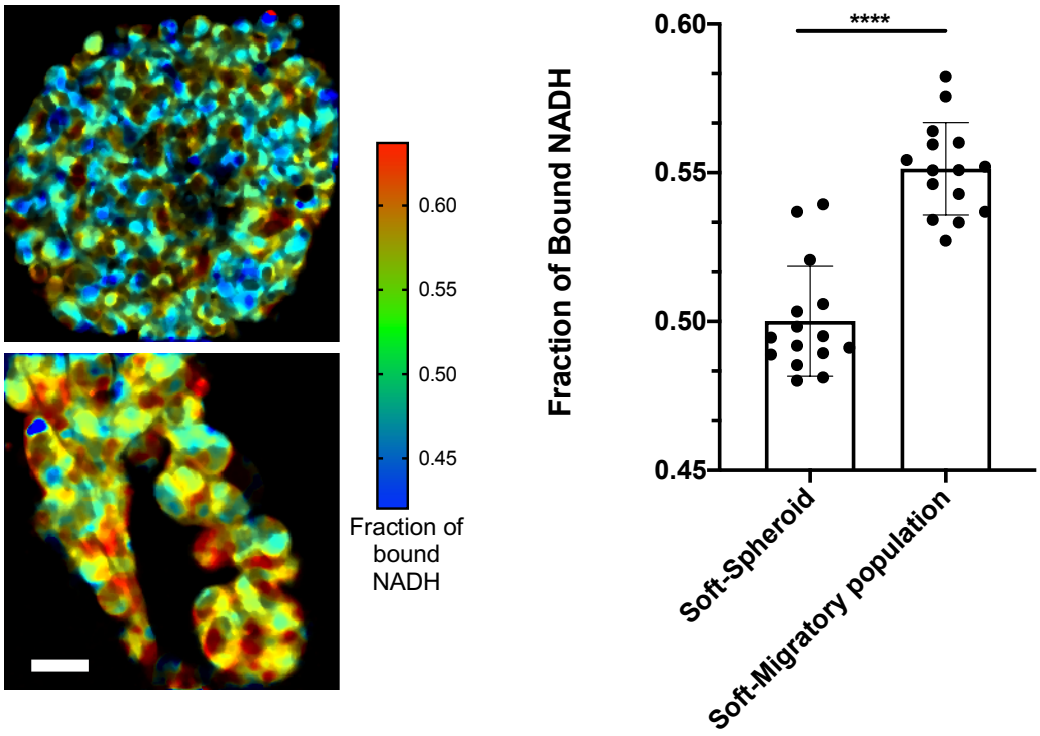

Figure 3.9: FLIM comparison of a GBM spheroid and GBM migratory population is soft hydrogels. The migratory cells, originated from the same sphere on top, adopt a more OXPHOS metabolism pathway. (Scale bar = 50 μm) (****: p-value <0.0001).

Discussion:

These studies investigated effects of mechanical properties of the matrix on GBM cells. We first measured stiffness of GBM tumors xenografted into murine brains and correlated that with overall survival. In **Figure 3. 1**, we showed that GBM tumor core stiffness increases to approximately 10X of the adjacent brain tissue before a mouse met euthanasia criteria. This increase in the stiffness potentially could contribute to mice outcome since the stiffer tumor presses against the adjacent brain tissue and could cause cell death in the adjacent brain tissue. In addition, our results suggest that tumor stiffness is heterogenous, where tumor edge is softer than non-necrotic core and non-cancerous brain tissue is softer than both. This mechanical heterogeneity may contribute to the observed heterogeneity in GBM cells residing at the core of the tumor compared to ones residing at the edge. For instance, Minata, *et al.,* 2019*,* reported that while GSCs at the tumor core resemble the mesenchymal subtype, GSCs at the edge are more similar to the proneural subtype[233].

We sought to study the role of this mechanical landscape on GBM spheroids. Therefore, we utilized HA-based hydrogels to mimic the stiffness of a GBM tumor core and adjacent brain tissue (**Figure 3. 2**). Although many studies have shown that matrix stiffness has effects on GBM cells phenotype/genotype[68,147,234], few have explored stiffness-induced changes in GBM metabolism. Chen et al., 2017, reported a decrease in GBM invasion (U251) with increasing the stiffness but they did not observe any changes in metabolic activity of U251 cells[235]. Hughes et al., 2020, showed that in GBM tumor-initiating cells, OXPHOS genes' expression is regulated by matrix stiffness where L0 patient-derived classical subtype GBM cells differentially overexpressed OXPHOS

genes on stiff substrates when compared with soft substrates[236]. Interestingly, Randall *et al.*, 2020, demonstrated that in a GBM xenograft model, GBM cells at the edge of the tumor overexpress genes related to fatty acid metabolism[237]. Fatty acid metabolism has been shown to be a possible key factor in GBM prognosis, where addition of Atorvastatin increased rats' survival with xenografted GBM[238]. Atorvastatin is a competitive inhibitor of HMG-CoA reductase which reduces HMG-CoA to mevalonate. Mevalonate pathway is an important metabolic pathway in biosynthesis of sterols and isoprenoids which are integral to tumor growth[239]. It is possible that these observed differences in fatty acid metabolism may arise from different ECM stiffness at the tumor core and edge. Our results from RNA-sequencing (**Figure 3. 5**) and FLIM (**Figure 3. 6**) clearly showed that GBM cells, depending on the microenvironment stiffness, adopt a different metabolic mechanism (OXPHOS vs. GLY). This result is similar to Hughes et al., 2020, findings described above. The primary GBM gliomasphere culture condition (used in our studies) enriches the GSCs population which have phenotypical/genotypical similarities to L0 GBM tumor initiating cells used in Hughes et al., 2020, studies[240].

Furthermore, we showed that GBM cell migration in soft hydrogels is concurrent with a lower pH in the microenvironment (**Figure 3.8**). This is particularly interesting as enzymes responsible for matrix degradation (i.e., MMPs, hyaluronidase) are more active in acidic pH[241,242]. For GBM cells to migrate in a microenvironment, they either need to degrade the matrix around them or squeeze through the matrix pores. Since GBM gliomaspheres switch to GLY in soft hydrogels, we hypothesize that the lower pH in the soft condition is due to the production of lactic acid as a by-product of glycolysis[243]. This lower pH, in turn activates matrix remodeling enzymes (MMPs and Hyaluronidase) to

facilitate cell migration. Sullivan *et al.*, 2018, demonstrated that in breast cancer, degradation of HA by hyaluronidase triggers an increase in glycolysis[216]. These findings, in conjunction with ours, suggest a possible positive feedback loop where degradation of HA by hyaluronidase increases GBM cell glycolysis. This increase in glycolysis in turn lowers the pH and activates more hyaluronidase to increase HA degradation. The order in which these events may occur is not clear and needs further investigation.

To investigate this more thoroughly, we propose 3 future experiments: 1) lowering the pH manually in both soft and stiff conditions and compare it with the control samples. 2) measuring hyaluronidase activity using a hyaluronidase activity assay kit (Razie assay kits, Amsbio)[244,245], and 3) interrupting glycolysis, using a lactate dehydrogenase (LDH) inhibitor, and observing effects on GBM cell migration.

To summarize this chapter, data showed that the stiffness of a GBM tumor plays a direct role (through HA/CD44 interaction) in GBM cell metabolism and cell migration. GBM in stiff hydrogels, mimicking the stiffness of the core of the tumor, utilize OXPHOS more than glycolysis. On the other hand, GBM cells in soft hydrogels, mimicking the stiffness of the edge of the tumor, utilize glycolysis more. This switch to GLY in soft hydrogels potentially decreases the microenvironment pH and facilitates GBM migration by activating ECM-remodeling enzymes. Based on these, we hypothesize that inhibition of GBM glycolysis, through LDH activity, could be beneficial in controlling GBM cell invasion. There are few evidences in literature exhibiting the efficacy of LDH inhibition in GBM. Daniele et al., 2015, showed that LDH-A inhibitors (NHI-1 and NHI-2) lowered U87MG cell viability[246]. Nevertheless, none has studied the role of LDH (and glycolysis) in GBM cell migration. There have been multiple clinical trials, targeting metabolism in

different cancers, summarized in a recent review by Clem *et al.*, 2016 [247]. For example, a phase II trial of AT-101 (a LDH-A inhibitor) showed stabilization of tumors in 16% of GBM patients[248]. Other LDH-A inhibitors such as galloflavin[249],JQ[250], and FX11[251] are still in preclinical stages. Nevertheless, since many metabolic alterations in GBM can exist across various GBM genotypes, it is not farfetched to hypothesize that targeting GBM metabolic abnormalities might gain more success than targeting genomic alterations[252]. In addition, many preclinical studies have showed the benefit of targeting metabolism in combination with current clinical methods[252]. For instance, in many cancers, a high rate of glycolysis is correlated with radio-resistance, while inhibition of glycolysis appears to sensitize cancer cells to radiation[252]. Dwarakanath *et al.*, 2009, showed that inhibition of glycolysis using 2-deoxy-glucose enhances radiation-induced GBM cell damage[253]. Similarly, studies have showed that inhibition of glycolysis induces a modest sensitization to the treatment with TMZ, an alkylating chemotherapy commonly used in GBM patients, in GBM cells both *in vitro* and in murine models[254,255]. These studies, combined with our findings presented here, accentuate the need for a more suitable preclinical model (such as our HA hydrogel platform) of GBM metabolism.

Chapter 4: Future development

The overarching goal of this dissertation has been to develop a three-dimensional (3D), biomimetic platform to enable human-relevant investigations of glioblastoma (GBM) *in vitro*. We have successfully developed an HA-based hydrogel system formed via the facile thiol-ene photochemical technique. This method allowed us to fabricate HA-based hydrogels with tunable chemical and mechanical properties to investigate various aspects of GBM microenvironment. Using this platform, we were able to investigate the role of perivascular niche on GBM migration (Chapter 2). Additionally, we showed that how tumor stiffness alters GBM cells phenotype/genotype (Chapter 3). To improve upon the current HA platform, we are working on two aspects, discussed below.

Interfacing hydrogels (IH)

Most of the hydrogel constructs used for experiments presented in this dissertation, can only represent a single property of the GBM microenvironment. For example, in Chapter 3, GBM cells are encapsulated either in a soft or a stiff hydrogel. These hydrogels are not able to mimic the microenvironment transition in human GBM tumors where GBM cells at the edge of a tumor experience multiple stiffness, a stiff tumor and a softer non-cancerous tissue. To resolve this, we have been developing an "Interfacing Hydrogel" (IH) system, which can mimic this mechanical transition. A first prototype of this system was used in Chapter 2, **Figure 2. 5**. We are working on improving the throughput of the method as well as adopting it to model mechanical transitions in GBM tumor microenvironment. **Figure 4. 1**, shows a schematic view of the IH platform, which allows us to accurately position a smaller hydrogel in the center of a larger one. In contrast to the prototype in Chapter 2, the position of each hydrogel can be accurately

controlled which would allow us to separate hydrogels from the interface, extract cells from each hydrogel and study them separately (using single cell RNA sequencing).

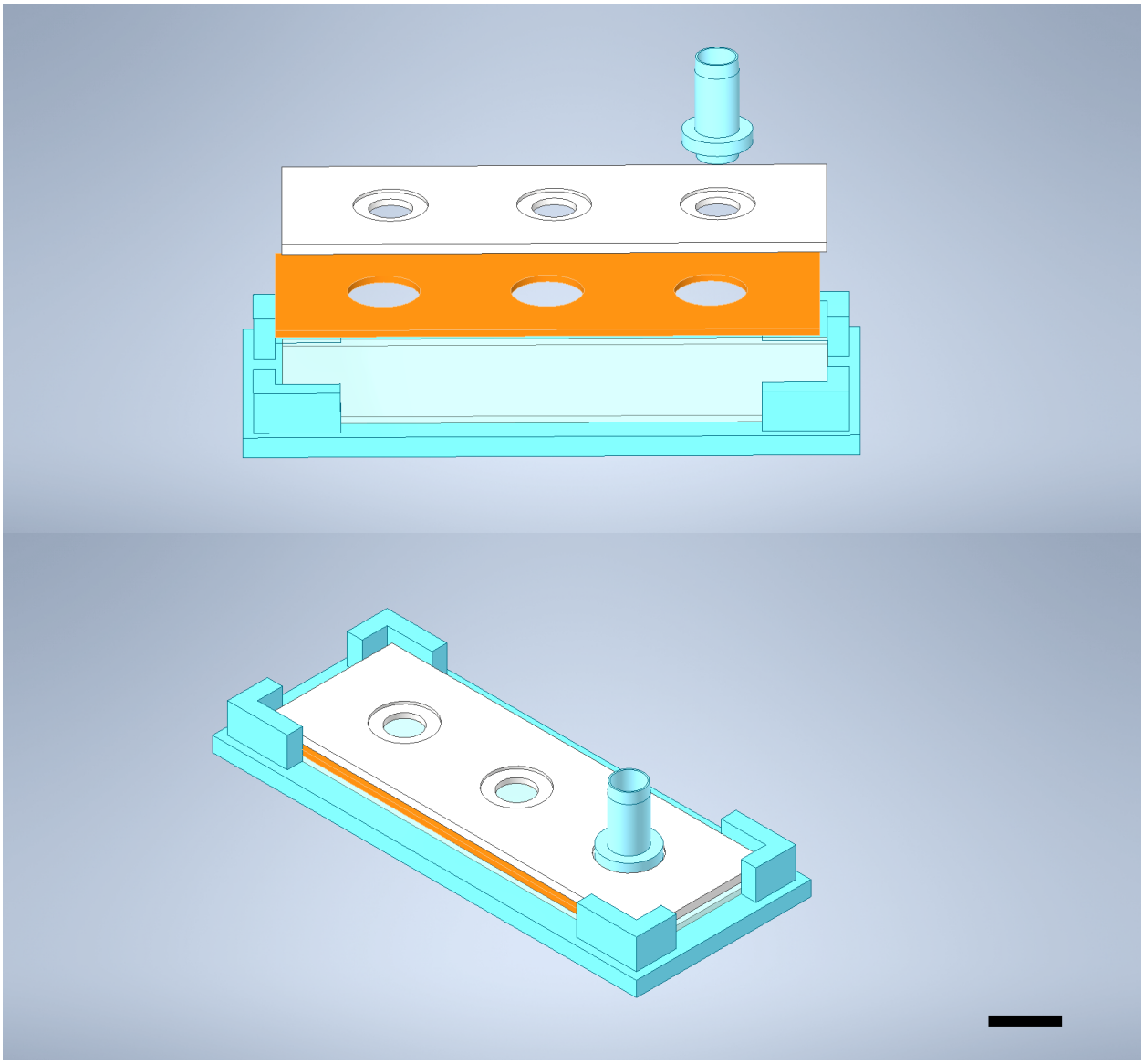

Figure 4. 1: Schematic representation of a new Interfacing hydrogel system. (Top) deconstructed view and (Bottom) assembled view. (Scale bar = 10mm)

We used the thiol-ene photochemical technique in conjunction with the IH system to form concentric hydrogels in which mechanical properties of each hydrogel could be tuned separately. A concentric IH hydrogel in which a stiff inner hydrogel (mimicking tumor) was embedded in a soft outer hydrogel (mimicking surrounding non-cancerous brain tissue) (**Figure 4. 2**). We performed micro-compression studies using atomic force microscopy (AFM) to measure mechanical properties of various locations along the X-axis. As can be seen, the center (x=0) with modulus of around 30 kPa is around 10-15X stiffer than the softer side (x=3500) with modulus of around 2-3 kPa. Meanwhile the interface (x=2000) is only 3X softer than the core with modulus of 10 kPa. These results clearly show the capability of the IH system to mimic our data from xenografts studies (**Figure 3. 1**).

We encapsulated GBM cells in IH constructs of different interfaces. To mimic a GBM tumor interfacing with the adjacent non-cancerous tissue, GBM cells were encapsulated in a stiff inner hydrogel. Then the inner gel was embedded in a soft hydrogel (Stiff-Soft IH). As a control, GBM cells were encapsulated in a soft inner hydrogel and then embedded in a soft hydrogel (Soft-Soft IH). We did not encapsulate cells in Soft-Stiff and Stiff-Stiff IH since based on our previous data, GBM cells do not show any migratory phenotype when encapsulated in a stiff microenvironment. Interestingly, cells encapsulated in Stiff-Soft IH construct exhibited a faster migratory behavior where they migrated further away from the interface (**Figure 4. 3**). We will use these constructs to separate the migratory population from the stationary ones. Then, we will perform single cell RNA-sequencing to study differential gene expressions in two cell populations.

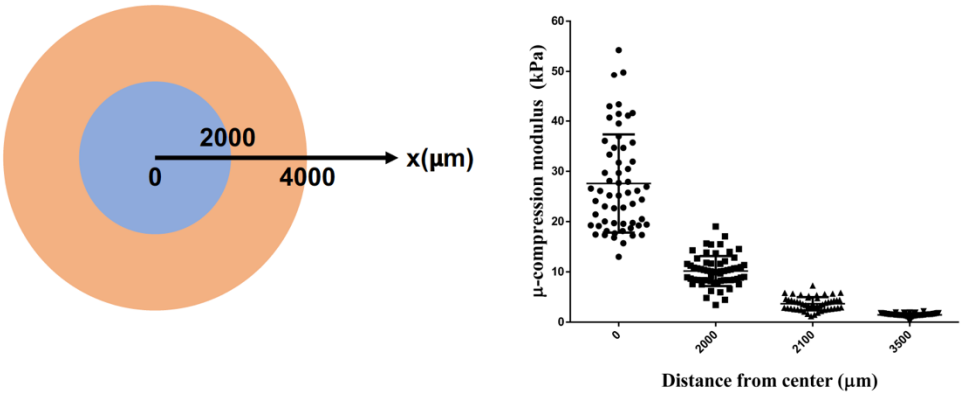

Figure 4. 2: The interfacing gel can be used to mimic the stiffness transition of the microenvironment in a GBM tumor. (left) the inside hydrogel with radius of 2mm was actuarily formed in a larger hydrogel. (right) AFM micro-compression measurements from the center of two hydrogels (0) to the outer hydrogel shows the ability of interfacing hydrogels to mimic the mechanical transition in GBM microenvironment.

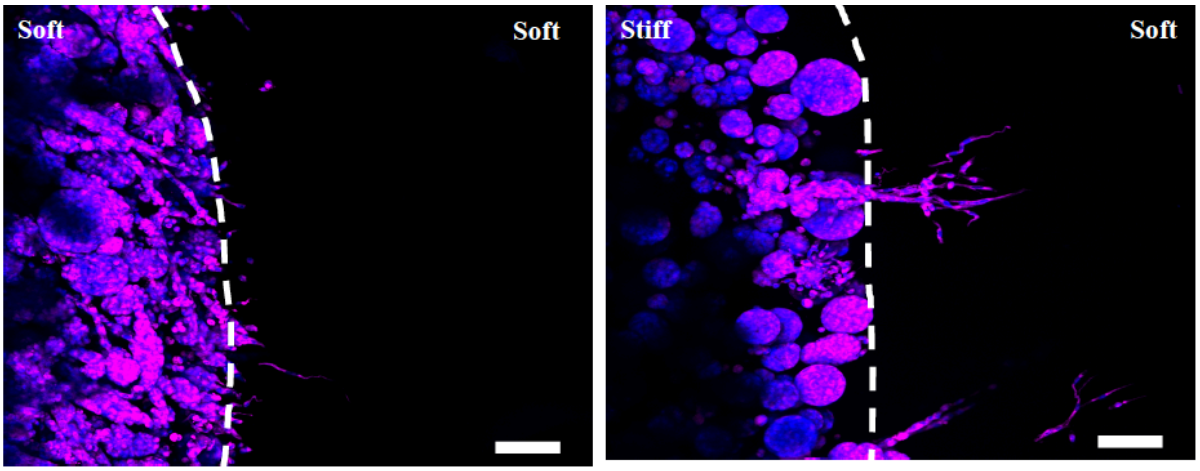

Figure 4. 3: GBM cells were encapsulated in the inner hydrogel. (Left) GBM cells encapsulated in an IH construct where both inner and outer hydrogel were soft. (right) GBM encapsulation in a tumor mimicking IH where the inner gel was stiffer than the outer gel. In the tumor mimicking IH, GBM cells migrated faster and further away from the interface. (Red=Phalloidin actin staining, Blue= Hoechst nuclei staining) (Scale bar= 250 μm)

Stress-relaxing hydrogels

In Chapter 3, we presented a thiol-ene photochemical method to fabricate hydrogels with a wide range of mechanical properties. We have observed that GBM cells only show migratory behavior in soft hydrogels while in stiff hydrogels no migration was noticed (**Figure 3. 8**). Beside the differences in pH and enzyme activity (discussed in Chapter 3), differences in GBM migration when cultured in soft and stiff hydrogels could be partially attributed to the elastic nature of our hydrogels. As can be seen in **Figure 4. 4**, based on dynamic modulus measurements (with a rheometer), while increasing crosslink density (via increasing SH concentration) increases the storage moduli (G') by 10-fold, it only increases the loss moduli of hydrogels (G") by 3-fold. This mismatch would make the hydrogels more elastic than viscous in stiffer conditions. The viscosity of a hydrogel is an important parameter for cells to be able to move in between hydrogel network, since it would allow cells to deform the hydrogel network[256].

To solve this, we have been working on a stress-relaxing hydrogel system based on imine bond formation between hydrazide and aldehyde functional groups. A hydrogel network formed from this reaction is shown to be stress-relaxing in which encapsulated cells are able to move through the hydrogel network by locally deforming imine bonds. The imine bonds would form quickly enough to be suitable for cell-laden hydrogel formation[257,258].

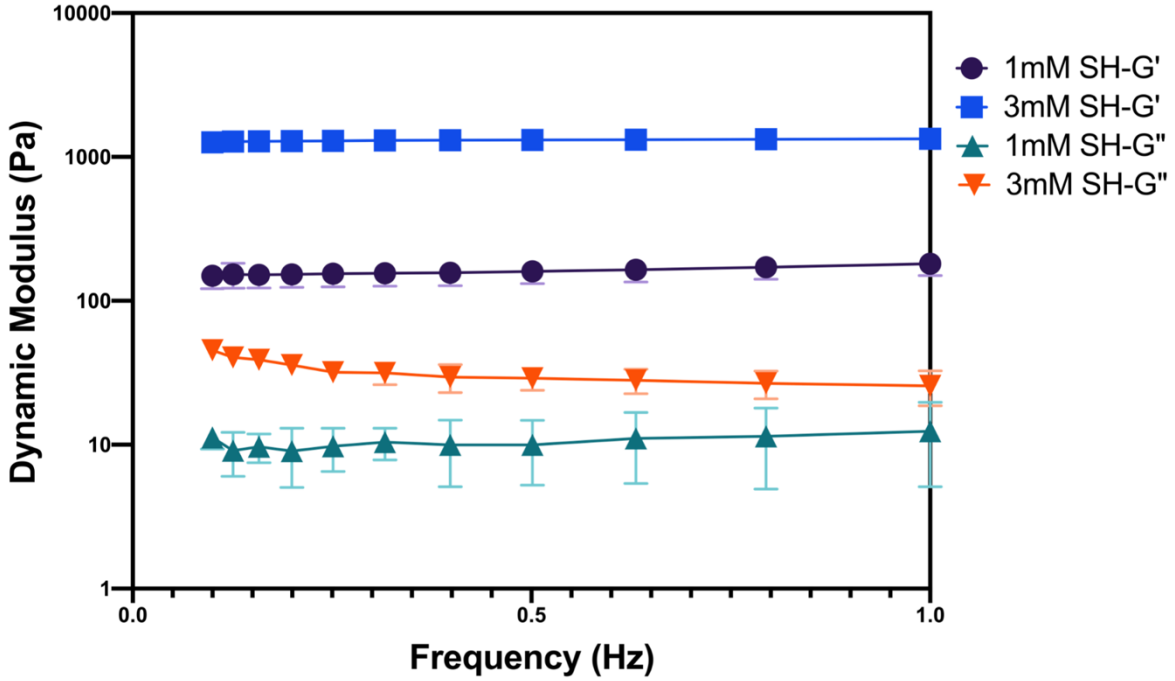

Figure 4. 4: Rheology data of soft and stiff hydrogels.

To prepare necessary precursors for hydrogel formation, we are functionalizing HA with a hydrazide group (HA-Hyd). In addition, we will add hydrazide functional groups on a 4-arm PEG to achieve 4 arm PEG-hydrazide (PEG-Hyd). Hydrogels will be formed by mixing the HA-Hyd+PEG-Hyd solution with a solution of PEG-dialdehyde. To perform these steps, we will use two separate methods:

EDC/NHS conjugation

We are using the EDC/NHS chemistry to conjugate adipic acid dihydrazide (ADH) on HA carboxyl groups (**Figure 4. 5.A**). This aqueous reaction is similar to what we have used to functionalize HA with thiols (SH) (**Figure 2. 1**). To assess the extent of modification, we will use TNBS (2,4,6-trinitrobenzene sulfonic acid) assay. So far, we have successfully achieved 14% modification on HA. Same method will be used to conjugate ADH to arms of a 4-arm PEG-acetic acid (PEG-COOH) (**Figure 4. 5.B**). So far, this method only yielded 50% modification success. To increase the yield, we will need to use higher molar ratio is EDC/NHS/ADH and/or perform the reaction in an anhydrous organic solvent (like DMSO) to prevent EDC/NHS hydrolysis.

Michael-addition chemistry

As an alternative method, we will use Michael-addition chemistry to functionalize HA and PEG. To do so, we will conjugate a maleimide-PEG-hydrazide to thiolated HA (HA-SH) through the maleimide-thiol click chemistry (**Figure 4. 6.A**). Same linker will be used to modify a 4-arm PEG-SH (**Figure 4. 6.B**).

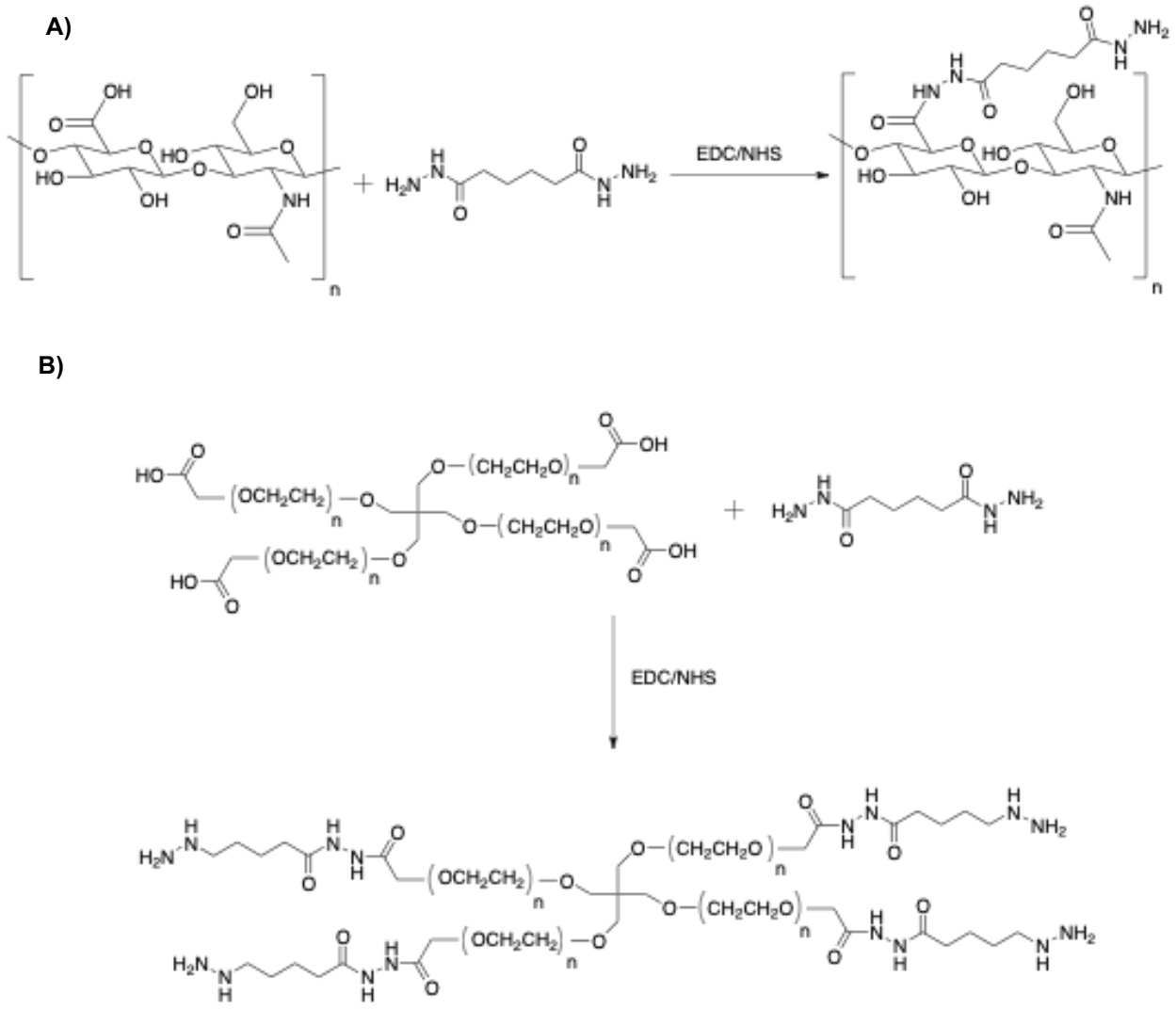

Figure 4. 5: EDC/NHS modification of A) HA and B)4-arm PEG-COOH to add hydrazide functional groups.

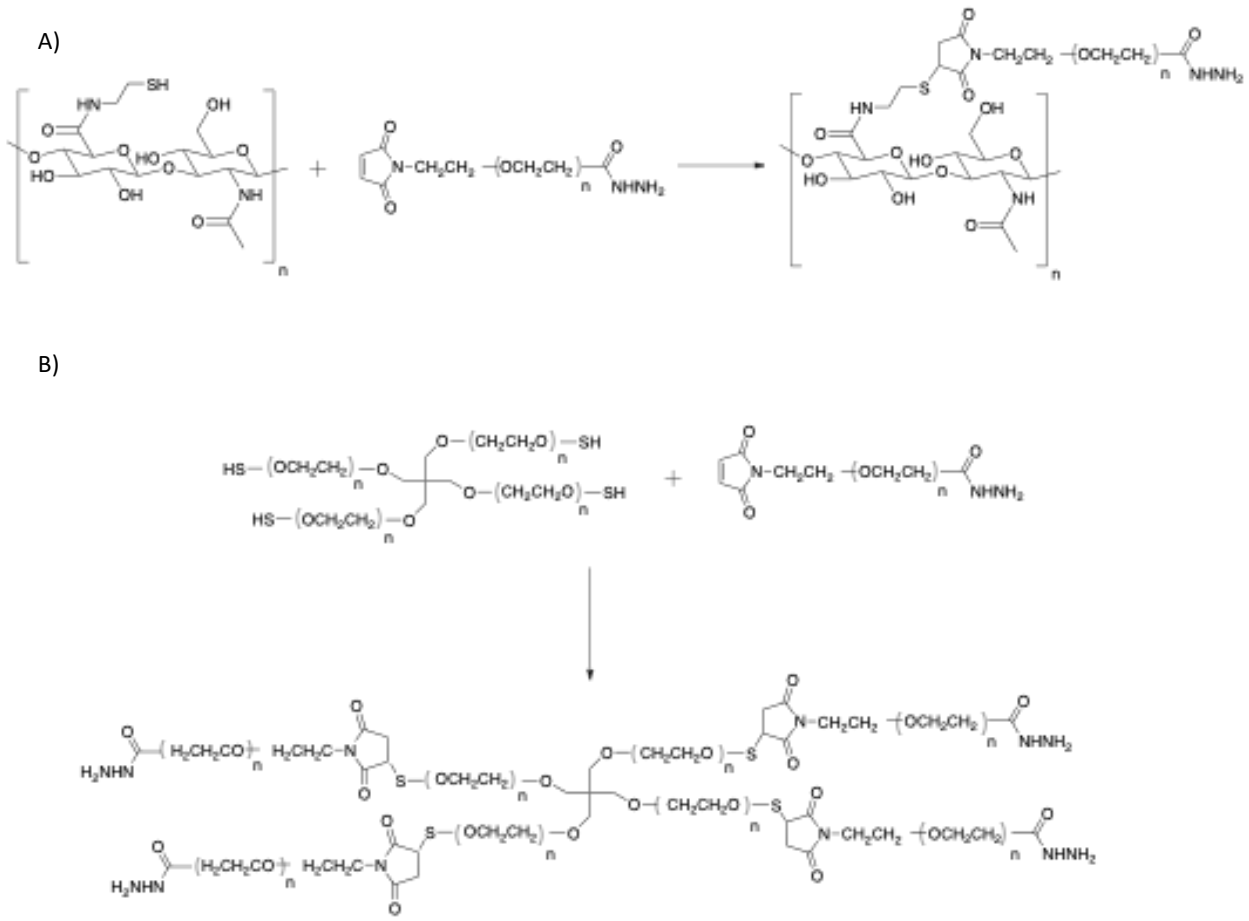

Figure 4. 6: Michael-addition click chemistry modification of A) HA-SH and B)4 arm PEG-SH to introduce hydrazide functional group

Chapter 5: Broader impact

For any type of disease, drug development is a time-consuming, expensive, and labor-intensive process that has many steps including target identification, compound discovery, preclinical verification, and clinical trials[259]. One major step in this procedure is high-throughput (HTP) characterization of pharmaceutical targets and agents. Currently, most HTP assessments are done on 2D-cultured cells (i.e., cells cultured in a well plate). Many studies[260,261], as well as our previous work[152,262], have shown the necessity of 3D culture models with biomimetic properties for a better drug response. For example, we showed that patient-derived GBM cells encapsulated in the 3D HA hydrogels better exhibit the acquired resistance to the EGFR inhibition than gliomasphere culture[152].

Therefore, we believe that integrating our 3D hyaluronic acid (HA)-based hydrogels into an HTP system can fill the technological gap in preclinical studies. Relatively low viscosity of the hydrogel precursor solution, tunability of chemical and physical properties, and the on-demand hydrogel formation via photo-activated thiol-ene chemistry make our HA system a suitable candidate for integration into available HTP systems (such as MANTIS® liquid handler, Formulatrix). The integration of HA hydrogels with HTP systems would allow researchers to investigate the outcome of therapeutic agents, individually and in combination, on various GBM patient-derived cell lines in a biomimetic microenvironment. These studies normally require thousands of samples, which is impractical to do manually.

Another rapidly growing field to use the HA-based HTP system is personalized medicine. The goal of the personalized medicine is to develop therapeutic regimens for targeted group of people whom the traditional methods have failed. The belief is that as

each individual possess unique molecular, and physiological characteristics, tailored clinical intervention may be required[263]. In GBM, current standard treatment includes maximal surgical removal followed by radiotherapy and concomitant temozolomide (TMZ) with further adjuvant therapies like bevacizumab[264,265]. We discussed the different subtypes and various unique nuances in each patient-derived cell line (Chapter 1). This unique molecular signature in each subtype/group emphasizes on a need for a more tailored therapeutics regimen. Recent advancements in nucleic acid sequencing methods has enabled researchers to characterize GBM molecular signatures more accurately and driven the field to more personalized therapeutic approaches[266]. This has led to the development of a new generation of GBM therapeutics based on molecular inhibitors, antibodies, *etc*. As sequencing might not be an option for each individual GBM patient, the HA-based HTP system could be beneficial to examine the efficacy of these new drugs cells derived from a specific patient's tumor. In addition, acquired resistance to therapeutic agents is a complication that cannot be predicted from 2D HTP screens (Due to lack of a 3D microenvironment)[262]. On the other hand, the HA hydrogel platform has shown the capability in conserving the GBM therapeutic resistance[152]. The HA HTP platform potentially could overcome these by screening the patient-specific GBM cells' response (efficacy, resistance etc.) to a wide range of available therapeutic agents to provide a better insight on the most applicable drug regimen for each patient.

Working toward a personalized medicine in GBM, patients' GBM cells can be obtained from surgical biopsies or after the surgical removal of the tumor. These cells would be directly encapsulated in HA hydrogels through a HTP system. Patient-specific drug responses would be obtained by comparing the GBM cell proliferation, survival and

acquisition of resistance of multiple known GBM therapeutic agents. The outcome then could be used to design a patient-specific tailored drug regimen that is most effective against the specific patient tumor. Through this process, one can potentially determine the most effective drug combination as well as the lowest effective dosage for an individual patient. The personalized drug regimen could substitute the generic TMZ administration after the surgical removal of the tumor while being administered concurrently with the radiation.

Chapter 6: Bibliography

1. Ostrom, Q. T. *et al.* CBTRUS statistical report: Primary brain and other central nervous system tumors diagnosed in the United States in 2009-2013. *Neuro. Oncol.* **18**, v1–v75 (2016).

2. Tykocki, T. & Eltayeb, M. Ten-year survival in glioblastoma. A systematic review. *J. Clin. Neurosci.* **54**, 7–13 (2018).

3. McLendon, R. *et al.* Comprehensive genomic characterization defines human glioblastoma genes and core pathways. *Nature* **455**, 1061–1068 (2008).

4. Holland, E. C. *et al.* Combined activation of Ras and Akt in neural progenitors induces glioblastoma formation in mice. *Nat. Genet.* **25**, 55–57 (2000).

5. Sidaway, P. CNS cancer: Glioblastoma subtypes revisited. *Nat. Rev. Clin. Oncol.* **14**, 587 (2017).

6. Wang, Q. *et al.* Tumor Evolution of Glioma-Intrinsic Gene Expression Subtypes Associates with Immunological Changes in the Microenvironment. *Cancer Cell* **32**, 42-56.e6 (2017).

7. Huang, J. *et al.* Isocitrate dehydrogenase mutations in glioma: From basic discovery to therapeutics development. *Front. Oncol.* **9**, 1–7 (2019).

8. Zamecnik, J. The extracellular space and matrix of gliomas. *Acta Neuropathol.* **110**, 435–442 (2005).

9. Hsu, E. *et al.* Bone marrow metastasis in astrocytic gliomata. *J. Neurooncol.* **37**, 285–293 (1998).

10. Bellail, A. C., Hunter, S. B., Brat, D. J., Tan, C. & Van Meir, E. G. Microregional

extracellular matrix heterogeneity in brain modulates glioma cell invasion. *Int. J. Biochem. Cell Biol.* **36**, 1046–1069 (2004).

11. Virga, J. *et al.* Extracellular matrix differences in glioblastoma patients with different prognoses. *Oncol. Lett.* **17**, 797–806 (2019).

12. Charles, N. A., Holland, E. C., Gilbertson, R., Glass, R. & Kettenmann, H. The brain tumor microenvironment. *Glia* **59**, 1169–1180 (2011).

13. Day, A. J. & Prestwich, G. D. Hyaluronan-binding proteins: Tying up the giant. *J. Biol. Chem.* **277**, 4585–4588 (2002).

14. Jain, R. K. *et al.* Angiogenesis in brain tumours. *Nat. Rev. Neurosci.* **8**, 610–622 (2007).

15. Misra, S., Hascall, V. C., Markwald, R. R. & Ghatak, S. Interactions between hyaluronan and its receptors (CD44, RHAMM) regulate the activities of inflammation and cancer. *Front. Immunol.* **6**, (2015).

16. Varga, I. *et al.* Expression of invasion-related extracellular matrix molecules in human glioblastoma versus intracerebral lung adenocarcinoma metastasis. *Zentralbl. Neurochir.* **71**, 173–180 (2010).

17. Zhang, H., Kelly, G., Zeritlo, C., Jaworski, D. M. & Hockfield, S. Expression of a cleaved brain-specific extracellular matrix protein mediates glioma cell invasion in vivo. *J. Neurosci.* **18**, 2370–2376 (1998).

18. Mooney, K. L. *et al.* The role of CD44 in glioblastoma multiforme. *J. Clin. Neurosci.* **34**, 1–5 (2016).

19. Si, D., Yin, F., Peng, J. & Zhang, G. High Expression of CD44 Predicts a Poor

Prognosis in Glioblastomas. *Cancer Manag. Res.* **12**, 769–775 (2020).

20. Xu, Y., Stamenkovic, I. & Yu, Q. CD44 attenuates activation of the Hippo signaling pathway and is a prime therapeutic target for glioblastoma. *Cancer Res.* **70**, 2455–2464 (2010).

21. Herishanu, Y. *et al.* Activation of CD44, a receptor for extracellular matrix components, protects chronic lymphocytic leukemia cells from spontaneous and drug induced apoptosis through MCL-1. *Leuk. Lymphoma* **52**, 1758–1769 (2011).

22. Hao, J. *et al.* Co-expression of CD147 (EMMPRIN), CD44v3-10, MDR1 and monocarboxylate transporters is associated with prostate cancer drug resistance and progression. *Br. J. Cancer* **103**, 1008–1018 (2010).

23. Chopra, A. *et al.* Augmentation of integrin-mediated mechanotransduction by hyaluronic acid. *Biomaterials* **35**, 71–82 (2014).

24. Tschumperlin, D. J. *et al.* Mechanotransduction through growth-factor shedding into the extracellular space. *Nature* **429**, 83–86 (2004).

25. Bello, L. *et al.* Low-dose chemotherapy combined with an antiangiogenic drug reduces human glioma growth in vivo. *Cancer Res.* **61**, 7501–7506 (2001).

26. Zhang, B. *et al.* Biodegradable scaffold with built-in vasculature for organ-on-a-chip engineering and direct surgical anastomosis. *Nat. Mater.* **15**, 669–678 (2016).

27. Winkler, F. *et al.* Imaging glioma cell invasion in vivo reveals mechanisms of dissemination and peritumoral angiogenesis. *Glia* **57**, 1306–1315 (2009).

28. Watkins, S. *et al.* Disruption of astrocyte-vascular coupling and the blood-brain

barrier by invading glioma cells. *Nat. Commun.* **5**, (2014).

29. Wade, A. *et al.* Proteoglycans and their roles in brain cancer. *FEBS J.* **280**, 2399–2417 (2013).

30. Arslan, F. *et al.* The role of versican isoforms V0/V1 in glioma migration mediated by transforming growth factor-β2. *Br. J. Cancer* **96**, 1560–1568 (2007).

31. Hu, B., Kong, L. L., Matthews, R. T. & Viapiano, M. S. The proteoglycan brevican binds to fibronectin after proteolytic cleavage and promotes glioma cell motility. *J. Biol. Chem.* **283**, 24848–24859 (2008).

32. Phillips, J. J. *et al.* Heparan sulfate sulfatase SULF2 regulates PDGFRα signaling and growth in human and mouse malignant glioma. *J. Clin. Invest.* **122**, 911–922 (2012).

33. Hoelzinger, D. B., Demuth, T. & Berens, M. E. Autocrine factors that sustain glioma invasion and paracrine biology in the brain microenvironment. *J. Natl. Cancer Inst.* **99**, 1583–1593 (2007).

34. Zhu, V. F., Yang, J., LeBrun, D. G. & Li, M. Understanding the role of cytokines in Glioblastoma Multiforme pathogenesis. *Cancer Lett.* **316**, 139–150 (2012).

35. Nazarenko, I. *et al.* PDGF and PDGF receptors in glioma. *Ups. J. Med. Sci.* **117**, 99–112 (2012).

36. Huang, L. & Fu, L. Mechanisms of resistance to EGFR tyrosine kinase inhibitors. *Acta Pharm. Sin. B* **5**, 390–401 (2015).

37. Hong, S. I., Park, M. J., Kim, M. S., Rhee, C. H. & Lee, S. H. PTEN suppresses hyaluronic acid-induced matrix metalloproteinase-9 expression in U87MG

glioblastoma cells through focal adhesion kinase dephosphorylation. *Cancer Res.* **62**, 6318–6322 (2002).

38. Pedron, S., Becka, E. & Harley, B. A. C. Regulation of glioma cell phenotype in 3D matrices by hyaluronic acid. *Biomaterials* **34**, 7408–7417 (2013).

39. Pedron, S., Becka, E. & Harley, B. A. Spatially gradated hydrogel platform as a 3D engineered tumor microenvironment. *Adv. Mater.* **27**, 1567–1572 (2015).

40. Tsatas, D., Kanagasundaram, V., Kaye, A. & Novak, U. EGF receptor modifies cellular responses to hyaluronan in glioblastoma cell lines. *J. Clin. Neurosci.* **9**, 282–288 (2002).

41. Reynés, G. *et al.* Circulating markers of angiogenesis, inflammation, and coagulation in patients with glioblastoma. *J. Neurooncol.* **102**, 35–41 (2011).

42. Bruna, A. *et al.* High TGFβ-Smad Activity Confers Poor Prognosis in Glioma Patients and Promotes Cell Proliferation Depending on the Methylation of the PDGF-B Gene. *Cancer Cell* **11**, 147–160 (2007).

43. Dieterich, L. C. *et al.* Transcriptional profiling of human glioblastoma vessels indicates a key role of VEGF-A and TGFβ2 in vascular abnormalization. *J. Pathol.* **228**, 378–390 (2012).

44. Platten, M., Wick, W. & Weller, M. Malignant glioma biology: Role for TGF-β in growth, motility, angiogenesis, and immune escape. *Microsc. Res. Tech.* **52**, 401–410 (2001).

45. Thomas, D. A. & Massagué, J. TGF-β directly targets cytotoxic T cell functions during tumor evasion of immune surveillance. *Cancer Cell* **8**, 369–380 (2005).

46. Martinez, F. O. & Gordon, S. The M1 and M2 paradigm of macrophage activation: Time for reassessment. *F1000Prime Rep.* **6**, 1–13 (2014).

47. Novak, U., Stylli, S. S., Kaye, A. H. & Lepperdingerm, G. Hyaluronidase-2 Overexpression Accelerates Intracerebral but not Subcutaneous Tumor Formation of Murine Astrocytoma Cells. *Cancer Res.* **59**, 6246 LP – 6250 (1999).

48. Campo, G. M. *et al.* Molecular size hyaluronan differently modulates toll-like receptor-4 in LPS-induced inflammation in mouse chondrocytes. *Biochimie* **92**, 204–215 (2010).

49. Powell, J. D. & Horton, M. R. Threat matrix: Low-molecular-weight hyaluronan (HA) as a danger signal. *Immunol. Res.* **31**, 207–218 (2005).

50. Wu, M. *et al.* A novel role of low molecular weight hyaluronan in breast cancer metastasis. *FASEB J.* **29**, 1290–1298 (2015).

51. Hagemann, C. A complete compilation of matrix metalloproteinase expression in human malignant gliomas. *World J. Clin. Oncol.* **3**, 67 (2012).

52. Le, D. M. *et al.* Exploitation of astrocytes by glioma cells to facilitate invasiveness: A mechanism involving matrix metalloproteinase-2 and the urokinase-type plasminogen activator-plasmin cascade. *J. Neurosci.* **23**, 4034–4043 (2003).

53. Coniglio, S. J. & Segall, J. E. Review: Molecular mechanism of microglia stimulated glioblastoma invasion. *Matrix Biol.* **32**, 372–380 (2013).

54. Jäälinojä, J., Herva, R., Korpela, M., Höyhtyä, M. & Turpeenniemi-Hujanen, T. Matrix metalloproteinase 2 (MMP-2) immunoreactive protein is associated with poor grade and survival in brain neoplasms. *J. Neurooncol.* **46**, 81–90 (2000).

55. Li, Q. *et al.* Comparative analysis of matrix metalloproteinase family members reveals that MMP9 predicts survival and response to temozolomide in patients with primary glioblastoma. *PLoS One* **11**, 1–15 (2016).

56. Misko, A., Ferguson, T. & Notterpek, L. Matrix metalloproteinase mediated degradation of basement membrane proteins in Trembler J neuropathy nerves. *J. Neurochem.* **83**, 885–894 (2002).

57. Brooks, P. C. *et al.* Localization of matrix metalloproteinase MMP-2 to the cell surface by interaction with integral αvβ3. *FASEB J.* **10**, 683–693 (1996).

58. Lakka, S. S. *et al.* Inhibition of cathepsin B and MMP-9 gene expression in glioblastoma cell line via RNA interference reduces tumor cell invasion, tumor growth and angiogenesis. *Oncogene* **23**, 4681–4689 (2004).

59. Yu, Q. & Stamenkovic, I. Cell surface-localized matrix metalloproteinase-9 proteolytically activates TGF-β and promotes tumor invasion and angiogenesis. *Genes Dev.* **14**, 163–176 (2000).

60. Engler, A. J., Sen, S., Sweeney, H. L. & Discher, D. E. Matrix Elasticity Directs Stem Cell Lineage Specification. *Cell* **126**, 677–689 (2006).

61. Bouchonville, N. *et al.* AFM mapping of the elastic properties of brain tissue reveals kPa μm-1 gradients of rigidity. *Soft Matter* **12**, 6232–6239 (2016).

62. Kim, Y. & Kumar, S. CD44-mediated adhesion to hyaluronic acid contributes to mechanosensing and invasive motility. *Mol. Cancer Res.* **12**, 1416–29 (2014).

63. Lamontagne, C. A. & Grandbois, M. PKC-induced stiffening of hyaluronan/CD44 linkage; local force measurements on glioma cells. *Exp. Cell Res.* **314**, 227–236

(2008).

64. DuFort, C. C., Paszek, M. J. & Weaver, V. M. Balancing forces: architectural control of mechanotransduction. *Nat. Rev. Mol. Cell Biol.* **12**, 308 (2011).

65. Sharili, A. S. & Connelly, J. T. Nucleocytoplasmic shuttling: A common theme in mechanotransduction. *Biochem. Soc. Trans.* **42**, 645–649 (2014).

66. Umesh, V., Rape, A. D., Ulrich, T. A. & Kumar, S. Microenvironmental stiffness enhances glioma cell proliferation by stimulating epidermal growth factor receptor signaling. *PLoS One* **9**, 1–8 (2014).

67. Zustiak, S. P. *et al.* Three-dimensional matrix stiffness and adhesive ligands affect cancer cell response to toxins. *Biotechnol. Bioeng.* **113**, 443–452 (2016).

68. Grundy, T. J. *et al.* Differential response of patient-derived primary glioblastoma cells to environmental stiffness. *Sci. Rep.* **6**, 23353 (2016).

69. Pathak, A. & Kumar, S. Independent regulation of tumor cell migration by matrix stiffness and confinement. *Proc. Natl. Acad. Sci. U. S. A.* **109**, 10334–10339 (2012).

70. Rape, A. D., Zibinsky, M., Murthy, N. & Kumar, S. A synthetic hydrogel for the high-throughput study of cell-ECM interactions. *Nat. Commun.* **6**, 8129 (2015).

71. Ulrich, T. A., Jain, A., Tanner, K., MacKay, J. L. & Kumar, S. Probing cellular mechanobiology in three-dimensional culture with collagen-agarose matrices. *Biomaterials* **31**, 1875–1884 (2010).

72. Netti, P. A., Berk, D. A., Swartz, M. A., Grodzinsky, A. J. & Jain, R. K. Role of extracellular matrix assembly in interstitial transport in solid tumors. *Cancer Res.*

60, 2497–2503 (2000).

73. Netti, P. A., Berk, D. A., Swartz, M. A., Grodzinsky, A. J. & Jain, R. K. Role of Extracellular Matrix Assembly in Interstitial Transport in Solid Tumors Role of Extracellular Matrix Assembly in Interstitial Transport in Solid Tumors 1. 2497–2503 (2000).

74. Pogoda, K. *et al.* Compression stiffening of brain and its effect on mechanosensing by glioma cells. *New J. Phys.* **16**, (2014).

75. Umesh, V., Rape, A. D., Ulrich, T. A. & Kumar, S. Microenvironmental Stiffness Enhances Glioma Cell Proliferation by Stimulating Epidermal Growth Factor Receptor Signaling. *PLoS One* **9**, e101771 (2014).

76. Schregel, K. *et al.* Magnetic Resonance Elastography reveals effects of anti-angiogenic glioblastoma treatment on tumor stiffness and captures progression in an orthotopic mouse model. *Cancer Imaging* **20**, 35 (2020).

77. Lin, H. H. *et al.* Mechanical phenotype of cancer cells: Cell softening and loss of stiffness sensing. *Oncotarget* **6**, 20946–20958 (2015).

78. Nguyen, A. V. *et al.* Stiffness of pancreatic cancer cells is associated with increased invasive potential. *Integr. Biol. (United Kingdom)* **8**, 1232–1245 (2016).

79. Shivashankar, G. V. Mechanosignaling to the cell nucleus and gene regulation. *Annu. Rev. Biophys.* **40**, 361–378 (2011).

80. Gritsenko, P. G., Ilina, O. & Friedl, P. Interstitial guidance of cancer invasion. *J. Pathol.* **226**, 185–199 (2012).

81. Munson, J. M. & Shieh, A. C. Interstitial fluid flow in cancer: Implications for

disease progression and treatment. *Cancer Manag. Res.* **6**, 317–318 (2014).

82. Munson, J. M., Bellamkonda, R. V & Swartz, M. A. Interstitial Flow in a 3D Microenvironment Increases Glioma Invasion by a CXCR4-Dependent Mechanism. *Cancer Res.* **73**, 1536 LP – 1546 (2013).

83. Kingsmore, K. M. *et al.* Interstitial flow differentially increases patient-derived glioblastoma stem cell invasion: Via CXCR4, CXCL12, and CD44-mediated mechanisms. *Integr. Biol. (United Kingdom)* **8**, 1246–1260 (2016).

84. Gielen, P. R. *et al.* Connexin43 confers Temozolomide resistance in human glioma cells by modulating the mitochondrial apoptosis pathway. *Neuropharmacology* **75**, 539–548 (2013).

85. Péglion, F. & Etienne-Manneville, S. N-cadherin expression level as a critical indicator of invasion in non-epithelial tumors. *Cell Adhes. Migr.* **6**, 327–332 (2012).

86. Camand, E., Peglion, F., Osmani, N., Sanson, M. & Etienne-Manneville, S. N-cadherin expression level modulates integrin-mediated polarity and strongly impacts on the speed and directionality of glial cell migration. *J. Cell Sci.* **125**, 844–857 (2012).

87. Shinoura, N. *et al.* Expression of N-cadherin and α-catenin in astrocytomas and glioblastomas. *Br. J. Cancer* **72**, 627–633 (1995).

88. Yuan, X. *et al.* Isolation of cancer stem cells from adult glioblastoma multiforme. *Oncogene* **23**, 9392–9400 (2004).

89. Heddleston, J. M. *et al.* Glioma Stem Cell Maintenance: The Role of the

Microenvironment. *Current Pharmaceutical Design* **17**, 2386–2401 (2011).

90. Lathia, J. D. *et al.* Laminin alpha 2 enables glioblastoma stem cell growth. *Ann. Neurol.* **72**, 766–778 (2012).

91. Hitomi, M. *et al.* Differential Connexin Function Enhances Self-Renewal in Glioblastoma. *Cell Rep.* **11**, 1031–1042 (2015).

92. Seano, G. & Jain, R. K. Vessel co-option in glioblastoma: emerging insights and opportunities. *Angiogenesis* **23**, 9–16 (2020).

93. Das, S. & Marsden, P. A. Angiogenesis in glioblastoma. *N. Engl. J. Med.* **369**, 1561–1563 (2013).

94. Hardee, M. E. & Zagzag, D. Mechanisms of glioma-associated neovascularization. *Am. J. Pathol.* **181**, 1126–1141 (2012).

95. Caspani, E. M., Crossley, P. H., Redondo-Garcia, C. & Martinez, S. Glioblastoma: A pathogenic crosstalk between tumor cells and pericytes. *PLoS One* **9**, (2014).

96. Soda, Y. *et al.* Transdifferentiation of glioblastoma cells into vascular endothelial cells. *Proc. Natl. Acad. Sci. U. S. A.* **108**, 4274–4280 (2011).

97. Cheng, L. *et al.* Glioblastoma stem cells generate vascular pericytes to support vessel function and tumor growth. *Cell* **153**, 139–152 (2013).

98. Calabrese, C. *et al.* A Perivascular Niche for Brain Tumor Stem Cells. *Cancer Cell* **11**, 69–82 (2007).

99. Infanger, D. W. *et al.* Glioblastoma stem cells are regulated by interleukin-8 signaling in a tumoral perivascular niche. *Cancer Res.* **73**, 7079–7089 (2013).

100. Pietras, A. *et al.* Osteopontin-CD44 signaling in the glioma perivascular niche enhances cancer stem cell phenotypes and promotes aggressive tumor growth. *Cell Stem Cell* **14**, 357–369 (2014).

101. Schneider, S. W. *et al.* Glioblastoma cells release factors that disrupt blood-brain barrier features. *Acta Neuropathol.* **107**, 272–276 (2004).

102. Lathia, J. D. *et al.* Integrin Alpha 6 regulates glioblastoma stem cells. *Cell Stem Cell* **6**, 421–432 (2010).

103. Allen, M., Bjerke, M., Edlund, H., Nelander, S. & Westermark, B. Origin of the U87MG glioma cell line: Good news and bad news. *Sci. Transl. Med.* **8**, (2016).

104. Huszthy, P. C. *et al.* Pitfalls and Perspectives. *Neuro. Oncol.* **14**, 979–993 (2012).

105. Zheng, X. *et al.* Proteomic analysis for the assessment of different lots of fetal bovine serum as a raw material for cell culture. Part IV. Application of proteomics to the manufacture of biological drugs. *Biotechnol. Prog.* **22**, 1294–1300 (2006).

106. Hughes, C. S., Postovit, L. M. & Lajoie, G. A. Matrigel: a complex protein mixture required for optimal growth of cell culture. *Proteomics* **10**, 1886–1890 (2010).

107. Ledur, P. F., Onzi, G. R., Zong, H. & Lenz, G. Culture conditions defining glioblastoma cells behavior: what is the impact for novel discoveries? *Oncotarget* **8**, 69185–69197 (2017).

108. Lee, J. *et al.* Tumor stem cells derived from glioblastomas cultured in bFGF and EGF more closely mirror the phenotype and genotype of primary tumors than do serum-cultured cell lines. *Cancer Cell* **9**, 391–403 (2006).

109. Sarkaria, J. N. *et al.* Identification of molecular characteristics correlated with

glioblastoma sensitivity to EGFR kinase inhibition through use of an intracranial xenograft test panel. *Mol. Cancer Ther.* **6**, 1167–1174 (2007).

110. Wakimoto, H. *et al.* Maintenance of primary tumor phenotype and genotype in glioblastoma stem cells. *Neuro. Oncol.* **14**, 132–144 (2012).

111. Zhang, P., Xia, Q., Liu, L., Li, S. & Dong, L. Current Opinion on Molecular Characterization for GBM Classification in Guiding Clinical Diagnosis, Prognosis, and Therapy . *Frontiers in Molecular Biosciences* **7**, 241 (2020).

112. Iwadate, Y. Epithelial-mesenchymal transition in glioblastoma progression. *Oncol. Lett.* **11**, 1615–1620 (2016).

113. Li, R. *et al.* Genetic and clinical characteristics of primary and secondary glioblastoma is associated with differential molecular subtype distribution. *Oncotarget* **6**, 7318–7324 (2015).

114. Codrici, E., Enciu, A. M., Popescu, I. D., Mihai, S. & Tanase, C. Glioma Stem Cells and Their Microenvironments: Providers of Challenging Therapeutic Targets. *Stem Cells Int.* **2016**, (2016).

115. Hubert, C. G. *et al.* A three-dimensional organoid culture system derived from human glioblastomas recapitulates the hypoxic gradients and cancer stem cell heterogeneity of tumors found in vivo. *Cancer Res.* **76**, 2465–2477 (2016).

116. Oh, Y. T. *et al.* Translational validation of personalized treatment strategy based on genetic characteristics of glioblastoma. *PLoS One* **9**, 1–11 (2014).

117. Joo, K. M. *et al.* Patient-Specific Orthotopic Glioblastoma Xenograft Models Recapitulate the Histopathology and Biology of Human Glioblastomas In Situ. *Cell*

Rep. **3**, 260–273 (2013).

118. Oh, T. *et al.* Immunocompetent murine models for the study of glioblastoma immunotherapy. *J. Transl. Med.* **12**, 1–10 (2014).

119. Maes, W. & Van Gool, S. W. Experimental immunotherapy for malignant glioma: Lessons from two decades of research in the GL261 model. *Cancer Immunol. Immunother.* **60**, 153–160 (2011).

120. Hambardzumyan, D., Parada, L. F., Holland, E. C. & Charest, A. Genetic modeling of gliomas in mice: New tools to tackle old problems. *Glia* **59**, 1155–1168 (2011).

121. Heyer, J., Kwong, L. N., Lowe, S. W. & Chin, L. Non-germline genetically engineered mouse models for translational cancer research. *Nat. Rev. Cancer* **10**, 470–480 (2010).

122. Tibbitt, M. W. & Anseth, K. S. Hydrogels as extracellular matrix mimics for 3D cell culture. *Biotechnol. Bioeng.* **103**, 655–663 (2009).

123. Ulrich, T. A., de Juan Pardo, E. M. & Kumar, S. The Mechanical Rigidity of the Extracellular Matrix Regulates the Structure, Motility, and Proliferation of Glioma Cells. *Cancer Res.* **69**, 4167 LP – 4174 (2009).

124. Rape, A. D. & Kumar, S. A composite hydrogel platform for the dissection of tumor cell migration at tissue interfaces. *Biomaterials* **35**, 8846–8853 (2014).

125. Thomas, T. W. & DiMilla, P. a. Spreading and motility of human glioblastoma cells on sheets of silicone rubber depend on substratum compliance. *Med. Biol. Eng. Comput.* **38**, 360–370 (2000).

126. Lees, J. G. *et al.* Role of dynamin in elongated cell migration in a 3D matrix. *Biochim. Biophys. Acta - Mol. Cell Res.* **1853**, 611–618 (2015).

127. Xiao, W., Sohrabi, A. & Seidlits, S. K. Integrating the glioblastoma microenvironment into engineered experimental models. *Futur. Sci. OA* **3**, FSO189 (2017).

128. Rao, S. S. *et al.* Mimicking white matter tract topography using core-shell electrospun nanofibers to examine migration of malignant brain tumors. *Biomaterials* **34**, 5181–5190 (2013).

129. Johnson, J. *et al.* Quantitative analysis of complex glioma cell migration on electrospun polycaprolactone using time-lapse microscopy. *Tissue Eng. Part C. Methods* **15**, 531–40 (2009).

130. Ananthanarayanan, B., Kim, Y. & Kumar, S. Elucidating the mechanobiology of malignant brain tumors using a brain matrix-mimetic hyaluronic acid hydrogel platform. *Biomaterials* **32**, 7913–7923 (2011).

131. Fraley, S. I. *et al.* A distinctive role for focal adhesion proteins in three-dimensional cell motility. *Nat. Cell Biol.* **12**, 598–604 (2010).

132. Wolfenson, H., Lavelin, I. & Geiger, B. Dynamic Regulation of the Structure and Functions of Integrin Adhesions. *Dev. Cell* **24**, 447–458 (2013).

133. Vartanian, A. *et al.* GBM's multifaceted landscape: Highlighting regional and microenvironmental heterogeneity. *Neuro. Oncol.* **16**, 1167–1175 (2014).

134. Jin, S. G. *et al.* The effect of hyaluronic acid on the invasiveness of malignant glioma cells: Comparison of invasion potential at hyaluronic acid hydrogel and

Matrigel. *J. Korean Neurosurg. Soc.* **46**, 472–478 (2009).

135. Sarkar, S., Nuttall, R. K., Liu, S., Edwards, D. R. & Yong, V. W. Tenascin-C stimulates glioma cell invasion through matrix metalloproteinase-12. *Cancer Res.* **66**, 11771–11780 (2006).

136. Jiguet Jiglaire, C. *et al.* Ex vivo cultures of glioblastoma in three-dimensional hydrogel maintain the original tumor growth behavior and are suitable for preclinical drug and radiation sensitivity screening. *Exp. Cell Res.* **321**, 99–108 (2014).

137. Rao, S. S. *et al.* Glioblastoma behaviors in three-dimensional collagen-hyaluronan composite hydrogels. *ACS Appl. Mater. Interfaces* **5**, 9276–9284 (2013).

138. Wang, C., Tong, X., Jiang, X. & Yang, F. Effect of matrix metalloproteinase-mediated matrix degradation on glioblastoma cell behavior in 3D PEG-based hydrogels. *J. Biomed. Mater. Res. - Part A* **105**, 770–778 (2017).

139. Coquerel, B. *et al.* Elastin-derived peptides: Matrikines critical for glioblastoma cell aggressiveness in a 3-D system. *Glia* **57**, 1716–1726 (2009).

140. Azagarsamy, M. A. & Anseth, K. S. Bioorthogonal click chemistry: An indispensable tool to create multifaceted cell culture scaffolds. *ACS Macro Lett.* **2**, 5–9 (2013).

141. Williams, C. G., Malik, A. N., Kim, T. K., Manson, P. N. & Elisseeff, J. H. Variable cytocompatibility of six cell lines with photoinitiators used for polymerizing hydrogels and cell encapsulation. *Biomaterials* **26**, 1211–1218 (2005).

142. Monteiro, N. *et al.* Photopolymerization of cell-laden gelatin methacryloyl

hydrogels using a dental curing light for regenerative dentistry. *Dent. Mater.* **34**, 389–399 (2018).

143. Cha, J., Kang, S.-G. & Kim, P. Strategies of Mesenchymal Invasion of Patient-derived Brain Tumors: Microenvironmental Adaptation. *Sci. Rep.* **6**, 24912 (2016).

144. Kievit, F. M. *et al.* Proliferation and enrichment of CD133+ glioblastoma cancer stem cells on 3D chitosan-alginate scaffolds. *Biomaterials* **35**, 9137–9143 (2014).

145. Ulrich, T. A., Jain, A., Tanner, K., MacKay, J. L. & Kumar, S. Probing cellular mechanobiology in three-dimensional culture with collagen-agarose matrices. *Biomaterials* **31**, 1875–1884 (2010).

146. Heffernan, J. M., Overstreet, D. J., Le, L. D., Vernon, B. L. & Sirianni, R. W. Bioengineered Scaffolds for 3D Analysis of Glioblastoma Proliferation and Invasion. *Ann. Biomed. Eng.* **43**, 1965–1977 (2015).

147. Wang, C., Tong, X. & Yang, F. Bioengineered 3D brain tumor model to elucidate the effects of matrix stiffness on glioblastoma cell behavior using peg-based hydrogels. *Mol. Pharm.* **11**, 2115–2125 (2014).

148. Florczyk, S. J. *et al.* Porous chitosan-hyaluronic acid scaffolds as a mimic of glioblastoma microenvironment ECM. *Biomaterials* **34**, 10143–10150 (2013).

149. Pedron, S. & Harley, B. A. C. Impact of the biophysical features of a 3D gelatin microenvironment on glioblastoma malignancy. *J. Biomed. Mater. Res. - Part A* **101**, 3404–3415 (2013).

150. Belousov, A. *et al.* The Extracellular Matrix and Biocompatible Materials in Glioblastoma Treatment. *Front. Bioeng. Biotechnol.* **7**, 341 (2019).

151. Logun, M. T. *et al.* Glioma cell invasion is significantly enhanced in composite hydrogel matrices composed of chondroitin 4- and 4,6-sulfated glycosaminoglycans. *J. Mater. Chem. B* **4**, 6052–6064 (2016).

152. Xiao, W. *et al.* Brain-mimetic 3D culture platforms allow investigation of cooperative effects of extracellular matrix features on therapeutic resistance in glioblastoma. *Cancer Res.* (2018). doi:10.1158/0008-5472.CAN-17-2429

153. Seidlits, S. K. *et al.* Peptide-modified, hyaluronic acid-based hydrogels as a 3D culture platform for neural stem/progenitor cell engineering. *J. Biomed. Mater. Res. - Part A* **107**, 704–718 (2019).

154. Tay, A., Sohrabi, A., Poole, K., Seidlits, S. & Di Carlo, D. A 3D Magnetic Hyaluronic Acid Hydrogel for Magnetomechanical Neuromodulation of Primary Dorsal Root Ganglion Neurons. *Adv. Mater.* **30**, 1–8 (2018).

155. Caliari, S. R. & Burdick, J. A. A practical guide to hydrogels for cell culture. *Nat. Methods* **13**, 405–414 (2016).

156. Kaphle, P., Li, Y. & Yao, L. The mechanical and pharmacological regulation of glioblastoma cell migration in 3D matrices. *J. Cell. Physiol.* **234**, 3948–3960 (2019).

157. Sood, D. *et al.* Fetal Brain Extracellular Matrix Boosts Neuronal Network Formation in 3D Bioengineered Model of Cortical Brain Tissue. *ACS Biomater. Sci. Eng.* **2**, 131–140 (2016).

158. Heffernan, J. M., Overstreet, D. J., Le, L. D., Vernon, B. L. & Sirianni, R. W. Bioengineered Scaffolds for 3D Analysis of Glioblastoma Proliferation and

Invasion. *Ann. Biomed. Eng.* **43**, 1965–1977 (2015).

159. Han, L. H., Tong, X. & Yang, F. Photo-crosslinkable PEG-based microribbons for forming 3D macroporous scaffolds with decoupled niche properties. *Adv. Mater.* **26**, 1757–1762 (2014).

160. Wang, H. & Heilshorn, S. C. Adaptable Hydrogel Networks with Reversible Linkages for Tissue Engineering. *Adv. Mater.* **27**, 3717–3736 (2015).

161. Griffin, D. R., Weaver, W. M., Scumpia, P., Di Carlo, D. & Segura, T. Scaffolds Assembled From Annealed Building Blocks. *Nat. Mater.* **14**, 737–744 (2015).

162. Werner, M. *et al.* Surface Curvature Differentially Regulates Stem Cell Migration and Differentiation via Altered Attachment Morphology and Nuclear Deformation. *Adv. Sci. (Weinheim, Baden-Wurttemberg, Ger.* **4**, 1600347 (2016).

163. Pieuchot, L. *et al.* Curvotaxis directs cell migration through cell-scale curvature landscapes. *Nat. Commun.* **9**, 3995 (2018).

164. Rath, B. H., Wahba, A., Camphausen, K. & Tofilon, P. J. Coculture with astrocytes reduces the radiosensitivity of glioblastoma stem-like cells and identifies additional targets for radiosensitization. *Cancer Med.* **4**, 1705–1716 (2015).

165. Chen, Z. *et al.* In vitro angiogenesis by human umbilical vein endothelial cells (HUVEC) induced by three-dimensional co-culture with glioblastoma cells. *J. Neurooncol.* **92**, 121–128 (2009).

166. Yang, N. *et al.* A co-culture model with brain tumor-specific bioluminescence demonstrates astrocyte-induced drug resistance in glioblastoma. *J. Transl. Med.*

12, 1–9 (2014).

167. Brown, J. A. *et al.* Metabolic consequences of inflammatory disruption of the blood-brain barrier in an organ-on-chip model of the human neurovascular unit. *J. Neuroinflammation* **13**, 1–17 (2016).

168. Wang, Y. I., Abaci, H. E. & Shuler, M. L. Microfluidic blood–brain barrier model provides in vivo-like barrier properties for drug permeability screening. *Biotechnol. Bioeng.* **114**, 184–194 (2017).

169. Montana, V. & Sontheimer, H. Bradykinin promotes the Chemotactic invasion of primary brain tumors. *J. Neurosci.* **31**, 4858–4867 (2011).

170. Farin, A. *et al.* Transplanted glioma cells migrate and proliferate on host brain vasculature: A dynamic analysis. *Glia* **53**, 799–808 (2006).

171. Ramírez-Castillejo, C. *et al.* Pigment epithelium-derived factor is a niche signal for neural stem cell renewal. *Nat. Neurosci.* **9**, 331–339 (2006).

172. Shen, Q. *et al.* Endothelial cells stimulate self-renewal and expand neurogenesis of neural stem cells. *Science (80-.).* **304**, 1338–1340 (2004).

173. Fuchs, E., Tumbar, T. & Guasch, G. Socializing with the neighbors: Stem cells and their niche. *Cell* **116**, 769–778 (2004).

174. Colwell, N. *et al.* Hypoxia in the glioblastoma microenvironment: Shaping the phenotype of cancer stem-like cells. *Neuro. Oncol.* **19**, 887–896 (2017).

175. Lewis, C. E. & Pollard, J. W. Distinct role of macrophages in different tumor microenvironments. *Cancer Res.* **66**, 605–612 (2006).

176. Ribatti, D. & Crivellato, E. Immune cells and angiogenesis. *J. Cell. Mol. Med.* **13**,

2822–2833 (2009).

177. Gonzalez, H., Hagerling, C. & Werb, Z. Roles of the immune system in cancer: from tumor initiation to metastatic progression. *Genes Dev.* **32**, 1267–1284 (2018).

178. Iadecola, C. & Nedergaard, M. Glial regulation of the cerebral microvasculature. *Nat. Neurosci.* **10**, 1369–1376 (2007).

179. Mathiisen, T. M., Lehre, K. P., Danbolt, N. C. & Ottersen, O. P. The perivascular astroglial sheath provides a complete covering of the brain microvessels: An electron microscopic 3D reconstruction. *Glia* **58**, 1094–1103 (2010).

180. Zagzag, D. *et al.* Vascular apoptosis and involution in gliomas precede neovascularization: A novel concept for glioma growth and angiogenesis. *Lab. Investig.* **80**, 837–849 (2000).

181. Xiao, W., Ehsanipour, A., Sohrabi, A. & Seidlits, S. K. Hyaluronic-acid based hydrogels for 3-dimensional culture of patient-derived glioblastoma cells. *J. Vis. Exp.* **2018**, 1–9 (2018).

182. Tabet, A. *et al.* Mechanical Characterization of Human Brain Tissue and Soft Dynamic Gels Exhibiting Electromechanical Neuro-Mimicry. *Adv. Healthc. Mater.* **8**, 1–5 (2019).

183. Williams, P. A. & Peacocke, A. R. The physical properties of a glycoprotein from bovine cortical bone (bone sialoprotein). *Biochim. Biophys. Acta - Mucoproteins Mucopolysaccharides* **101**, 327–335 (1965).

184. Hunter, G. K. & Goldberg, H. A. Modulation of crystal formation by bone

phosphoproteins: role of glutamic acid-rich sequences in the nucleation of hydroxyapatite by bone sialoprotein. *Biochem. J.* **302 (Pt 1**, 175–179 (1994).

185. Taipaleenmäki, H. *et al.* Antagonizing miR-218-5p attenuates Wnt signaling and reduces metastatic bone disease of triple negative breast cancer cells. *Oncotarget* **7**, 79032–79046 (2016).

186. Tu, Q. *et al.* Targeted overexpression of BSP in osteoclasts promotes bone metastasis of breast cancer cells. *J. Cell. Physiol.* **218**, 135–145 (2009).

187. Zhang, J. H. *et al.* Bone sialoprotein promotes bone metastasis of a non-bone-seeking clone of human breast cancer cells. *Anticancer Res.* **24**, 1361–1368 (2004).

188. Detry, C. *et al.* Detection of bone sialoprotein in human (pre)neoplastic lesions of the uterine cervix. *Calcif. Tissue Int.* **73**, 9–14 (2003).

189. Ghochani, Y., Kawaguchi, R., Coppola, G. & Kornblum, H. TMIC-11: NOVEL ANGIOCRINE CANDIDATES IN GLIOBLASTOMA PROGENITOR CELL PERIVASCULAR NICHE INTERACTIONS. *Neuro. Oncol.* **17**, v216–v216 (2015).

190. Cooper, L. A. D. *et al.* The Proneural Molecular Signature Is Enriched in Oligodendrogliomas and Predicts Improved Survival among Diffuse Gliomas. *PLoS One* **5**, e12548 (2010).

191. Liu, Q. *et al.* Molecular properties of CD133+ glioblastoma stem cells derived from treatment-refractory recurrent brain tumors. *J. Neurooncol.* **94**, 1–19 (2009).

192. Lingineni, K., Belekar, V., Tangadpalliwar, S. R. & Garg, P. The role of multidrug resistance protein (MRP-1) as an active efflux transporter on blood-brain barrier

(BBB) permeability. *Mol. Divers.* **21**, 355–365 (2017).

193. Mas-Moruno, C., Rechenmacher, F. & Kessler, H. Cilengitide: the first anti-angiogenic small molecule drug candidate design, synthesis and clinical evaluation. *Anticancer. Agents Med. Chem.* **10**, 753–768 (2010).

194. Stupp, R. *et al.* Cilengitide combined with standard treatment for patients with newly diagnosed glioblastoma with methylated MGMT promoter (CENTRIC EORTC 26071-22072 study): a multicentre, randomised, open-label, phase 3 trial. *Lancet. Oncol.* **15**, 1100–1108 (2014).

195. Tucci, M., Stucci, S. & Silvestris, F. Does cilengitide deserve another chance? *Lancet Oncol.* **15**, e584–e585 (2014).

196. Ellert-Miklaszewska, A., Poleszak, K., Pasierbinska, M. & Kaminska, B. Integrin signaling in glioma pathogenesis: From biology to therapy. *Int. J. Mol. Sci.* **21**, (2020).

197. Zhao, Y.-Z. *et al.* Glioma-targeted therapy using Cilengitide nanoparticles combined with UTMD enhanced delivery. *J. Control. Release* **224**, 112–125 (2016).

198. Chauvet, D. *et al.* In Vivo Measurement of Brain Tumor Elasticity Using Intraoperative Shear Wave Elastography. *Ultraschall der Medizin* **37**, 584–590 (2016).

199. Miroshnikova, Y. A. *et al.* Feedback To Regulate Glioblastoma Aggression. *Nat Cell Biol* **18**, 1336–1345 (2016).

200. Ciasca, G. *et al.* Nano-mechanical signature of brain tumours. *Nanoscale* **8**,

19629–19643 (2016).

201. Seano, G. *et al.* Solid stress in brain tumours causes neuronal loss and neurological dysfunction and can be reversed by lithium. *Nat. Biomed. Eng.* **3**, 230–245 (2019).

202. Hanahan, D. & Weinberg, R. A. Hallmarks of cancer: The next generation. *Cell* **144**, 646–674 (2011).

203. Raimundo, N., Baysal, B. E. & Shadel, G. S. Revisiting the TCA cycle: Signaling to tumor formation. *Trends Mol. Med.* **17**, 641–649 (2011).

204. Warburg, O., Posener, K. & Nägelein, E. Über den Stoffwechsel der Carcinomzelle_Warburg_1924-1.pdf. *Klin Wochenschr Berl* **4**, 310–343 (1924).

205. Romero-Garcia, S., Lopez-Gonzalez, J. S., Báez-Viveros, J. L., Aguilar-Cazares, D. & Prado-Garcia, H. Tumor cell metabolism: an integral view. *Cancer Biol. Ther.* **12**, 939–948 (2011).

206. Pauwels, E. K. J., Coumou, A. W., Kostkiewicz, M. & Kairemo, K. [18F] Fluoro-2-deoxy-D-glucose positron emission tomography/computed tomography imaging in oncology: Initial staging and evaluation of cancer therapy. *Med. Princ. Pract.* **22**, 427–437 (2013).

207. Garnier, D., Renoult, O., Alves-Guerra, M.-C., Paris, F. & Pecqueur, C. Glioblastoma Stem-Like Cells, Metabolic Strategy to Kill a Challenging Target. *Front. Oncol.* **9**, 118 (2019).

208. Menendez, J. A. & Alarcón, T. Metabostemness : a new cancer hallmark. *Front. Oncol.* **4**, 1–21 (2014).

209. Marin-valencia, I. *et al.* Article Analysis of Tumor Metabolism Reveals Mitochondrial Glucose Oxidation in Genetically Diverse Human Glioblastomas in the Mouse Brain In Vivo. *Cell Metab.* 827–837 (2012). doi:10.1016/j.cmet.2012.05.001

210. Semenza, G. L. HIF-1 : upstream and downstream of cancer metabolism. *Curr. Opin. is Genet. Dev.* 51–56 (2010). doi:10.1016/j.gde.2009.10.009

211. Sonveaux, P. *et al.* Targeting lactate-fueled respiration selectively kills hypoxic tumor cells in mice. *J Clin Invest* **118**, 3930–3942 (2008).

212. Martinez-outschoorn, U. E., Lisanti, M. P. & Sotgia, F. Seminars in Cancer Biology Catabolic cancer-associated fibroblasts transfer energy and biomass to anabolic cancer cells , fueling tumor growth. *Semin. Cancer Biol.* **25**, 47–60 (2014).

213. Cuyàs, E., Corominas-faja, B. & Menendez, J. A. The nutritional phenome of EMT-induced cancer stem-like cells. *Oncotarget* **5**, 3970–3982 (2014).

214. Bertero, T., Gaggioli, C. & Bertero, T. Mechanical forces rewire metabolism in the tumor niche Mechanical forces rewire metabolism in the tumor niche. *Mol. Cell. Oncol.* **6**, 1–3 (2019).

215. Via, G. & Signaling, M. Stiffer Matrix Accelerates Migration of Hepatocellular Carcinoma Cells through Enhanced Aerobic. *Cancers (Basel).* **12**, 490–505 (2020).

216. Sullivan, W. J. *et al.* Extracellular Matrix Remodeling Regulates Glucose Metabolism through TXNIP Destabilization. *Cell* **175**, 117-132.e21 (2018).

217. Sahai, S. *et al.* A cost-effective method to immobilize hydrated soft-tissue samples for atomic force microscopy. *Biotechniques* 206–209 (2016). doi:10.2144/000114461

218. Amsden, B. Solute Diffusion within Hydrogels. Mechanisms and Models. *Macromolecules* 8382–8395 (1998).

219. Singh, S. K. *et al.* Reports Critical role of three-dimensional tumorsphere size on experimental outcome. *Biotechniques* **69**, 333–338 (2020).

220. Dobin, A. *et al.* STAR: ultrafast universal RNA-seq aligner. *Bioinformatics* **29**, 15–21 (2013).

221. Kramer, A., Green, J., Pollard, J., Tugendreich, S. & Kra, A. Systems biology Causal analysis approaches in Ingenuity Pathway Analysis. *Bioinformatics* **30**, 523–530 (2014).

222. Hull, R. V, Iii, P. S. C. & U, R. J. H. Conformation of NADH studied by fluorescence excitation transfer spectroscopy. 9–16 (2001).

223. Mah, E. J., Lefebvre, A. E. Y. T., Mcgahey, G. E., Yee, A. F. & Digman, M. A. Collagen density modulates triple-negative breast cancer cell metabolism through adhesion- mediated contractility. *Sci. Rep.* 1–11 (2018). doi:10.1038/s41598-018-35381-9

224. Ranjit, S., Malacrida, L., Jameson, D. M. & Gratton, E. Fit-free analysis of fl uorescence lifetime imaging data using the phasor approach. **13**, 1979–2004 (2018).

225. Zhao, R., Jiang, S., Zhang, L. & Yu, Z. Mitochondrial electron transport chain,

ROS generation and uncoupling (Review). *Int J Mol Med* **44**, 3–15 (2019).

226. Digman, M. A., Caiolfa, V. R., Zamai, M. & Gratton, E. The Phasor Approach to Fluorescence Lifetime Imaging Analysis. *Biophys. J.* **94**, L14–L16 (2008).

227. Schaefer, P. M., Kalinina, S., Rueck, A. & Arnim, C. A. F. Von. NADH Auto fl uorescence — A Marker on its Way to Boost Bioenergetic Research. *Cytom. Part A* **95A**, 34–46 (2019).

228. Ghukasyan, V. V & Kao, F.-J. Monitoring Cellular Metabolism with Fluorescence Lifetime of Reduced Nicotinamide Adenine Dinucleotide. *J. Phys. Chem. C* **113**, 11532–11540 (2009).

229. Mas-Moruno, C., Rechenmacher, F. & Kessler, H. Cilengitide: the first anti-angiogenic small molecule drug candidate design, synthesis and clinical evaluation. *Anticancer. Agents Med. Chem.* **10**, 753–768 (2010).

230. Vaheri, A. *et al.* The ezrin protein family: membrane-cytoskeleton interactions and disease associations. *Curr. Opin. Cell Biol.* **9**, 659–666 (1997).

231. Bulut, G. *et al.* Small molecule inhibitors of ezrin inhibit the invasive phenotype of osteosarcoma cells. *Oncogene* **31**, 269–281 (2012).

232. Held, P., Ph, D. & Instruments, B. p p l i c a t i o n o t e Using Phenol Red to Assess pH in Tissue Culture Media. (1966).

233. Minata, M. *et al.* Phenotypic Plasticity of Invasive Edge Glioma Stem-like Cells in Response to Ionizing Radiation. *Cell Rep.* **26**, 1893-1905.e7 (2019).

234. Palamà, I. E., D'Amone, S. & Cortese, B. Microenvironmental Rigidity of 3D Scaffolds and Influence on Glioblastoma Cells: A Biomaterial Design Perspective.

Front. Bioeng. Biotechnol. **6**, 131 (2018).

235. Chen, J.-W. E., Pedron, S. & Harley, B. A. C. The Combined Influence of Hydrogel Stiffness and Matrix-Bound Hyaluronic Acid Content on Glioblastoma Invasion. *Macromol. Biosci.* **17**, 10.1002/mabi.201700018 (2017).

236. Hughes, J. H. *et al.* Transcriptomic analysis reveals that BMP4 sensitizes glioblastoma tumor-initiating cells to mechanical cues. *Matrix Biol.* **85**–**86**, 112–127 (2020).

237. Randall, E. C. *et al.* Localized Metabolomic Gradients in Patient-Derived Xenograft Models of Glioblastoma. *Cancer Res.* **80**, 1258 LP – 1267 (2020).

238. Bhat, K. *et al.* Dopamine Receptor Antagonists, Radiation, and Cholesterol Biosynthesis in Mouse Models of Glioblastoma. *JNCI J. Natl. Cancer Inst.* (2021). doi:10.1093/jnci/djab018

239. Mullen, P. J., Yu, R., Longo, J., Archer, M. C. & Penn, L. Z. The interplay between cell signalling and the mevalonate pathway in cancer. *Nat. Rev. Cancer* **16**, 718–731 (2016).

240. Liu, J., Albrecht, A. M., Ni, X., Yang, J. & Li, M. Glioblastoma tumor initiating cells: therapeutic strategies targeting apoptosis and microRNA pathways. *Curr. Mol. Med.* **13**, 352–357 (2013).

241. Jung, H. Hyaluronidase: An overview of its properties, applications, and side effects. *Arch. Plast. Surg.* **47**, 297–300 (2020).

242. Amaral, S. F. *et al.* Dynamic Influence of pH on Metalloproteinase Activity in Human Coronal and Radicular Dentin. *Caries Res.* **52**, 113–118 (2018).

243. Rogatzki, M. J., Ferguson, B. S., Goodwin, M. L. & Gladden, L. B. Lactate is always the end product of glycolysis. *Front. Neurosci.* **9**, 22 (2015).

244. Martin, L. *et al.* The β-d-Endoglucuronidase Heparanase Is a Danger Molecule That Drives Systemic Inflammation and Correlates with Clinical Course after Open and Endovascular Thoracoabdominal Aortic Aneurysm Repair: Lessons Learnt from Mice and Men . *Frontiers in Immunology* **8**, 681 (2017).

245. Martin, L. *et al.* The synthetic antimicrobial peptide 19-2.5 interacts with heparanase and heparan sulfate in murine and human sepsis. *PLoS One* **10**, 1–13 (2015).

246. Daniele, S. *et al.* Lactate dehydrogenase-A inhibition induces human glioblastoma multiforme stem cell differentiation and death. *Sci. Rep.* **5**, 1–17 (2015).

247. Clem, B. F., O'Neal, J., Klarer, A. C., Telang, S. & Chesney, J. Clinical development of cancer therapeutics that target metabolism. *QJM An Int. J. Med.* **109**, 367–372 (2016).

248. Fiveash, J. B. *et al.* NABTT-0702: A phase II study of R-(-)-gossypol (AT-101) in recurrent glioblastoma multiforme (GBM). *J. Clin. Oncol.* **27**, 2010 (2009).

249. Manerba, M. *et al.* Galloflavin (CAS 568-80-9): a novel inhibitor of lactate dehydrogenase. *ChemMedChem* **7**, 311–317 (2012).

250. Qiu, H. *et al.* JQ1 suppresses tumor growth through downregulating LDHA in ovarian cancer. *Oncotarget* **6**, 6915–6930 (2015).

251. Le, A. *et al.* Inhibition of lactate dehydrogenase A induces oxidative stress and inhibits tumor progression. *Proc. Natl. Acad. Sci. U. S. A.* **107**, 2037–2042

(2010).

252. Zhou, W. & Wahl, D. R. Metabolic Abnormalities in Glioblastoma and Metabolic Strategies to Overcome Treatment Resistance. *Cancers (Basel).* **11**, 1231 (2019).

253. Dwarakanath, B. S. *et al.* Clinical studies for improving radiotherapy with 2-deoxy-D-glucose: present status and future prospects. *J. Cancer Res. Ther.* **5 Suppl 1**, S21-6 (2009).

254. Wicks, R. T. *et al.* Local delivery of cancer-cell glycolytic inhibitors in high-grade glioma. *Neuro. Oncol.* **17**, 70–80 (2015).

255. Koukourakis, M. *et al.* Blocking LDHA glycolytic pathway sensitizes glioblastoma cells to radiation and temozolomide. *Biochem. Biophys. Res. Commun.* **491**, 932–938 (2017).

256. Chaudhuri, O. *et al.* Hydrogels with tunable stress relaxation regulate stem cell fate and activity. *Nat. Mater.* **15**, 326–334 (2016).

257. McKinnon, D. D., Domaille, D. W., Cha, J. N. & Anseth, K. S. Biophysically defined and cytocompatible covalently adaptable networks as viscoelastic 3D cell culture systems. *Adv. Mater.* **26**, 865–872 (2014).

258. Liu, A. *et al.* Tunable Fast Relaxation in Imine-Based Nanofibrillar Hydrogels Stimulates Cell Response through TRPV4 Activation. *Biomacromolecules* **21**, 3745–3755 (2020).

259. Vogenberg, F. R., Isaacson Barash, C. & Pursel, M. Personalized medicine: part 1: evolution and development into theranostics. *P T* **35**, 560–576 (2010).

260. Pampaloni, F., Reynaud, E. G. & Stelzer, E. H. K. The third dimension bridges the

gap between cell culture and live tissue. *Nat. Rev. Mol. Cell Biol.* **8**, 839–845 (2007).

261. Ravi, M., Paramesh, V., Kaviya, S. R., Anuradha, E. & Solomon, F. D. P. 3D Cell Culture Systems: Advantages and Applications. *J. Cell. Physiol.* **230**, 16–26 (2015).

262. Xiao, W. *et al.* Bioengineered scaffolds for 3D culture demonstrate extracellular matrix-mediated mechanisms of chemotherapy resistance in glioblastoma. *Matrix Biol.* **85**, 128–146 (2020).

263. Goetz, L. H. & Schork, N. J. Personalized medicine: motivation, challenges, and progress. *Fertil. Steril.* **109**, 952–963 (2018).

264. Gilbert, M. R. *et al.* Dose-dense temozolomide for newly diagnosed glioblastoma: a randomized phase III clinical trial. *J. Clin. Oncol. Off. J. Am. Soc. Clin. Oncol.* **31**, 4085–4091 (2013).

265. Tan, A. C. *et al.* Management of glioblastoma: State of the art and future directions. *CA. Cancer J. Clin.* **70**, 299–312 (2020).

266. Szopa, W., Burley, T. A., Kramer-Marek, G. & Kaspera, W. Diagnostic and Therapeutic Biomarkers in Glioblastoma: Current Status and Future Perspectives. *Biomed Res. Int.* **2017**, 8013575 (2017).